Diatom-based reconstructions of earthquake-induced paleoenvironmental change in coastal Alaska and Washington, USA

Jessica Marie DePaolis

Dissertation submitted to the faculty of the Virginia Polytechnic Institute and State University in partial fulfillment of the requirements for the degree of

Doctor of Philosophy
In
Geosciences

Christina Dura, Chair
Robert C. Witter
Brian W. Romans
James A. Spotila

December 8, 2023
Blacksburg, Virginia

Keywords: diatom, subduction zone, earthquake, paleoseismology, paleoecology

Diatom-based reconstructions of earthquake-induced paleoenvironmental change in coastal Alaska and Washington, USA

Jessica M. DePaolis

ABSTRACT

Great (Mw >8.5) earthquakes occur over long temporal intervals that extend beyond current historical (written and oral) records along most subduction zone coastlines often leading to the underestimation of magnitude, recurrence, and spatial extent of these events. Paleoseismic studies target low energy depositional environments that record primary and secondary evidence of earthquake occurrence within the coastal stratigraphy over much longer temporal scale, thus improving our understanding of the behavior of subduction zone earthquakes. Diatoms preserved within coastal stratigraphic records are sensitive to earthquake-induced environmental change and are useful bioindicators in paloesiesmology studies. The two studies in this dissertation employ diatoms to create novel approaches to investigate behavior and recurrence of earthquakes along two subductions zones: Alaska-Aleutian subduction zone and the Cascadia subduction zone. In these chapters we use diatoms to explore 1) the potential for combined slip along the Patton Bay splay fault system and the eastern Alaska-Aleutian subduction zone within Prince William Sound, Alaska, and 2) lacustrine turbidite source mechanisms in Ozette Lake, Washington to potentially improve the spatial and temporal earthquake record for the northern Cascadia subduction zone. This work has implications for improving our earthquake chronologies along subduction zone coastlines and making important contributions to coastal hazards assessments.

Diatom-based reconstructions of earthquake-induced paleoenvironmental change in coastal Alaska and Washington, USA

Jessica M. DePaolis

GENERAL AUDIENCE ABSTRACT

Subduction zones are capable of producing great (>Mw 8.5) earthquakes with accompanying tsunamis that can impact nearby coastlines with devastating force. Great earthquakes occur over long timescales (thousands of years) and are often not captured in short historical records, leaving questions about the recurrence, behavior, and range of potential future earthquakes along these boundaries. Paleoseismology, the study of earthquake history, employs methods that use the earthquake-induced environmental changes along subduction zone coastlines to provide long-term records of earthquake occurrence. Diatoms, a type of siliceous microalgae entrained in coastal sediments, react to changes in pH, salinity, water depth, and sediment type, and are important indicators of environmental change that can be used to expand our understanding of earthquake behavior. This dissertation uses diatoms in two projects that explore the earthquake history along the Alaska-Aleutian subduction zone and the Cascadia subduction zone. First, we determine that secondary faults, called splay faults, in Prince William Sound are likely triggered only by slip along the Alaska-Aleutian subduction zone, suggesting that combined slip has occurred during four of the eight total megathrust earthquakes in the last ~4,200 years. Second, we investigate the sediment origins of the youngest six deposits (turbidites) in Ozette Lake, linking them to diatoms located on the subaqueous delta and shallow lake surfaces, leading us to infer the source is likely earthquake-induced slope failure. Both projects help to expand our understanding of subduction zone earthquake behavior, and will help inform future hazards assessments for coastal communities.

“My diatoms, they’re small but they’re lovely”

Ruth Patrick

ACKNOWLEDGMENTS

To my advisor and fearless leader, Tina Dura, I sincerely thank you for your support throughout this journey. You have been instrumental in my growth as a scientist and human, and I am thankful for your patience, guidance, and friendship for the last six years. To be your first student is the biggest honor.

To my external committee member, Rob Witter, an embodiment of "team work makes the dream work" mentality. Thanks for being a great teammate and mentor - your guidance has been so valuable and I'm incredibly grateful that you agreed to be a part of my PhD journey. I hope we get to crack more apples in the field together one day.

To you both, I hope this is the start of many epic research projects together.

To Brian Romans and Jim Spotila, thank you both for the constructive feedback, thoughtful comments, and unwavering support through the years. It has been incredible to have your ideas and expertise on my committee.

I am indebted to the wizardry of the faculty and staff at Virginia Tech. A big thanks to Mary Jane, Sharon, Bera, and April from the Department of Geosciences for their support and willingness to share chocolate.

A very special thank you to the collaborators who graciously allowed me to join them in Chile (Marco Cisternas, Lisa Ely, Bre MacInnes), Alaska (Rob Witter, Peter Haeussler, Adrian Bender, Janet Curran), and Washington (Danny Brothers, Brian Sherrod, Andy Ritchie, Drake Singleton) to help with various field work trips. I am so grateful for the opportunities to join you in some

incredible adventures and I appreciate your patience, kindness, and guidance. I look forward to seeing many of you again in future research endeavors.

To the Coastal Hazards Lab past and present, especially the Campfire Conversations crew, you were a huge part of my growth as a scientist and I thank you for all of those conversations around the conference table “campfire”.

To my fellow grad students, the Hokies past and present, who have made this journey a little easier, and Derring a little brighter, with your support and friendship. I hope we cross paths again.

To Ben, who has been my go-to companion for absolutely everything over the last four years. I’m looking forward to the return of our weekend camping trips, long walks without curfew, and relaxing dinners at home. Thanks for being steady and reliable when life has gotten chaotic. I love you so much, bugs.

To my cat, Shaun White, you are my favorite. Don’t tell Ben.

To my wonderful, dear friends who have been asking for years when I’d be finished. The time is finally here. Thank you for the support, the long phone calls, the pep talks, the cat videos, the visits, the messages, and the mail. Your support has been felt and it’s made such a huge difference. I owe you all a visit.

To my family, thank you for understanding when I can’t make it home for the holidays, for nodding along to my silly conversations about academia, and laughing at my graying hair. You never fall

short of giving the best hugs around, showing your love with food, and saying “yes” to watching my cat for *another* couple months. I love you all!

Finally, this dissertation would not have been possible without additional financial support from USGS, NSF, SEPM, and the Virginia Tech Department of Geosciences. A special thanks to the VT Department of Geosciences Heath Robinson-Roy J. Holden Scholarship, Wallace D. Lowry and Alumni Research Scholarship, and the Petroleum Industry Summer Scholarship.

ATTRIBUTION

Chapter 2 is a manuscript that has been submitted for publication to the *Journal of Geophysical Research: Solid Earth*: DePaolis, J.M., Dura, T., Witter, R.C., Haeussler, P.J., Bender, A., Curran, J.H., Corbett, D.R., *Repeated coseismic uplift above the Patton Bay splay fault system, Montague Island, Alaska, USA.* (2023). Journal of Geophyscial Research: Solid Earth (In Review).

JMD participated in field sampling, conducted all diatom, cluster, and DCA analyses, wrote the original manuscript draft, and produced all of the figures. TD contributed to the manuscript drafts, main text to the DCA and cluster analysis, and provided extensive feedback at all stages of the manuscript. RCW led field work, provided OxCal analysis, produced Table 2, provided the original concept for Figure 8, and provided extensive feedback to the manuscript text and figures. PJH, AB, JHC participated in field sampling and provided helpful feedback and reviewed later drafts of the manuscript. DRC provided Cs/Pb analysis and interpretation, and contributed text to the methods section of the manuscript.

TABLE OF CONTENTS

Chapter 1: Introduction

1.1 SUBDUCTION ZONE PALEOSEISMOLOGY

Subduction zones, also referred to as megathrusts, are tectonically active boundaries scaling hundreds to thousands of kilometers of coastline. These boundaries are capable of producing great (>Mw 8.5) earthquakes that can be accompanied by devastating tsunamis as seen during the Maule (2010; Mw 8.8), Tohoku-Oki (2011; Mw 9), and Anchorage (1964; Mw 9.2) earthquakes (Plafker, 1965; Ozawa et al., 2011; Moreno et al., 2012). Long-lasting, intense shaking and accompanying tsunami trains can lead to loss of life, infrastructure damage, and displaced communities (McGuire et al., 2017). However, because great earthquakes occur relatively infrequently, and because there is significant spatial variability in rupture location over time, their recurrence and past rupture behavior are often not captured within the short historical and instrumental records of most subduction zone coastlines (Satake and Atwater, 2007). The limited temporal window of historical and instrumental records of subduction zone earthquakes leaves questions about subduction zone behavior through time, highlighting the importance of studying earthquakes on centennial and millennial timescales. So how do we begin to forecast when, where, and how great earthquakes may behave along subduction zone coastlines?

Subduction zone paleoseismology, which combines the methods of coastal stratigraphy, sedimentology, micropaleontology, and sea-level research provides a framework for reconstructing centennial to millennial-scale histories of earthquakes and tsunami inundation along subduction zone coastlines over multiple seismic cycles. Subduction zone seismic cycles are broadly described as having two stages: 1) interseismic (between earthquakes) period characterized by strain accumulation between coupled (stuck) tectonic plates creating gradual deformation of the upper plate and 2) coseismic (during an earthquake) period characterized by

release of strain and sudden deformation of the upper plate (Fig. 1.1). Low energy, organic-rich, depositional environments, such as tidal marshes, coastal lagoons, and coastal lakes, can effectively record upper plate coseismic deformation as primary (i.e., changes in relative sea level – RSL – created by coseismic vertical land motion, tsunami inundation, etc.) or secondary (i.e., shaking-induced subaqueous slope failure, etc.) evidence (Nelson et al., 2006; Sabatier et al., 2022). By employing stratigraphic methods in these ecologically sensitive coastal environments, paleoseismologist identify primary and secondary evidence of the largest, but least frequent subduction zone earthquakes which extends the earthquake chronology available to study.

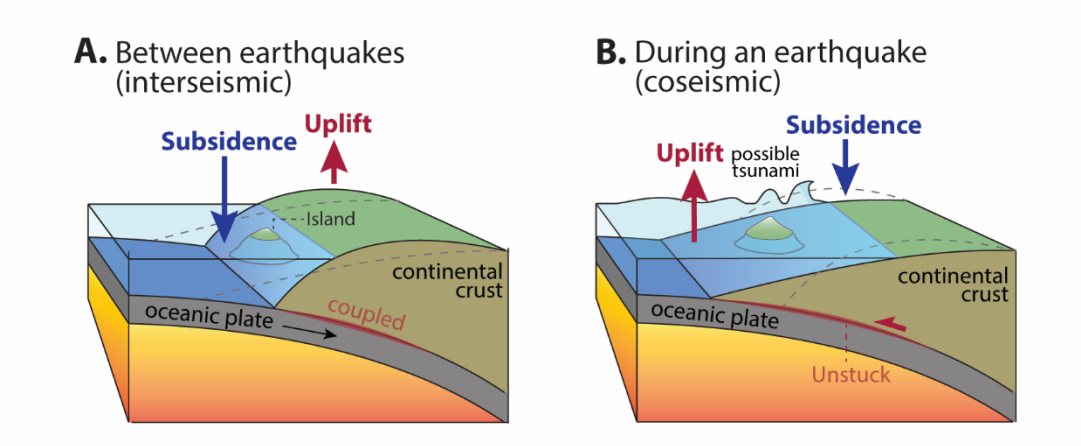

Figure 1.1 Subduction zone behavior during a) interseismic and b) coseismic periods of the earthquake deformation cycle. Modified from Walton and Staisch, et al. (2020).

Primary evidence records great earthquakes as widespread vertical land motion reflected in RSL changes. Low-energy, depositional environments along the coast may preserve laterally continuous, sharp (1-3 mm) stratigraphic contacts between silt and overlying peat (coseismic uplift, RSL fall) or peat and overlying silt (coseismic subsidence, RSL rise). Ecological changes, such as draining lagoons and salinity change, are also recorded in the stratigraphy, reflecting long-term preservation of coseismic vertical land motion (Fig. 1.2).

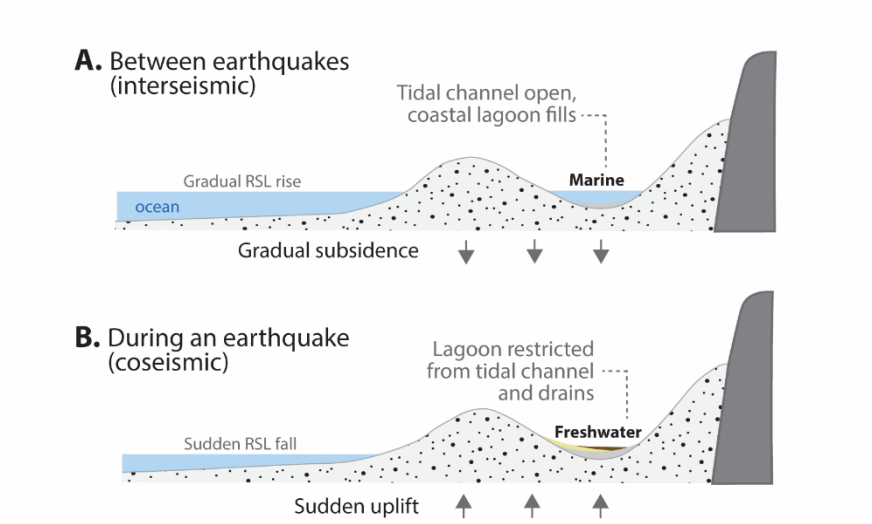

Figure 2.1 Schematic representing a cross-sectional view of the geomorphological and ecological changes of a coastal lagoon system during a) interseismic and b) coseismic periods of the earthquake deformation cycle.

Secondary evidence records great earthquakes as deposition caused by intense shaking along the coastline. In sensitive depositional settings, such as coastal lakes, earthquake-induced subaqueous landslides, subaerial landslides, or resuspended lake sediments may produce coarse, anomalous, widespread deposition that interrupts normal lake sedimentation as turbidites or other mass transport (Sabatier et al., 2022; Fig. 1.3).

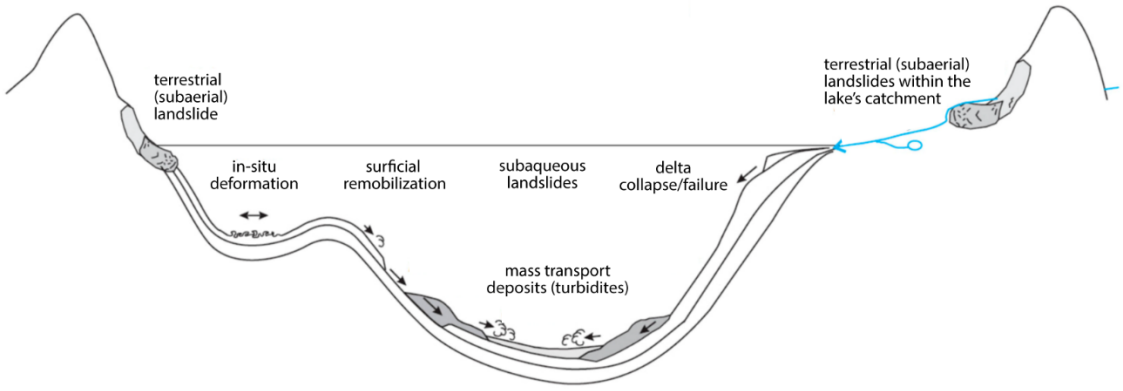

Figure 1.3 Cross-sectional view of a coastal lake and the possible secondary depositional mechanisms triggered by intense seismic activity. Adjusted from Sabatier et al. (2022).

1.2 DIATOMS AS PALEOSEISMIC INDICATORS

Diatoms, an important group of siliceous microalgae, are often incorporated into the stratigraphy of coastal environments and may provide crucial ecological information that can be used to improve earthquake chronologies. Diatoms are critical in providing detailed environmental reconstructions that can be used to link environmental change to the earthquake record. Sensitive to variables like pH, water depth, salinity, and substrate, diatoms are some of the first organisms to reflect earthquake-induced ecological change (Horton et al., 2013; Pilarczyk et al., 2014). During a subduction zone earthquake, diatoms preserved in low-energy depositional environments may record the sudden change in RSL as salinity, substrate, water depth, or nutrient change, reflecting the earthquake-induced land motion as environmental response. Similarly, secondary effects like shaking-induced subaqueous landslides will transport diatom-rich sediment from one locality of a lake to another, potentially leaving a signal showing where the sediment was sourced from. When preserved in Holocene geologic records, diatoms can provide long-term records of ecological response to primary or secondary seismic indicators over multiple earthquake cycles (Hemphill-Haley, 1996; Pilarczyk et al., 2014; Dura et al., 2016).

1.3 SUMMARY OF CHAPTERS

This dissertation will focus on two studies that demonstrate how diatom-based methods provide necessary, and often novel, answers to large-scale paleoseismic questions. The chapters are briefly outlined below.

Chapter 2 discusses the rupture history of the Patton Bay splay fault system, a series of secondary faults that connect directly to the Alaska-Aleutian subduction zone (megathrust) at seismogenic depths within Prince William Sound, Alaska. We explore the stratigraphic record of

the western coast of Montague Island where a distinct, widespread sedimentological contact representing the 1964 M9.2 Great Alaska Earthquake and three additional prehistoric earthquake contacts (760-870 yr BP, 2500-2700 yr BP, 4120-4500 yr BP) are recorded (Shennan et al., 2014, 2016). During the 1964 earthquake, combined megathrust and splay fault slip created 3.7-4.3 m of uplift at our field locality (Hidden Lagoons) on western Montague Island, and compounded tsunami hazards for Prince William Sound coastal communities (Plafker, 1969) leaving questions: Are the prehistoric earthquakes evidence of past combined megathrust-splay fault slip? Or do they represent megathrust-only or splay-only slip? We describe the sedimentological and diatom signature across the 1964 CE earthquake contact and use it as an analog to study the prehistoric earthquakes and determine their past slip patterns (i.e., independent or combined). Diatoms contribute to understanding ecological and geomorphological coastal change and semi-quantify earthquake-induced RSL changes at Hidden Lagoons. We conclude that each of the prehistoric contacts likely represent repeated, combined megathrust-splay fault slip and highlights a significant contribution to understanding Alaska's splay fault and subduction zone behavior. This work has been submitted for publication to *Geological Society of America Bulletin*.

Chapter 3 discusses a novel approach of using diatoms to identify the source mechanism (i.e., seismic versus climate) of turbidite deposition in Ozette Lake, located on the western coast of Washington state, to improve long-term earthquake history of the northern Cascadia subduction zone (CSZ). The most recent great (Mw >8.5) earthquake produced by the fault boundary occurred in early 1700 CE, however, the CSZ has remained quiet since that rupture leaving questions about expected recurrence, magnitude, and behavior of future earthquakes (Atwater, 1987; Satake, 2003). Onshore coastal records along the northern CSZ are much shorter than the southern CSZ, creating challenges for developing the spatial and temporal variability of past events along the entire boundary (Nelson et al., 2020; Walton et al., 2021). Coastal lakes are sensitive recorders of

sediment accumulation and may contain secondary evidence (e.g., subaqueous slope failure) for earthquake occurrence along coastlines that may have shorter and weaker coastal sedimentary records. Therefore, long-term lake records may be used to fill spatial and temporal gaps in earthquake chronologies where other onshore records are insufficient. Sedimentary similarities between seismic- and climate-induced deposition within lakes may cause under- or over-estimation of earthquake recurrence, inhibiting accurate assessment of earthquake histories (Sabatier et al., 2022). In this chapter, we use diatoms in a novel approach to differentiate the source mechanism of turbidites within Ozette Lake. We conclude that: 1) diatoms in Ozette Lake record distinctly different signatures during seismic- and flood-induced deposition, enhancing our ability to use diatoms to distinguish the source of deposits in the fossil record and; 2) turbidites are likely sourced from sediment displaced from the Umbrella Creek delta and resuspended shallow lake environments during intense earthquakes and not from floods. This work highlights important potential uses of diatoms in lacustrine paleoseismology and will be submitted for publication at a later time.

In summary, diatoms offer unique and novel ways of approaching paleoseismic questions. We present two examples of how diatoms make significant contributions to regional paleoseismology by providing new context for Alaska neotectonics and expanding northern Cascadia subduction zone earthquake chronologies. This work has broader implications for offering improvements to earthquake preparedness and enhancing hazards assessments for regional coastal communities.

REFERENCES CITED

Atwater, B.F., 1987, Evidence for Great Holocene Earthquakes along the Outer Coast of: Source:

Science, New Series, v. 236, p. 942–944.

Dura, T., Hemphill-Haley, E., Sawai, Y., and Horton, B.P., 2016, The application of diatoms to reconstruct the history of subduction zone earthquakes and tsunamis: Earth-Science Reviews, v. 152, p. 181–197, doi:10.1016/j.earscirev.2015.11.017.

Hemphill-Haley, E., 1996, Diatoms as an aid in identifying late-Holocene tsunami deposits: The Holocene, v. 6, p. 439–448, doi:10.1177/095968369600600406.

Horton, B.P., Engelhart, S.E., Kemp, A.C., and Sawai, Y., 2013, Microfossils in Tidal Settings as Indicators of Sea-Level Change, Paleoearthquakes, Tsunamis, and Tropical Cyclones, *in* Treatise on Geomorphology, p. 292–314.

McGuire, J.J., Plank, T., Barrientos, S., Becker, T., Brodsky, E. and Cottrell, E., 2017. The SZ4D initiative: Understanding the processes that underlie subduction zone hazards in 4D. *Vision Document Submitted to the National Science Foundation*.

Moreno, M., Melnick, D., Rosenau, M., Baez, J., Klotz, J., Oncken, O., Tassara, A., Chen, J., Bataille, K., and Bevis, M., 2012, Toward understanding tectonic control on the Mw 8.8 2010 Maule Chile earthquake: Earth and Planetary Science Letters, v. 321, p. 152–165.

Nelson, A.R., Hawkes, A.D., Sawai, Y., Engelhart, S.E., Witter, R., Grant-Walter, W.C., Bradley, L.-A., Dura, T., Cahill, N., and Horton, B., 2020, Identifying the Greatest Earthquakes of the Past 2000 Years at the Nehalem River Estuary, Northern Oregon Coast, USA: Open Quaternary, v. 6, doi:10.5334/oq.70.

Nelson, A.R., Kelsey, H.M., and Witter, R.C., 2006, Great earthquakes of variable magnitude at the Cascadia subduction zone: Quaternary Research, v. 65, p. 354–365, doi:10.1016/j.yqres.2006.02.009.

Ozawa, S., Nishimura, T., Suito, H., Kobayashi, T., Tobita, M., and Imakiire, T., 2011, Coseismic and postseismic slip of the 2011 magnitude-9 Tohoku-Oki earthquake: Nature, v.

475, p. 373–376.

Pilarczyk, J.E., Dura, T., Horton, B.P., Engelhart, S.E., Kemp, A.C., and Sawai, Y., 2014, Microfossils from coastal environments as indicators of paleo-earthquakes, tsunamis and storms: Palaeogeography, Palaeoclimatology, Palaeoecology, v. 413, p. 144–157, doi:10.1016/j.palaeo.2014.06.033.

Plafker, G., 1965, Tectonic Deformation Associated with the 1964 Alaska Earthquake: Science, v. 148, p. 1675–1687.

Plafker, G., 1969, Tectonics of the March 27, 1964 Alaska Earthquake: US Geological Survey Professional Paper,.

Plafker, G., and Savage, J.C., 1970, Mechanism of the Chilean Earthquakes of May 21 and 22, 1960: Geological Society of America Bulletin, v. 81, p. 1001–1030.

Sabatier, P., Moernaut, J., Bertrand, S., Van Daele, M., Kremer, K., Chaumillon, E., and Arnaud, F., 2022, A Review of Event Deposits in Lake Sediments: Quaternary, v. 5, p. 1–49, doi:10.3390/quat5030034.

Satake, K., 2003, Fault slip and seismic moment of the 1700 Cascadia earthquake inferred from Japanese tsunami descriptions: Journal of Geophysical Research, v. 108, doi:10.1029/2003jb002521.

Satake, K. and Atwater, B.F., 2007. Long-term perspectives on giant earthquakes and tsunamis at subduction zones. *Annu. Rev. Earth Planet. Sci.*, *35*, pp.349-374.

Shennan, I., Barlow, N., Combellick, R., Pierre, K., and Stuart-Taylor, O., 2014, Late Holocene paleoseismology of a site in the region of maximum subsidence during the 1964 Mw 9.2 Alaska earthquake: Journal of Quaternary Science, v. 29, p. 343–350, doi:10.1002/jqs.2705.

Shennan, I., Garrett, E., and Barlow, N., 2016, Detection limits of tidal-wetland sequences to identify variable rupture modes of megathrust earthquakes: Quaternary Science Reviews, v.

150, p. 1–30, doi:10.1016/j.quascirev.2016.08.003.

Walton, M.A.L., Staisch, L.M., Dura, T., Pearl, J.K., Sherrod, B., Gomberg, J., Engelhart, S., Tréhu, A., Watt, J., and Perkins, J., 2021, Toward an integrative geological and geophysical view of Cascadia subduction zone earthquakes: Annual Review of Earth and Planetary Sciences, v. 49, p. 367–398.

Chapter 2: Repeated coseismic uplift of coastal lagoons above the Patton Bay Splay Fault System, Montague Island, Alaska, USA

Jessica M. DePaolis[1], Tina Dura[1], Robert C. Witter[2], Peter J. Haeussler[2], Adrian Bender[2], Janet H. Curran[2], D. Reide Corbett[3]

[1]*Department of Geosciences, Virginia Tech, Blacksburg, VA, USA*
[2]*United States Geological Survey, Alaska Science Center, Anchorage, Alaska, USA*
[3]*Department of Coastal Studies, East Carolina University, Wanchese, NC, USA*

ABSTRACT

Coseismic slip on the Patton Bay Splay Fault System during the 1964 M_w 9.2 Great Alaska Earthquake contributed to local tsunami generation and vertically uplifted shorelines as much as 11m on Montague Island in Prince William Sound (PWS). Sudden uplift of the island caused coastal lagoons along the island's northwestern coast to gradually drain. The resulting change in depositional environment from marine lagoon to freshwater muskeg created a sharp, laterally continuous stratigraphic contact between silt and overlying peat. Here, we characterize the geomorphology, sedimentology, and diatom ecology across the 1964 earthquake contact and three similar prehistoric contacts within the stratigraphy of the Hidden Lagoons locality. We find that the contacts signal instances of abrupt coastal uplift that, within error, overlap the timing of independently constrained megathrust earthquakes in PWS – 1964 CE, 760-870 yr BP, 2500-2700 yr BP, and 4120-4500 yr BP. Changes in fossil diatom assemblages across the inferred prehistoric earthquake contacts reflect ecological shifts consistent with repeated draining of a lagoon system caused by >3 m of coseismic uplift. Our observations provide evidence for four instances of combined megathrust-splay fault ruptures that have occurred in the past ~4,200 years in PWS. We recommend that the tsunami risks associated with future combined megathrust-splay fault system ruptures be considered in hazards assessments.

2.1 INTRODUCTION

The 1964 M_w 9.2 Great Alaska Earthquake ruptured >900 km of the Alaska-Aleutian subduction zone (AASZ) and produced a regional and Pacific-wide tsunami that impacted coastlines in Alaska, British Columbia, Hawaii, Oregon, and California (Plafker, 1969). The earthquake triggered a series of reverse faults that connect with the AASZ at seismogenic depths (Plafker, 1965; 1967; 1969; Haeussler et al., 2015; Fig. 2.1). These secondary faults, collectively known as the Patton Bay splay fault system (herein referred to as the splay fault system) increased uplift of the overriding plate and generated destructive local tsunami waves that destroyed the port of Seward (Lemke, 1967) and elevated the impacts of inundation along the coast of the Kenai Peninsula (Wilson and Tørum, 1972; Suleimani and Freymueller, 2020). Because megathrust splay faults have the potential to contribute to the tsunami hazard in future earthquakes, tsunami hazard assessments require information about how often splay fault ruptures have occurred in the past and whether splay faults consistently rupture independently or concurrently with megathrust slip.

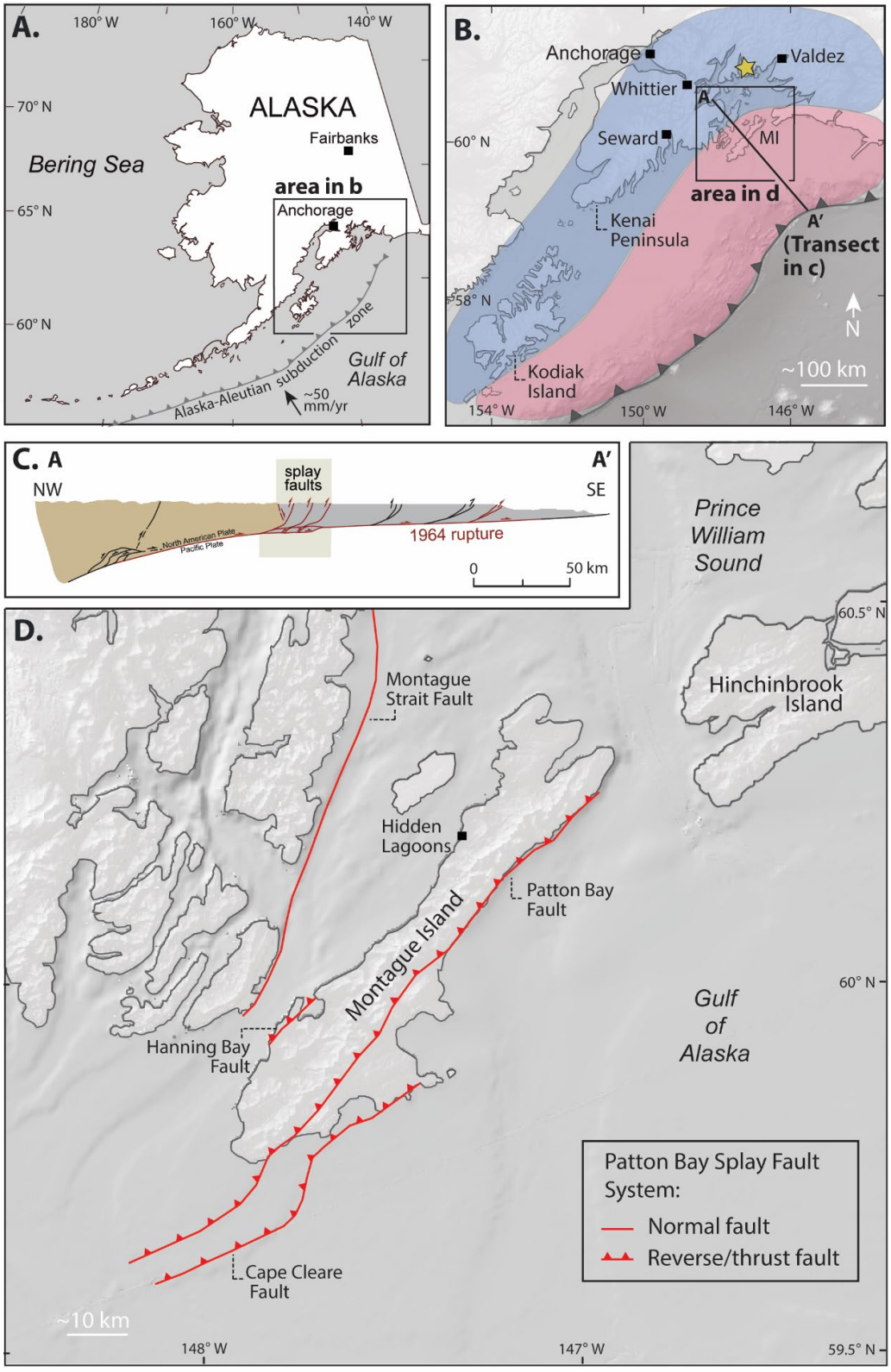
A.
180° W
160° W
140° W
70° N
65° N
60° N
ALASKA
Fairbanks
Bering Sea
area in b
Anchorage
Alaska-Aleutian subduction zone
~50 mm/yr
Gulf of Alaska
B.
Anchorage
Valdez
Whittier
A
Seward
MI
60° N
area in d
Kenai Peninsula
A'
(Transect in c)
58° N
N
~100 km
Kodiak Island
154° W
150° W
146° W
C. A
A'
NW
SE
splay faults
North American Plate
Pacific Plate
1964 rupture
0
50 km
Prince William Sound
60.5° N
D.
Montague Strait Fault
Hinchinbrook Island
Hidden Lagoons
Patton Bay Fault
Montague Island
60° N
Gulf of Alaska
Hanning Bay Fault
Patton Bay Splay Fault System:
Normal fault
Reverse/thrust fault
Cape Cleare Fault
~10 km
148° W
147° W
59.5° N

Figure 2.1. a) Regional and tectonic setting above the Alaska-Aleutian Subduction Zone. b) Estimated M_w 9.2 1964 CE earthquake rupture extent and deformation patterns (blue = subsidence, red = uplift) based on Plafker (1969). Gold star shows epicenter of the earthquake. MI = Montague Island. c) Cross section of 1964 CE deformation on the subduction zone and splay faults through the upper plate, modified from Haeussler et al. (2015). Faults shown in red ruptured during the earthquake. Small arrows show deformation direction. Gray shaded area shows the Patton Bay splay fault system. d) Normal (red line) and reverse (red line with teeth) faults of the Patton Bay splay fault system and their estimated onshore and offshore locations from Haeussler et al. (2015).

Splay faults are not unique to the AASZ and are known to contribute to the tsunami hazard at subduction zones around the world including Ecuador (Collot et al., 2008), Japan (Kodaira et al., 2002; Park et al., 2002), Cascadia (Han et al., 2017), and Chile (Melnick et al., 2012). Splay faults often exist offshore making it challenging to study their displacement and rupture dynamics through direct observations. However, it may be possible to reconstruct the long-term behavior of a splay fault system by examining the secondary effects that activation of the fault system has on proximal landforms and coastlines. For example, abrupt, earthquake-induced land-level change can be recorded in coastal sediments as geomorphic, stratigraphic, and microfossil changes over multiple earthquake cycles (centuries to millennia). This approach, known as coastal paleogeodesy, has been successfully applied in low-energy, intertidal coastal environments at subduction zones around the world (e.g., Witter et al., 2003; Sawai et al., 2016; Dura et al., 2017). At the AASZ, coastal paleogeodetic approaches have been applied in tidal marshes fringing Prince William Sound (PWS) to reconstruct megathrust deformation patterns during eight earthquakes in the past ~4,200 years (Shennan et al., 2014), but a study that employs coastal paleogeodesy to reconstruct the rupture history of the splay fault system has not been conducted until now.

Here, we use the geomorphic, stratigraphic, and fossil diatom signature of the 1964 M_w 9.2 Great Alaska Earthquake preserved within the informally-named Hidden Lagoons locality on Montague Island as an analog for identifying prehistoric environmental changes that may signal

past coseismic uplift of the coast. We document three inferred prehistoric earthquake contacts that record environmental shifts consistent with coseismic uplift, similar to that observed following the combined megathrust and splay-fault rupture in 1964 CE. Radiocarbon, ^{137}Cs, and ^{210}Pb dating constrain the ages of the four instances of sudden uplift in the past ~4,200 years. Our results suggest that past ruptures of the splay fault system occurred close in time, within less than a century, of four of eight megathrust earthquakes documented by coastal paleogeodesy (Shennan et al., 2014; Shennan et al., 2016).

2.1.1 The 1964 M9.2 Great Alaska Earthquake and the Megathrust Earthquake Cycle

The eastern AASZ, which includes the region west of Kodiak Island, is a convergent plate boundary that has produced numerous great (>M_w 8) megathrust earthquakes (Fig. 2.1a; Plafker, 1965; Shennan et al., 2014). The largest instrumentally recorded earthquake on the eastern AASZ occurred on March 27, 1964 (M_w 9.2) and produced widespread upper-plate deformation within two zones: a zone of uplift extending ~250 km from the trench and a zone of subsidence ~200 km landward from the zone of uplift (Brocher, 2014; Plafker, 1965; Fig. 2.1b). The hingeline (i.e., contour of zero uplift or subsidence) separating the deformation zones paralleled the trench from offshore Kodiak Island and the Kenai Peninsula to PWS. Coastlines in the zone of subsidence (e.g., Kenai Peninsula) were submerged 1-2 m below sea level (Plafker, 1969). Coastlines located within the zone of uplift emerged 1–3 m above sea level, except along the coast of Montague Island, where uplift reached as much as 11 m (Plafker, 1969).

Montague Island (60.1° N, 147.3° W), located in southern PWS, lies ~150 km from the Aleutian trench. Although the island uplifted during the 1964 earthquake, explorers reported evidence for subsidence along the coast during the interseismic period before the coseismic uplift

(Fig. 2.2). Captain George Vancouver visited the northwest shore of Montague Island in 1794 and described "rapid encroachments" of the sea and forests submerged by tides (Vancouver, 1801), consistent with subsidence preceding the 1964 CE earthquake. During the 1964 CE earthquake, Montague Island was uplifted 3.7-11.0 m (Plafker, 1969) due to slip on the underlying splay fault system, greatly exceeding uplift observed elsewhere in PWS. Aerial photographs taken before and after the earthquake show that coseismic uplift shifted Montague Island coastlines seaward and initiated draining of coastal lagoons that in one case stranded previously brackish-marine fish species in freshening environments (Plafker, 1967; Lescak et al., 2015; Fig. 2.2). Like Vancouver's observations before the 1964 earthquake, modern satellite geodetic data (CORS Station AC79, http://geodesy.unr.edu/NGLStationPages/stations/AC79.sta) show that Montague Island is subsiding at a rate of 0.95±0.76 mm/yr during the current interseismic interval (Blewitt and Hammond, 2018). The environmental changes observed on Montague Island resulting from the 1964 CE earthquake suggest that prehistoric earthquakes may have similarly impacted the coast thus providing an opportunity to apply paleogeodetic methods to reconstruct a long-term record of coastal deformation related to the earthquake cycle. Does the splay fault system always rupture with the megathrust? And what can the megathrust-splay fault relationship tell us about local and regional tsunami hazards?

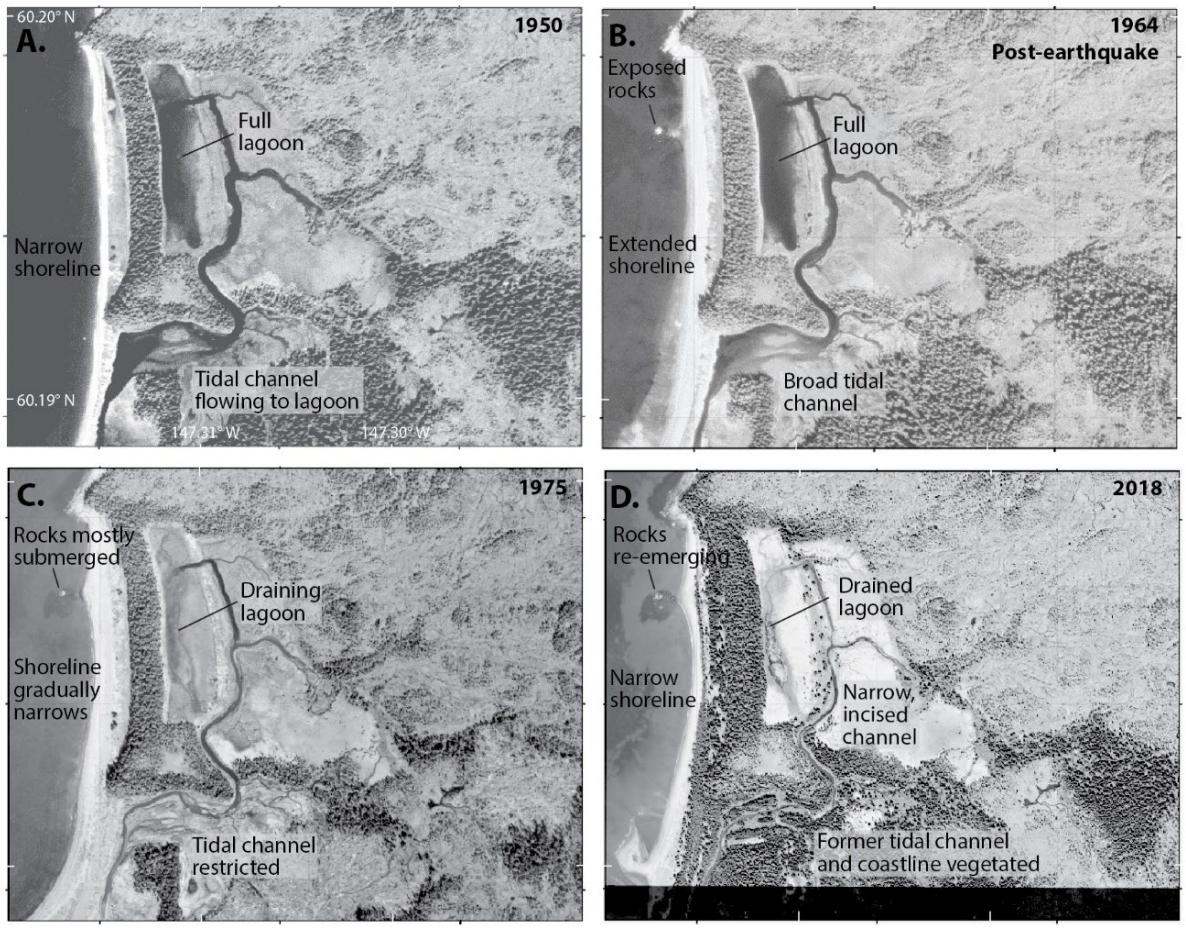

Figure 2.2. Aerial photography and satellite imagery of Hidden Lagoons before and after the March 1964 M 9.2 earthquake. a) 1950; b) August 1964; c) 1975; and d) 2018. Annotations reference important geomorphological and environmental changes.

2.2 PALEOGEODETIC METHODS AND APPROACH

We conducted a geomorphic, stratigraphic, and fossil diatom investigation of the Hidden Lagoons site on the northwest coast of Montague Island to search for evidence of sudden, coseismic uplift of the coast (Fig. 2.3). We targeted the site because aerial imagery acquired before and after the 1964 CE earthquake show that the tidally influenced lagoons gradually drained and shifted to a freshwater muskeg environment following the earthquake (Fig. 2.2), and Plafker's (1967) observations indicated 3.7–4.3 m of coastal uplift during the 1964 CE earthquake. Such an environmental change would be represented in the lagoon stratigraphy as a sudden transition from

an inorganic lagoon silt to an organic-rich deposit as the lagoon drained and dried and peat-forming vegetation colonized the drained surface. We would expect prehistoric earthquakes to produce similar environmental shifts and stratigraphic evidence. Our evaluation of the subsurface stratigraphy and geomorphic evolution of the site is based on analysis of 42 hand-driven sediment cores, 2 riverbank exposures, and 3 shallow (~1 m) pits (Fig. 2.3a). In the field we recorded detailed descriptions of site stratigraphy including color, sharpness of upper and lower contacts, and stratigraphy using the Troels-Smith method for describing organic-rich sediment (Troels-Smith, 1955; Nelson et al., 2015a). Computed tomography (CT) scans, which enhance characteristics of core sediment not visible to the naked eye, such as density variations and sediment inclusions, were crucial in defining and assessing contact location and sharpness. We chose a select number of cores to sample based on their representation of the site-wide stratigraphy (Fig. S1).

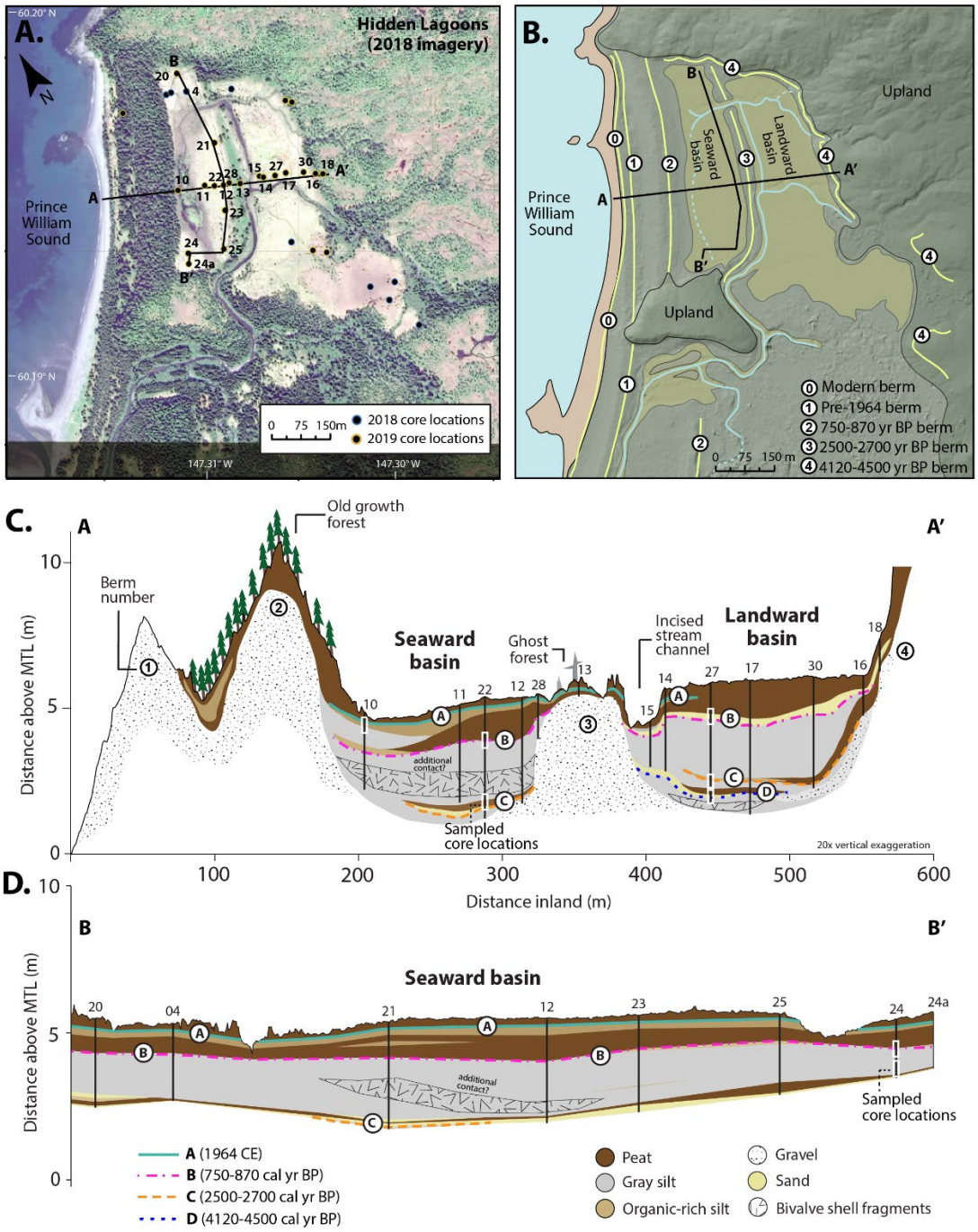

Figure 2.3. Hidden Lagoons site maps and cross sections. a) 2018 satellite imagery showing sample sites. b) Lidar annotated with geomorphological features including uplifted berms (yellow lines labeled 0-4) and modern streams (blue lines). c, d) Transects A-A' (coast-perpendicular) and B-B' (coast-parallel) show the stratigraphy of the seaward and landward basins of the Hidden Lagoons site. Vertical lines capped by numbers show core locations.

To reconstruct the paleoenvironmental history of Hidden Lagoons, including relative sea-level (RSL) changes caused by sudden coseismic uplift, we analyzed diatoms, a type of siliceous microalgae, preserved within coastal sediments (e.g., Briggs et al., 2014; Dura et al., 2016; Shennan et al., 1998). Following the methods of Dura and Hemphill-Haley (2020), we sampled the sediment cores at 1- to 2-cm intervals across stratigraphic contacts of interest. Diatoms were identified to the species level and a minimum of 300 diatom valves were counted in each of the 73 samples analyzed. To simplify interpretation, we used regional (Hamilton and Shennan, 2005; Nelson et al., 2015b) and global (Denys, 1991; Vos and de Wolf, 1993; Guiry et al., 2014; Dura and Hemphill-Haley, 2020; Spaulding et al., 2021) intertidal diatom ecological classifications to group species that exceeded 2% of the total diatoms counted into five categories. The intertidal diatom categories (e.g., marine lagoon, brackish lagoon) are defined by the dominant species' tolerance to varying practical salinity units (psu); the marine lagoon category includes marine and marine-brackish species that thrive in salinities exceeding 30 psu, while the brackish lagoon group includes brackish-marine and brackish species that tolerate salt concentrations between 0.2 and 30 psu. The freshwater diatom categories (e.g., freshwater coastal lake, freshwater peat bog, freshwater muskeg) include diatoms that tolerate low (below 0.2 psu) to no salinity and are defined by the dominant species' life form (e.g., benthic, planktonic, aerophilic) and preferred water depth conditions (Table 1, Fig. S2-S6, Table S1). Full species-level diatom counts can be found in the data release (DePaolis et al., 2023).

We applied stratigraphically constrained, unweighted pair-group average (UPGMA) cluster analysis to fossil diatom samples to identify samples with similar species composition (Fig. 2.5, S7). We also applied detrended correspondence analysis (DCA) to examine the pattern of diatom assemblage variation between samples. Samples with similar species assemblages and abundances are grouped together in the DCA plot and samples with statistically different species

assemblages and abundances plot farther apart (Fig. 2.6). Both the UPGMA cluster analysis and the DCA plots were calculated using the PAleontological STatistics (PAST) software program (Hammer, 2020).

We surveyed the positions of pits, cores and tidal benchmarks using a TRIMBLE Geo7x GNSS instrument to provide sub-meter vertical and horizontal accuracy. We processed survey data using TRIMBLE software and the nearest National Geodetic Survey Continuously Operating Reference Station (CORS), AC79 (https://www.unavco.org/instrumentation/networks/status/nota/overview/AC79). Pit and core elevations were determined from a lidar digital elevation model (Witter et al., 2020) and tied to local mean tide level (MTL) for the closest National Ocean Service tidal benchmark at Port Chalmers on Montague Island (https://tidesandcurrents.noaa.gov/stationhome.html?id=9454511). The diurnal tidal range (MLLW-MHHW) at the Port Chalmers tide station is 3.6 m.

To develop a chronology of episodic changes in depositional environment preserved at Hidden Lagoons, we collected buried macrofossils (i.e., rhizomes, seeds, and conifer needles and cones) found in cores for radiocarbon analyses. We used OxCal (version 4.4.3, Bronk Ramsey, 2021) and the IntCal20 atmospheric ^{14}C curve (Reimer et al., 2020) to calibrate ^{14}C dates to account for variations in atmospheric ^{14}C concentrations over time. We report calibrated ^{14}C ages in years before 1950 Common Era (CE). The full radiocarbon data release is available in Witter et al. (2023). Using our radiocarbon dates collected from above and below stratigraphic contacts, we constructed a Bayesian Sequence model in OxCal to compute probabilistic estimates of the time the contact formed (Lienkaemper & Ramsey, 2009; Bronk Ramsey, 2009). The OxCal code for our age model is included in the supplementary information. Inferred earthquake timing estimates are reported as the mean, 2-sigma uncertainty, and 95% confidence age ranges of the computed

probability density function (PDF) in calibrated years before CE 1950 (Table 2). Additionally, we used ^{137}Cs and ^{210}Pb (Corbett & Walsh, 2015; supplemental information) to verify the timing of the stratigraphic contact that marks uplift in 1964 CE (Fig. 2.4).

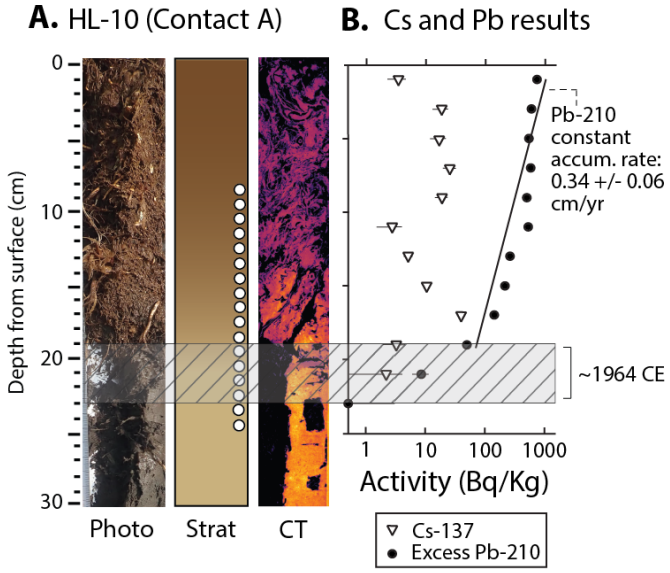

Figure 2.4. a) Photograph, stratigraphy schematic, and CT scan of the top 30 cm of core HL-10, encompassing Contact A (1964 CE). Colors used for stratigraphy schematic same as in Figure 3. Diatom sample depths shown by white circles. Gray, stripped rectangle shows the inferred depth (19-23 cm) of 1964 CE. b) Cesium (Cs-137) and Lead (Pb-210) results are shown with white triangles and black circles, respectively. Black line shows the estimated constant accumulation rate.

2.3 EVIDENCE FOR REPEATED COASTAL EMERGENCE

We mapped a series of four coast-parallel beach berms, numbered 1 through 4 progressing landward from the Hidden Lagoons shoreline creating a seaward basin and a landward basin at the site (Fig. 2.3b). Four primary stratigraphic contacts (A, B, C, and D) between silt or sand and peat units are evidence in the stratigraphy of the seaward and landward basins (Fig. 2.3c, d). Contacts B, C, and D are sharp, while contact A records a gradual transition. Contacts A, B, and C are laterally continuous across both the seaward and landward basins, whereas contact D is only

present in the landward basin. ^{137}Cs and ^{210}Pb analyses constrain the age of contact A to 1964 CE (Fig. 2.4), while our radiocarbon age model provides age ranges for contact B (760–870 cal yr BP), contact C (2500–2700 cal yr BP), and contact D (4120–4500 cal yr BP) (Fig. 2.5; Table 2). We summarize evidence for environmental shifts across each contact below.

Table 2. OxCal age model results for uplift events at Hidden Lagoons compared to the chronology of megathrust earthquakes on the eastern Alaska-Aleutian subduction zone.

Contact or event name	Modeled age estimate (years before 1950 CE)		Confidence interval (%)	Mean (μ)	Standard deviation (σ)	Median (m)
	From	To				
Hidden Lagoons, Montague Island chronology						
Contact A	[This contact records uplift during the 1964 Great Alaska earthquake]					
Contact B	872	760	95.4	811	29	808
Contact C	2705	2501	95.4	2594	58	2592
Contact D	4495	4125	95.4	4313	102	4324
Eastern AASZ earthquake chronology (Shennan et al., 2014 and Shennan et al., 2016*)						
EQ1	902	837	95.4	870	17	871
EQ2	1484	1397	95.4	1440	21	1441
EQ3	2102	2006	95.4	2052	27	2050
EQ4	2685	2540	95.4	2615	38	2618
EQ5	3216	3037	95.4	3131	43	3131
EQ6	3662	3475	95.4	3550	47	3541
EQ7*	4346	4151	95.4	--	20	4214

R code for the OxCal age model included in Supplementary Information.

2.3.1 Contact A: Evidence for Coseismic Uplift in 1964

The 3.7–4.3 m of coseismic uplift observed near Hidden Lagoons during the 1964 CE Alaska earthquake (Plafker, 1969) lowered the head of tide in the outlet stream and caused the water table in the lagoon to drain over the following decade. The gradual draining of the lagoon is captured in aerial photography and satellite imagery collected between 1950 and 2018 (Fig. 2.2). The area of the lagoon shows little change between photographs taken in 1950 prior to the 1964 earthquake and photographs taken 4 months after the earthquake (August 1964). However, by 1975, imagery shows the area of the lagoon reduced by about half. By 2018, wetland vegetation fills much of the area occupied by the lagoon before the 1964 earthquake.

Stratigraphy in the seaward basin records the 1964 uplift as a gradual (over 3 cm) peat-over-silt contact (contact A) at 21 cm depth in core HL-10 (Fig. 2.3c, 2.5a). The upward transition from silt to peat across contact A represents the slow (over >10 years), post-earthquake draining of the lagoon in the western part of the seaward basin as shown in the pre- and post-earthquake aerial imagery (Fig. 3). By 1975, part of the former lagoon was colonized by freshwater vegetation, and organic-rich peat accumulated over the lagoon silt.

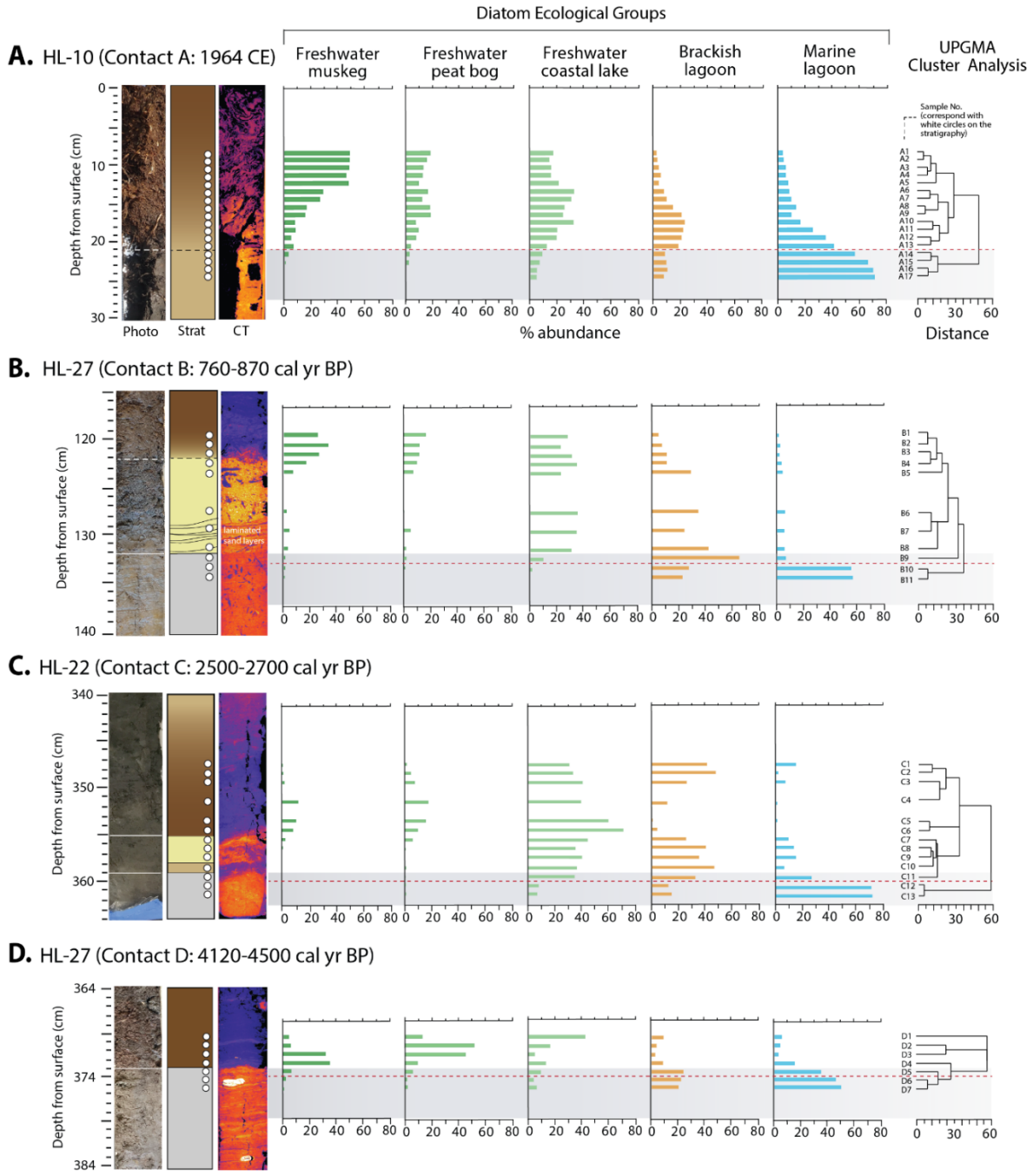

Figure 2.5. Photograph, stratigraphy schematic, and CT scans for a) contact A recovered in core HL-10; b) contact B in HL-27; c) contact C in HL-22; and d) contact D in HL-27. Colors used for stratigraphy schematic same as in Figure 3. Solid and dashed lines on the photos and schematics indicate sharp and gradual stratigraphic contacts, respectively. Diatom sample depths shown by white circles. Relative abundances of diatom are organized by five ecologic categories: Freshwater muskeg, freshwater peat bog, freshwater coastal lake, brackish lagoon, and marine lagoon. The results of the unweighted pair-group average (UPGMA) cluster analysis (far right) help to inform the stratigraphic level in each core section of strong environmental shifts in diatom assemblages (dotted red lines).

A gradual shift from marine to freshwater fossil diatom flora across contact A records the post-earthquake freshening of Hidden Lagoons (Fig. 2.5a). Below the contact, the diatom flora within the silt is characterized by marine taxa (e.g., *Cocconeis scutellum, C. costata)* common in coastal environments at or below MTL. This environmental interpretation is consistent with the pre-earthquake aerial imagery (Fig. 2.2a) that shows an active tidal channel connected with the lagoon in the seaward basin. Above contact A and continuing to 18 cm depth, the peat is characterized by a decrease in marine lagoon diatom species and an increase in brackish taxa (e.g., *Navicula subconcentrica, Nitzschia frustulum, Planothidium delicatulum*) and freshwater coastal lake taxa (e.g., *Tabellaria flocculosa),* consistent with a fall in RSL that cut off tidal communication to the lagoon and decreased its salinity. Over decades the lagoon continued to drain and freshen as shown by an increase, between 18-12 cm, in species consistent with a freshwater peat bog (e.g., *Pinnularia viridis, Eunotia incisa*) and freshwater muskeg (e.g., *Eunotia paludosa, E. curtagrunowii*). From 12 to 8 cm, the dominant diatom taxa are *E. intermedia* and *Chamaepinnularia spp*., freshwater species consistent with coastal muskeg environments above extreme tides showing the end result of compete draining of the lagoon and transition to a vegetated environment. UPGMA cluster and DCA analyses reflect the gradual diatom assemblage transition from marine lagoon to freshwater muskeg during the draining of the lagoon system (Fig. 2.5a, 2.6a).

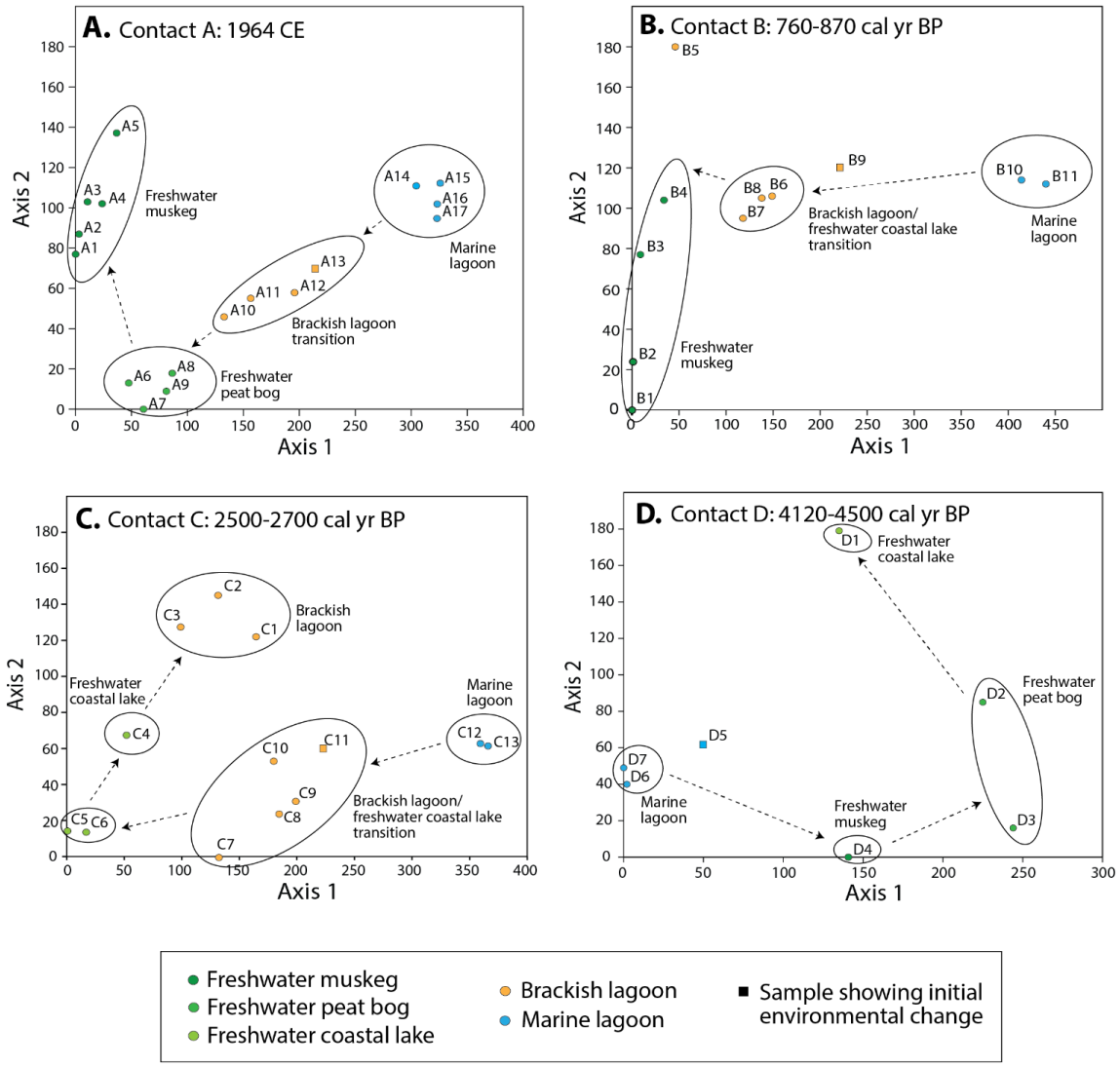

Figure 2.6. Results of detrended correspondence analysis (DCA) for a) Contact A (1964 CE) in core HL-10, b) Contact B (760-870 yr BP) in HL-27, c) Contact C (2500-2700 yr BP) in HL-22, and d) Contact D (4120-4500 yr BP) in HL-27. Samples that contain similar diatom assemblages and abundances are grouped together. Trend direction is indicated with dashed black arrows.

To confirm the age and depth of the 1964 CE earthquake contact we performed ^{137}Cs and ^{210}Pb analyses of the upper 25 cm of core HL-10 (Fig. 2.4). The downcore ^{210}Pb activity portrays an exponential decrease until approximately 18cm. Below this depth ^{210}Pb decreases rapidly. This rapid change in slope suggests a significant deposition change at approximately this depth, also evident in the CT scan. Assuming the CF:CS model (Corbett and Walsh, 2015) applies for the

younger portion of the core (0-18cm), this depth of transition (i.e., 18 cm) would correspond to circa 1966. A further constraint of age is the disappearance of excess (unsupported) ^{210}Pb at about 23 cm depth corresponding to circa 1900 CE. Although the highest ^{137}Cs activity measured was observed at this same depth, it is unclear if this truly represents the global maximum atmospheric ^{137}Cs deposition circa CE 1963 (Pennington et al., 1973) or if the true peak has been lost due to a sediment deposition transition. The summation of these results, although not definitive, implies an early 1960's age at the depth of 20-22cm.

2.3.2 Contact B: Rapid Emergence 760–870 cal yr BP

An earlier (760–870 cal yr BP) instance of coastal emergence is recorded in the landward basin at 132 cm depth (contact B) in core HL-27 (Fig. 2.5b). Here, a sharp stratigraphic contact separates silt from a 3-cm-thick fine to medium laminated sand. At 129 cm, the fine to medium sand is sharply overlain by a 7 -cm -thick, clean fine sand, which then gradually (over 1 cm) transitions into peat at 122 cm.

Clear shifts in diatom flora from marine to freshwater assemblages begin at 133 cm (1 cm below the obvious stratigraphic change) and continue across contact B (Fig. 2.5b). Below 133 cm, marine lagoon species (e.g., *C. costata*, *Surirella amphioxys*), common in coastal environments at or below MTL, dominate the silt. Between 132 cm and 133 cm, despite no change in sediment (silt), there is a nearly three-fold increase in brackish lagoon diatoms (e.g., *Tryblionella littoralis, Navicula salinarum*), signaling a fall in RSL that raised the lagoon out of the tidal frame and decreased its salinity. At 132 cm, there is a clear change in stratigraphy to fine to medium sand where brackish lagoon (e.g., *Navicula subconcentrica*, *Odontidium sp*.) and freshwater coastal lake (e.g., *Stauroforma exiguiformis, Fragilaria vaucheriae*) species are abundant. This assemblage,

which is consistent with freshening and draining of the lagoon, dominates the cleaner fine sand to 122 cm. In the peat above 122 cm, abundant freshwater muskeg species (e.g., *Eunotia spp*., *Pinnularia brebissonii*) common in coastal environments above MHHW signals the transition to a drier, vegetated freshwater environment. Despite contact B having a different stratigraphic signature compared to contact A, the gradual shift in diatom flora observed across contact B indicates RSL fall like that observed across contact A. We infer the sand unit above contact B represents fluvial deposits from the upland streams entering the lagoon from the east. UPGMA cluster and DCA analyses show a clear shift in fossil diatom assemblages starting 1 cm below contact B, with sample grouping reflecting a sudden shift from a marine lagoon to a brackish lagoon/freshwater lake, then transitioning to a freshwater muskeg environment (Fig. 2.5b, 2.6b).

Contact B also is preserved in the seaward basin as a stratigraphic peat-over-silt contact in cores 22 and 24 (Table 1, Fig. S1). However, the diatoms in the silt below the contact indicate a freshwater coastal lake (core 22) or freshwater peat bog (core 24) environment transitioning to a freshwater muskeg (core 22 and 24) environment following emergence. We infer that the transition from pre-emergence to post-emergence environment is muted because of the position of the core at the fringes of the seaward basin or that berm 3 prevented tidal exchange in the seaward basin (Fig. 2.3c, 2.3d).

2.3.3 Contact C: Rapid Emergence 2500–2700 cal yr BP

A peat-over-silt contact dated to 2500-2700 cal yr BP records coastal emergence in core HL-22 at 359 cm in the seaward basin (contact C; Fig. 2.5c). At 359 cm, there is a sharp contact between a silt and overlying a 1 -cm -thick organic-rich layer, and a sharp contact between the

organic layer and overlying 2 -cm -thick fine sand. At 356 cm, the fine sand gradually (over <1 cm) transitions upward to peat.

The first shifts in diatom flora begin at 360 cm (1 cm below the first obvious stratigraphic change) and remains consistent across the multiple stratigraphic changes. Below contact C marine lagoon taxa (e.g., *Paralia sulcate, C. scutellum*) common to coastal environments at or below MTL characterize the silt. At 360 cm, a centimeter below contact C, an abrupt decrease (>50%) in marine lagoon taxa and an abrupt increase in brackish (e.g., *Pinnunavis elegans, Amphora spp., Mastogloia smithii*) and freshwater coastal lake (e.g., *S. exiguiformis, Prestauroneis tumida*) species signal a sudden fall in RSL that signal reduced tidal communication to the lagoon. The fresh-brackish species, which are consistent with a freshening of the marine lagoon, remain abundant between 360-355 cm. Freshwater peat bog taxa (e.g., *Pinnularia interrupta, Pinnularia viridis*) increase in abundance between 355-350 cm representing a final transition to a drier, vegetated environment near MHHW. UPGMA cluster and DCA analyses show a clear shift in diatom assemblages starting 1 cm below contact C, with sample grouping reflecting a sudden shift from a marine lagoon to freshwater peat bog (Fig. 2.5c, 2.6c).

We note that contact C also is preserved in the landward basin as an organic-rich silt-over-silt contact in core HL-27 at 316 cm. The transition in diatom species begins at 318 cm, at least 2 cm below the stratigraphic contact (Fig. S7). The diatom species in the silt below the contact from 320-318 cm are dominated by brackish-marine lagoon species (e.g., *C. costata*, *Tabularia fasciculata*, *Rhoicosphenia abbreviata*). At 318 cm, there is a shift in diatom flora signaled by a slight decrease in marine lagoon species (e.g., *Cocconeis scutellum*) and a slight increase in brackish lagoon species (e.g., *Navicula subconcentrica*). The flora transitions to freshwater coastal lake species (e.g., *Stauroforma exiguiformis, Prestauroneis sp.*; Table 1) at 317 cm and stays

consistent through 313 cm. We take the absence of freshwater peat bog and muskeg diatom species to indicate the conversion of a brackish-marine lagoon to a freshwater coastal lake. We infer this environmental change reflects abrupt RSL fall which restricted tidal communication to the lagoon leading to the formation of a freshwater lake impounded by coastal landforms.

2.3.4 Contact D: Rapid Emergence 4120–4500 cal yr BP

A sharp peat-over-silt contact dated to 4120–4500 cal yr BP records the oldest evidence for coastal emergence in core HL-27 at 373 cm in the landward basin (contact D; Fig. 2.5d).

We observed slight changes in the diatom flora starting at 374 cm (1 cm below the stratigraphic contact). Between 376-374 cm, the silt is dominated by marine lagoon taxa (e.g., *Cocconeis costata*, *Cocconeis scutellum*, *Tabularia fasciculata)* common in coastal environments at or below MTL. At 374 cm there is a slight decrease in marine lagoon species and an abrupt increase in freshwater coastal lake species (e.g., *S. exiguiformis*) signaling a shift in the diatom flora just before the stratigraphic contact. Above the contact the diatom community continues to shift to freshwater diatom taxa with a significant increase of overall freshwater species abundance between 373-369 cm consistent with a draining and freshening lagoon. The diatom communities suggest that the environment first developed as a freshwater muskeg (e.g., *Eunotia spp.*) at 373 cm before shifting to a wetter freshwater environment with the increase in peat bog species (e.g., *Pinnularia viridis, Eunotia incisa*), and eventually a freshwater coastal lake with the appearance of common shallow freshwater species (e.g., *Stauroforma exiguiformis, Aulacoseira sp., Tabellaria flocculosa)* at 369 cm. We interpret these data as evidence for emergence of the coastline and subsequent sudden restriction of the landward lagoon by berm 3 which cuts off the lagoon from tidal communication. UPGMA cluster and DCA analyses show a slight shift in diatom

assemblages 1 cm below contact D, with sample groupings reflecting the shift from marine lagoon to freshwater environments (Fig. 2.5d, 2.6d).

2.3.5 Evidence for an Additional Emergence Event?

There is limited evidence for one additional emergence contact that is recorded in the seaward basin as a silt-over-silt contact at ~161 cm in core HL-22, between contacts B and C (Fig. 2.3c, d, S1). We identify the contact based on the presence of fossil marine bivalve shells below the contact and the absence of shells above the contact. We did not collect core samples across this contact and as a result we do not have the detailed diatom evidence that we do across other contacts. However, using available cores, we assess that the environmental transition is not detectable using diatoms because the silt below the contact (~315-317 cm) is dominated by marine species (e.g., *Cocconeis scutellum, Tabularia fasciculata*) and the silt above the contact (~140-143 cm) remains dominated by the same marine flora. The presence of marine bivalves suggests a previous intertidal zone that has been uplifted, but exact estimates are unresolvable. With limited stratigraphic data it is difficult to assess if there is another contact that could be present. We also note that while the silt at ~140 cm in HL-22 is characterized as a marine environment, the silt just below contact B at 121 cm in the same core is characterized as a freshwater coastal lake environment, suggesting that an ecological and/or geomorphological shift occurred in the time represented by ~20 cm of sediment (Table 1).

Table 1. Diatom summary and interpretation for each Hidden Lagoons uplift contact.

Stratigraphy	Sample depth* (cm)	Freshwater muskeg (%**)	Freshwater peat bog (%**)	Freshwater lake (%**)	Brackish lagoon (%**)	Marine lagoon (%**)	Inferred paleo-environment***	Prominent species
HL-10 contact A (1964 CE)								
PEAT	8-9	49.76	19.71	16.35	1.68	3.37	Drained lagoon - freshwater muskeg	*Chamaepinnularia soehrensis, Eunotia paludosa, E. intermedia, Pinnularia gibba, P. microstauron*
	9-10	49.64	15.57	14.84	1.95	4.14		
	10-11	48.80	13.46	15.14	3.37	5.53		
	11-12	46.19	11.32	15.70	5.54	6.00		
	12-13	48.51	9.61	20.59	3.66	7.09		
	13-14	28.47	16.47	32.00	8.47	8.24	Freshwater coastal lake	*Tabellaria flocculosa, Nitzschia frustulum*
	14-15	25.96	11.30	30.77	10.10	9.38		
	15-16	15.70	19.24	24.81	16.46	13.42		
	16-17	14.00	20.64	22.36	21.87	9.09		
	17-18	7.23	7.51	33.53	23.99	15.03	Brackish lagoon-freshwater coastal lake	*Navicula subconcentrica, Nitzschia linearis, Planothidium delicatulum, Stauroforma exiguiformis*
	18-19	7.63	9.81	20.44	22.34	25.61		
	19-20	3.41	7.74	20.43	21.98	34.06		
	20-21	6.42	2.75	12.54	19.88	41.90		
ORG. SILT	21-22	2.42	1.81	10.57	7.25	56.50	Marine lagoon	*Cocconeis scutellum, C. costata, Tabularia fasciculata*
	22-23	0.93	0.93	7.17	8.72	67.60		
	23-24	0.98	0.65	4.89	10.10	69.06		
	24-25	0.32	0.63	4.75	7.59	71.52		
HL-22 contact B (760-870 cal yr BP)								
PEAT	113-114	3.94	30.61	22.12	13.94	8.79	Drained lagoon - peat bog / freshwater muskeg	*Pinnularia sp., P. viridis, Eunotia diadema, E. incisa, Fragilariforma constricta*
	114-115	11.59	54.27	16.77	4.57	3.96		
	115-116	11.11	60.49	17.28	1.23	3.09		
	116-117	11.18	51.36	14.50	5.44	5.44		
	117-118	5.15	33.03	23.64	8.79	6.67		
	118-119	3.18	28.35	39.81	8.92	8.28		
	119-120	6.48	17.60	40.12	12.35	8.33		
	120-121	3.98	10.40	71.25	6.42	1.22	Freshwater coastal lake	*Stauroforma exiguiformis, Tabellaria flocculosa, Rossithidium pussilum*
SILT	121-122	5.66	10.38	66.36	8.49	2.20		
	122-123	3.26	8.30	53.41	11.57	3.56		
	123-124	4.64	3.48	59.13	15.07	3.19		
	124-125	4.31	5.23	55.38	9.23	1.54		
SILT	140-141	0.33	0.00	0.66	24.42	56.44	Marine Lagoon	*Cocconeis scutellum, Tabularia fasciculata*
	142-143	0.00	0.00	3.64	25.50	60.60		
HL-24 contact B (760-870 cal yr BP)								
PEAT	95-96	64.82	15.64	4.89	1.63	0.33	Drained lagoon - freshwater muskeg	*Pinnularia borealis, Eunotia curtgrunowii, E. horstii*
	96-97	73.20	9.15	10.13	0.98	0.00		
	97-98	68.08	11.73	9.45	2.28	0.33		
	98-99	19.74	53.95	8.22	4.61	1.64	Freshening lagoon-Freshwater peat bog	*Pinnularia nodosa, P. subcapitata, P. viridis*
SILT	99-100	13.91	46.36	15.89	1.32	2.65		
	100-101	4.62	32.34	20.13	7.26	8.91		
	101-102	9.27	20.86	18.54	11.59	15.89	Marine lagoon-Freshwater peat bog?	*Diploneis didyma, Cocconeis scutellum, Pinnularia viridis*
	102-103	3.99	22.59	8.64	10.30	23.92		
HL-27 contact B (760-870 cal yr BP)								
PEAT	119-120	26.32	17.43	29.61	6.58	0.99	Shallow to dry freshwater environment	*Pinnularia brebissonii* (appears only above the sand), *P. viridis , Eunotia macroglossa , Stauroforma exiguiformis*
	120-121	32.12	13.91	26.16	8.61	1.66		
	121-122	26.37	13.18	31.51	11.58	0.96		
	122-123	18.09	10.53	36.18	11.18	3.29	Freshwater lake	*Stauroforma exiguiformis*
SAND	123-124	8.22	8.22	26.32	29.93	3.29	Brackish lagoon - freshwater coastal lake	*Stauroforma exiguiformis, Staurosira construens var. venter, Nitzschia obtusa, Hippodonta hungarica, Amphora sp.*
	127-128	1.64	0.66	36.39	33.77	3.61		
	129-130	3.91	4.56	35.18	24.76	2.61		
	131-132	2.58	1.29	31.61	43.55	3.55		
SILT	132-133	0.97	1.29	11.61	65.16	7.74	Brackish lagoon	*Tryblionella littoralis, Navicula salinarum*
	133-134	0.33	0.33	1.97	27.30	55.26	Marine lagoon	*Thalassionema nitzschioides, Cocconeis costata, Surirella amphioxys*
	134-135	0.33	0.00	0.00	22.70	57.57		

Stratigraphy	Sample depth* (cm)	Freshwater muskeg (%**)	Freshwater peat bog (%**)	Freshwater lake (%**)	Brackish lagoon (%**)	Marine lagoon (%**)	Inferred paleo-environment***	Prominent species
HL-22 contact C (2500-2700 cal yr BP)								
ORG. SILT	314-315	0.29	0.29	4.13	31.26	49.26	Brackish-marine lagoon	*Tryblionella hungarica, Cocconeis scutellum*
	315-316	0.00	0.32	4.55	43.18	38.64		
PEAT	347-348	0.48	1.92	30.53	41.59	16.11	Brackish lagoon-freshwater lake	*Mastogloia smithii, Pinnunavis elegans, Stauroforma exiguiformis*
	348-349	0.46	4.87	33.18	49.88	2.78		
	349-350	1.79	8.93	43.75	25.89	7.74	Freshwater peat bog or coastal lake	*Staurosira construnes var. exigua, Aulacoseira sp., Pinnularia viridis*
	351-352	10.18	18.55	42.22	10.78	1.20		
	353-354	8.83	16.23	61.58	1.43	1.91		
	354-355	6.04	10.23	65.09	3.94	0.79		
SAND	355-356	2.11	6.33	45.91	25.07	10.29	Freshwater lake-brackish lagoon	*Stauroforma exiguiformis, Pinnunavis elegans*
	356-357	0.23	0.23	36.99	40.41	13.01		
	357-358	0.00	0.00	40.88	34.31	15.82		
ORG. SILT	358-359	0.00	0.96	37.83	47.95	6.99	Brackish lagoon-freshwater lake	*Stauroforma exiguiformis, Mastogloia smithii, Pinnunavis elegans*
SILT	359-360	0.00	0.24	35.35	31.23	26.88		
	360-361	0.00	0.31	8.05	12.69	70.28	Marine lagoon	*Paralia sulcata, Cocconeis scutellum*
	361-362	0.00	0.60	7.23	15.36	71.39		
HL-27 contact C (2500-2700 cal yr BP)								
ORG. SILT	313-314	0.00	0.00	58.22	15.46	2.30	Freshwater coastal lake	*Stauroforma exiguiformis*
	314-315	0.00	0.00	60.51	17.83	3.50		
	315-316	0.00	0.00	52.27	21.75	3.90		
SILT	316-317	0.00	0.00	39.54	25.16	10.78		
	317-318	0.00	0.00	18.36	43.28	18.36	Brackish lagoon	*Navicula subconcentrica*
	318-319	0.00	0.00	6.82	39.29	35.39	Brackish-marine lagoon	*Cocconeis scutellum , C. costata , Tabularia fasciculata, Navicula sp.*
	319-320	0.00	0.00	15.74	32.46	24.92		
HL-27 contact D (4120-4500 cal yr BP)								
PEAT	369-370	4.09	12.58	43.40	9.75	6.92	Freshwater lake	*Stauroforma exiguiformis* and *Aulacoseira sp.*
	370-371	5.90	51.29	17.34	7.01	4.43	Freshwater peat bog	*Pinnularia viridis* and *Pinnularia subcapitata*
	371-372	31.79	46.36	3.97	3.31	2.98		
	372-373	36.75	9.93	12.58	9.27	15.56	Freshwater muskeg	*Eunotia naegelii* and *E. praerupta*
SILT	373-374	5.98	6.64	8.97	23.92	36.54	Marine lagoon	*Cocconeis costata, C. scutellum, Tabularia fasciculata*
	374-375	1.98	1.32	3.96	22.77	48.51		
	375-376	0.33	2.33	5.32	20.93	50.83		
HL-24 (Between contacts B and C)								
ORG. SILT	137-138	0.50	0.50	1.00	17.00	76.00	Marine lagoon	*Cocconeis costata, C. scutellum, Gyrosigma sp., Tabularia fasciculata*
	140-141	0.00	0.66	0.33	13.20	79.87		
	143-144	0.00	0.00	0.33	10.96	82.06		
	149-150	0.00	0.00	0.99	17.82	71.28		
	155-156	0.00	0.00	1.32	22.85	68.21		
	161-162	0.00	0.33	0.99	26.64	60.86		
	167-168	0.66	0.33	4.95	32.67	47.85	Brackish-marine lagoon	*Tryblionella hungarica, Cocconeis scutellum, Rhoicosphenia abbreviata*
	173-174	0.65	0.33	6.19	29.64	48.21		
	176-177	3.96	1.32	17.82	19.80	32.67		
PEAT	185-186	3.96	37.29	31.02	4.62	9.57	Freshwater peat bog	*Pinnularia viridis*

* Permanent diatom slides were prepared

** Only species that exceed 2% abundance are included in summary ecological groups.

*** For ecological classifications and paleoenvironmental interpretations, see supplemental information

2.4 DISCUSSION

2.4.1 Evidence for Coseismic Uplift at Hidden Lagoons

Geomorphic, stratigraphic, and fossil diatom evidence supports a history of four instances of sudden coseismic uplift of Hidden Lagoons over the past 4,200 years (1964 CE, 750-870 cal yr BP, 2500-2700 cal yr BP, and 4120-4500 cal yr BP). We base our interpretation on criteria established by Nelson et al. (1996), Hemphill-Haley (1996), and Shennan et al. (2016) that help discriminate seismic vs. non-seismic (e.g., localized or gradual sea-level changes) origins for sharp (1-3 mm) stratigraphic contacts in coastal environments. Indicators of sudden coseismic land-level change include: (1) continuous lateral extent of contacts, (2) sharpness and suddenness of the contact, (3) significant and sustained environmental change (microfossil analysis) across contacts, and (4) synchronicity with other regional sites/earthquake history. All contacts recorded at Hidden Lagoons are laterally continuous over 100-200 meters within and between the landward and seaward basins, and they display relatively sudden stratigraphic change indicating sudden RSL fall consistent with coastal uplift. Fossil diatoms across the stratigraphic contacts shift from an environment at or below MTL to an environment above the reach of extreme tides indicating significant and sustained land-level change. Guided by these criteria, we infer that the sharp peat-over-silt and sand-over-silt stratigraphic contacts at Hidden Lagoons formed due to sudden, coseismic uplift.

We note that fossil diatom assemblages display a sudden decrease in marine species and an increase in fresh-brackish species at or below stratigraphic contacts A, B, C, and D. Because the microfossils often signal an ecological change before the sedimentological change, we infer that the timing of uplift is recorded by the diatom assemblage shift before the sedimentary

response. This inference is supported by the UPGMA cluster and DCA analyses, which show a clear shift in fossil diatom assemblage composition beginning 1-2-cm below contacts B, C, and D (Fig. 2.5, 2.6). We assume that this is a direct reflection of diatoms responding to the change in environment first followed by the sedimentary shift within the following year(s), hence, shifts in diatoms more precisely record earthquake-induced uplift than do sedimentological changes that may lag sedimentary response. The sensitivity of diatoms to sudden environmental changes is supported by a study simulating sudden RSL change along the Oregon coast that showed diatoms respond to abrupt change in an environment within at least 2 weeks after a sudden change in the frequency of tidal inundation (i.e., change in salinity; Horton et al. (2017).

2.4.2 Estimating Coseismic Uplift at Hidden Lagoons

Based on the ecological shifts observed in diatom assemblages across each contact, we can constrain the amount of coseismic uplift that occurred. Diatom assemblages across contacts A, B, C, and D indicate a shift between an environment at or below MTL, to an environment above extreme tides (i.e., storm tides or king tides). In the context of the 3.4 m (MHHW-MLLW) tidal range at Hidden Lagoons, this environmental shift corresponds to a minimum of ~3 m of coseismic uplift. Our estimates are minimums because diatom assemblages that commonly live at or below MTL, like those we observed in pre-earthquake silt units, are similar and thus cannot precisely resolve elevations below MTL. The upper range of our coseismic uplift estimate is constrained by the freshwater diatoms we observed in post-earthquake sediments that indicate an environment above the reach of extreme tides. Regional tide gauge records show the 50% annual exceedance probability level, the likelihood that water levels will exceed a given elevation, for extreme tides is 2.9 m above MTL (based on data for Seward, AK;

https://tidesandcurrents.noaa.gov/est/stickdiagram.shtml?stnid=9455090). Thus, we infer a minimum change from an environment at MTL, to an environment ~3 m above MTL across contacts A, B, C, and D.

We can further inform our estimates of coseismic uplift by placing the evidence into the context of Plafker's (1969) observation of 3.7–4.3 m of uplift near Hidden Lagoons in 1964, and by considering the current elevation of contact A (4.2 m above MTL). Although our minimum estimates can only resolve ~3 m of coseismic RSL change, we infer that the diatom shift observed across contact A represents the environmental shift that 4.2 m of uplift produces at Hidden Lagoons. Widespread environmental changes observed through fossil diatoms across contacts B, C, and D are comparable to contact A and we estimate coseismic uplift associated with each prehistoric contact to reflect a similar amount of uplift based on the similar fossil diatom transitions. Through this framework, we suggest that contacts B, C and D likely also record changes in depositional environment reflecting >3 m of coseismic uplift.

2.4.3 Evidence for Repeated, Combined Rupture of the Megathrust and Patton Bay Splay Fault System

Over the past ~4,200 years there have been at least eight megathrust earthquakes along the eastern AASZ (Shennan et al., 2014), four of which (including the 1964 CE earthquake) overlap with the timing of coseismic uplift events preserved at Hidden Lagoons (Fig. 2.7, Table 2). Here, we consider whether evidence at Hidden Lagoons represents combined megathrust and splay fault slip, or if there is evidence for megathrust- or splay fault-only slip.

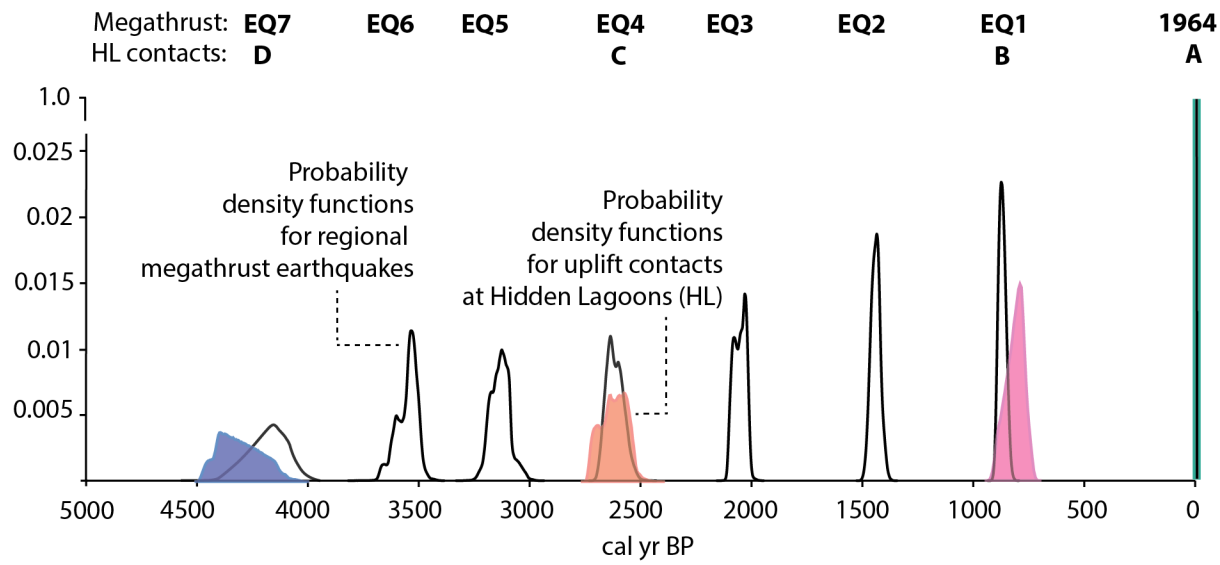

Figure 2.7. Graph showing probability density functions for Hidden Lagoons earthquake contacts (colored) relative to those for eastern AASZ earthquakes (black) determined by Shennan et. al. (2016).

Slip on the splay fault system during the 1964 CE earthquake increased the amount of coastal uplift on Montague Island relative to regional uplift attributable to megathrust slip alone. Based on the distance of Montague Island from the trench (~150 km), other coastal areas in the zone of tectonic uplift but away from splay faults that activated in 1964 were raised between 1-3 m (Plafker, 1965). However, the distinct, widespread peat-over-silt contact records a greater amount (3.7–4.3 m) of uplift that Plafker (1969) observed near Hidden Lagoons following the combined rupture of the megathrust and splay faults. Considering the similarity in the fossil diatom transitions across contact A and contacts B, C, and D, we infer that the three prehistoric earthquake contacts preserved at Hidden Lagoons may also be the result of greater uplift due to combined megathrust and splay fault slip compared to shorelines along-strike to Montague Island.

Longer-term evidence for repeated activation of the splay fault system comes from bathymetric and seismic surveys of offshore splay faults, and thermochronology data from Montague Island. Liberty et al. (2019) interpreted high-resolution bathymetric and seismic

reflection data as indicating simultaneous rupture of the splay fault system and megathrust during 20–30 Holocene earthquakes in western PWS. Thermochronology data reveal spatial patterns of rapid and focused exhumation on Montague Island in the hanging wall of the splay fault system within the past 5 Ma that mimics coseismic uplift in the 1964 CE earthquake (Haeussler et al., 2015). These observations suggest that repeated 1964-style combined megathrust-splay fault rupture patterns have been sustained over many millennia and bring context to the earthquake evidence at Hidden Lagoons.

We interpret the earthquake record at Hidden Lagoons to represent repeated instances of 1964-style combined ruptures, where our evidence for exaggerated uplift overlaps with roughly every other or every couple of megathrust earthquakes over the past 4,200 years. Our interpretation relies on three crucial observations: 1) combined megathrust-splay fault slip occurred during the 1964 earthquake and created 3.7-4.3 m of uplift at Hidden Lagoons; 2) the inferred prehistoric splay fault earthquakes at Hidden Lagoons overlap, within less than a century, of megathrust earthquakes on the eastern AASZ and; 3) diatoms across all prehistoric contacts (B, C, and D) reflect ecological shifts consistent with >3 m of uplift, similar to the fossil diatom transitions across the 1964 earthquake contact. We note, however, that the uncertainties in radiocarbon age estimates for the individual megathrust and inferred splay fault earthquakes are broad enough that Montague Island splay faults may have ruptured independently of the megathrust within a century. Therefore, we cannot rule out the possibility that our contacts at Hidden Lagoons represent independent splay fault ruptures that occur close in time with megathrust earthquakes.

We develop a conceptual model of shoreline response to the earthquake deformation cycle on Montague Island (Fig. 2.8). Prior to 4120–4500 cal yr BP, interseismic subsidence allowed berm 3 to grow which provided a seaward barrier for a basin to form and silt to accumulate in a

shallow lagoon. At the time, the shoreline occupied the seaward flank of berm 4, which now backs the landward Hidden Lagoon basin. Fossil diatoms across contact D at Hidden Lagoons imply a sudden change from a marine to freshwater environment around 4,300 years ago, which we interpret as uplift produced by megathrust-splay fault rupture beneath Montague Island. Following uplift, the lagoon drained, freshwater peat accumulated above the lagoon sediment, and the seaward-displaced shoreline formed west of berm 3. Over several centuries following earthquake D, interseismic subsidence caused RSL to rise gradually allowing berm 2 to form. Rising tides reentered the newly formed seaward basin and flooded it with sea water and silt. Fossil diatoms across contact C indicate that the environment suddenly shifted again from a marine to a brackish lagoon ~2500-2700 years ago which we interpret to reflect combined megathrust-splay fault rupture that again raised Hidden Lagoons. Following uplift, the basin accumulated peat and organic-rich silt above the drained lagoon sediment. Centuries following earthquake C, interseismic subsidence caused gradual RSL rise and flooding of the lagoons once again. Interseismic subsidence between earthquakes C and B in the seaward basin is recorded in core HL-24 as a gradual change from freshwater peat bog to marine lagoon over ~40 cm (Fig. 2.3d, Table 1, Fig. S1, S8). Fossil diatoms across contact B infer a sudden shift from marine lagoon to freshwater muskeg environment which we interpret to reflect splay fault rupture that raised the lagoons around 760-870 years ago. Following earthquake B, renewed interseismic subsidence led to the continued growth of berm 2, which grew in height and width over more than eight centuries. Subsidence was great enough during this period to flood part of the seaward basin via the tidal channel at Hidden Lagoons based on pre-1964 (contact A) earthquake aerial photography. Finally, contact A was formed during the rupture of the splay fault system in conjunction with the 1964 Great Alaska Earthquake which uplifted Hidden Lagoons 3.7–4.3 m, reconfigured the shoreline, and slowly drained the seaward lagoon.

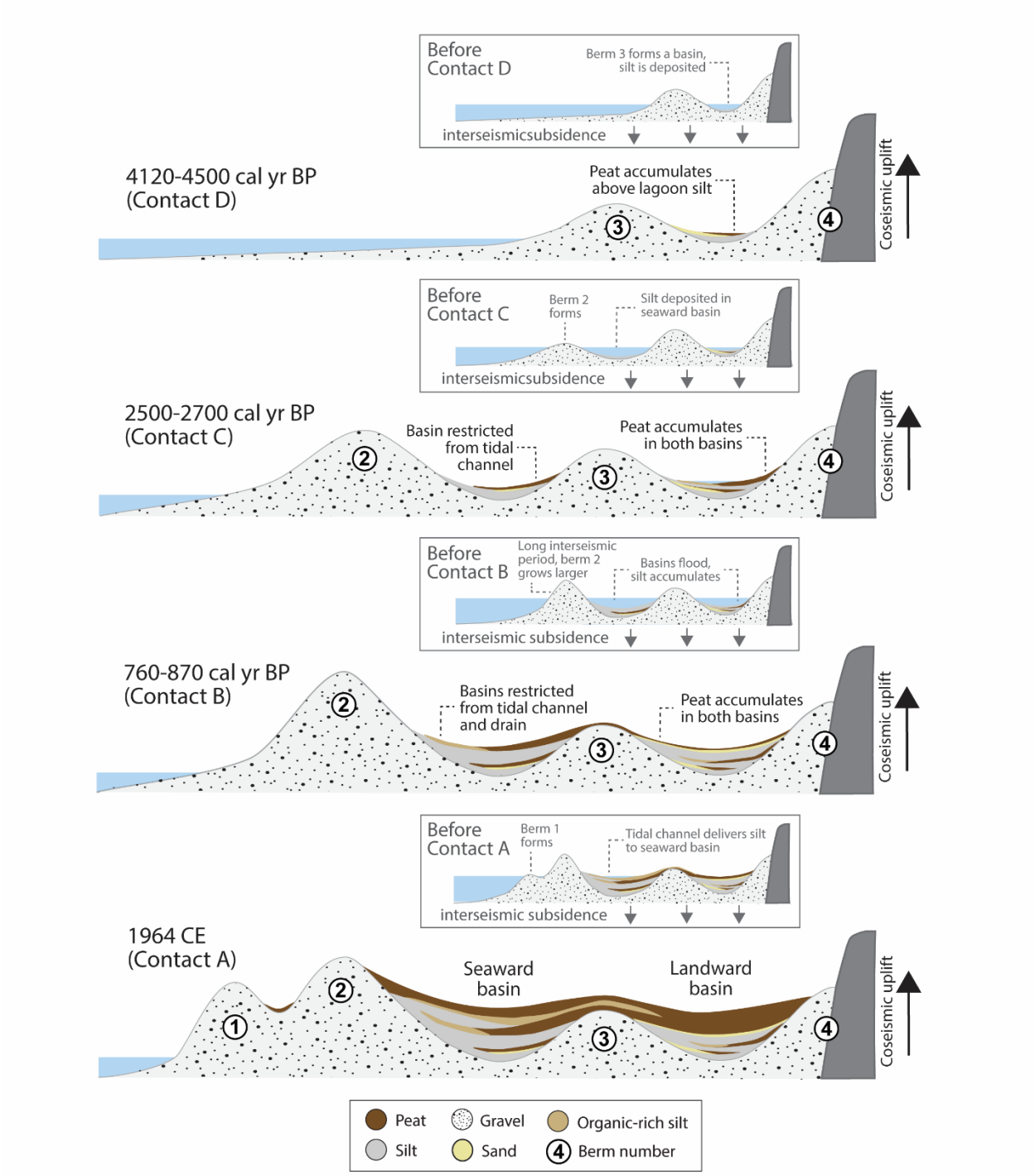

Figure 2.8. Schematic showing the geomorphological changes to the seaward and landward basins at Hidden Lagoons during and between major earthquakes (Contacts A-D).

If we infer all the contacts preserved at Hidden Lagoons record combined megathrust and splay fault ruptures, then where is evidence for the off-interval megathrust ruptures preserved? Does Hidden Lagoons site record megathrust-only events? It is possible that the missing megathrust earthquakes did not trigger the splay fault system, thus not enough displacement was created at Hidden Lagoons to raise marine lagoon environments out of the reach of tides and produce a distinct change in stratigraphy and diatom assemblages. We note only one instance of possible megathrust-only rupture in the Hidden Lagoons stratigraphy between contacts B and C where we observe a shift in bivalve presence across a silt-silt contact suggesting a fall in RSL (i.e., coseismic uplift). The magnitude of the change was not sufficient to produce a peat-over-silt contact, suggesting relatively less (<3 m) uplift than the other earthquakes recorded. We lack precise age constraints of this RSL shift, but given adjacent stratigraphic constraints, we speculate that the change may coincide with a megathrust rupture in ~1,440 or ~2,052 cal yr BP (Shennan et al., 2014).

2.5 CONCLUSION

Based on our observations at Hidden Lagoons, we suggest that rupture of the splay fault system is closely timed with four megathrust earthquakes on the AASZ, but not every great earthquake in PWS. The evidence further suggests that the splay faults may be rupturing in conjunction with megathrust slip. Shennan et al. (2014) provides a history of megathrust ruptures along the eastern AASZ with a mean recurrence interval of ~535 (419-883) years (Fig. 2.7). Earthquakes recorded at Hidden Lagoons, inferred to represent splay fault ruptures, recur every ~1030 years on average, which suggests that the splay fault system may rupture jointly with the megathrust every other or every couple of megathrust earthquakes. As the 1964 earthquake demonstrated, slip on the splay fault system can contribute to tsunamis generated during

megathrust earthquakes and thus enhance the tsunami hazards along coastlines in south-central Alaska.

Our record at Hidden Lagoons indicates that the eastern AASZ has the potential to produce 1964-style, combined megathrust-splay fault ruptures and may produce similar rupture patterns in the future, highlighting the need to understand the rupture dynamics of combined megathrust-splay fault rupture and the hazards associated with it (Liberty et al., 2019). Communities adjacent to subduction zones with similar splay fault structures (e.g., Cascadia, Ecuador, Chile) also may need to consider the tsunami potential when developing hazard maps. The record of splay fault ruptures at Hidden Lagoons provides data to improve hazard assessments in south-central Alaska that consider the tsunami potential with 1964-style combined megathrust-splay fault ruptures.

2.6 ACKNOWLEDGMENTS

The U.S. Geological Survey Earthquake Hazards Program supported field work for JMD, RCW, PJH, AB, and JHC, radiocarbon analysis, and student contract for JMD.

We would like to thank Captain Paul Tate of the USGS vessel *R/V Alaskan Gyre* and Marguerite Leoni for her assistance in the field. We would also like to thank SeanPaul La Selle (USGS) for providing the CT scans for our cores and Eileen Hemphill-Haley (USGS) for her discussions of Montague Island diatom results and providing an initial review.

REFERENCE CITED

Blewitt, G., and Hammond, W., 2018, Harnessing the GPS data explosion for interdisciplinary science: Eos, v. 99.

Briggs, R.W., Engelhart, S.E., Nelson, A.R., Dura, T., Kemp, A.C., Haeussler, P.J., Corbett, D.R., Angster, S.J., and Bradley, L.-A., 2014, Uplift and subsidence reveal a nonpersistent megathrust rupture boundary (Sitkinak Island, Alaska): Geophysical Research Letters, v. 41, p. 2289–2296, doi:10.1002/2014GL059380.Received.

Brocher, J., 2014, Qualitative and quantitative evaluation of two new histogram limiting binarization algorithms: Int. J. Image Process, v. 8, p. 30–48.

Bronk Ramsey, C., 2009, Bayesian analysis of radiocarbon dates: Radiocarbon, v. 51, p. 337–360.

Bronk Ramsey, C., 2021, OxCal v4. 4.4: Available at: Retrieved from https://c14. arch. ox. ac. uk/oxcal. html,.

Collot, J.Y., Agudelo, W., Ribodetti, A., and Marcaillou, B., 2008, Origin of a crustal splay fault and its relation to the seismogenic zone and underplating at the erosional north Ecuador-south Colombia oceanic margin: Journal of Geophysical Research: Solid Earth, v. 113, p. 1–19, doi:10.1029/2008JB005691.

Corbett, D.R., and Walsh, J.P., 2015, 210Lead and137Cesium: Establishing a chronology for the last century: Handbook of Sea-Level Research, p. 361–372, doi:10.1002/9781118452547.ch24.

Denys, L., 1991, A check-list of the diatoms in the Holocene deposits of the western Beligan coastal plain with a survey of their apparent ecological requirements:

DePaolis, J.M. and Witter, R.C., 2023, Diatom data from coastal environments on Montague Island, Alaska: U.S. Geological Survey data release

Dura, T., and Hemphill-Haley, E., 2020, Diatoms in tsunami deposits, *in* Geologic Records of Tsunamis and Other Extreme Waves, p. 291–322.

Dura, T., Hemphill-Haley, E., Sawai, Y., and Horton, B.P., 2016, The application of diatoms to reconstruct the history of subduction zone earthquakes and tsunamis: Earth-Science Reviews, v. 152, p. 181–197, doi:10.1016/j.earscirev.2015.11.017.

Dura, T., Horton, B.P., Cisternas, M., Ely, L.L., Hong, I., Nelson, A.R., Wesson, R.L., Pilarczyk, J.E., Parnell, A.C., and Nikitina, D., 2017, Subduction zone slip variability during the last millennium, south-central Chile: Quaternary Science Reviews, v. 175, p. 112–137, doi:10.1016/j.quascirev.2017.08.023.

Guiry, M.D., Guiry, G.M., Morrison, L., Rindi, F., Miranda, S.V., Mathieson, A.C., Parker, B.C., Langangen, A., John, D.M., and Bárbara, I., 2014, AlgaeBase: an on-line resource for algae: Cryptogamie, Algologie, v. 35, p. 105–115.

Hamilton, S., and Shennan, I., 2005, Late Holocene great earthquakes and relative sea-level change at Kenai, southern Alaska: Journal of Quaternary Science, v. 20, p. 95–111, doi:10.1002/jqs.903.

Hammer, Ø., 2020, PAST paleontological statistics v. 4.03: Reference Manual. Oslo: University of Oslo,.

Han, S., Bangs, N.L., Carbotte, S.M., Saffer, D.M., and Gibson, J.C., 2017, Links between sediment consolidation and Cascadia megathrust slip behaviour: Nature Geoscience, v. 10, p. 954–959, doi:10.1038/s41561-017-0007-2.

Hemphill-Haley, E., 1996, Diatoms as an aid in identifying late-Holocene tsunami deposits: The Holocene, v. 6, p. 439–448, doi:10.1177/095968369600600406.

Kodaira, S., Kurashimo, E., Park, J.O., Takahashi, N., Nakanishi, A., Miura, S., Iwasaki, T., Hirata, N., Ito, K., and Kaneda, Y., 2002, Structural factors controlling the rupture process

of a megathrust earthquake at the Nankai trough seismogenic zone: Geophysical Journal International, v. 149, p. 815–835, doi:10.1046/j.1365-246X.2002.01691.x.

Lemke, R., 1967, Effects of the earthquake of March 27, 1964 at Seward, Alaska: Geological Survey Professional Paper, v. 542-E, p. 53.

Lescak, E.A., Bassham, S.L., Catchen, J., Gelmond, O., Sherbick, M.L., Von Hippel, F.A., and Cresko, W.A., 2015, Evolution of stickleback in 50 years on earthquake-uplifted islands: Proceedings of the National Academy of Sciences, v. 112, p. E7204–E7212, doi:10.1073/pnas.1512020112.

Liberty, L.M., Brothers, D.S., and Haeussler, P.J., 2019, Tsunamigenic splay faults imply a long-term asperity in southern Prince William Sound, Alaska: Geophysical Research Letters, doi:10.1029/2018gl081528.

Lienkaemper, J.J., and Bronk Ramsey, C., 2009, OxCal: Versatile tool for developing paleoearthquake chronologies—A primer: Seismological Research Letters, v. 80, p. 431–434.

Melnick, D., Moreno, M., Motagh, M., Cisternas, M., and Wesson, R.L., 2012, Splay fault slip during the Mw 8.8 2010 Maule Chile earthquake: Geology, v. 40, p. 251–254, doi:10.1130/g32712.1.

Nelson, A.R., Briggs, R.W., Dura, T., Engelhart, S.E., Gelfenbaum, G., Bradley, L.A., Forman, S.L., Vane, C.H., and Kelley, K.A., 2015a, Tsunami recurrence in the eastern Alaska-Aleutian arc: A Holocene stratigraphic record from Chirikof Island, Alaska: Geosphere, v. 11, p. 1172–1203, doi:10.1130/GES01108.1.

Nelson, A.R., Briggs, R.W., Dura, T., Engelhart, S.E., Gelfenbaum, G., Bradley, L.A., Forman, S.L., Vane, C.H., and Kelley, K.A., 2015b, Tsunami recurrence in the eastern Alaska-Aleutian arc: A Holocene stratigraphic record from Chirikof Island, Alaska: Geosphere, v.

11, p. 1172–1203, doi:10.1130/GES01108.1.

Nelson, A.R., Jennings, A.E., and Kashima, K., 1996, An earthquake history derived from stratigraphic and microfossil evidence of relative sea-level change at Coos Bay, southern coastal Oregon: GSA Bulletin, v. 108, p. 141–154, doi:10.1130/0016-7606(1996)108.

Park, J.O., Tsuru, T., Kodaira, S., Cummins, P.R., and Kaneda, Y., 2002, Splay fault branching along the Nankai subduction zone: Science, v. 297, p. 1157–1160, doi:10.1126/science.1074111.

Pennington, W., Tutin, T.G., Cambray, R.S., and Fisher, E.M., 1973, Observations on lake sediments using fallout 137Cs as a tracer: Nature, v. 242, p. 324–326.

Plafker, G., 1967, Surface faults on Montague Island associated with the 1964 Alaska earthquake: U. S. Geological Survey Professional Paper, p. 1–42.

Plafker, G., 1965, Tectonic Deformation Associated with the 1964 Alaska Earthquake: Science, v. 148, p. 1675–1687.

Plafker, G., 1969, Tectonics of the March 27, 1964 Alaska Earthquake: US Geological Survey Professional Paper,.

Reimer, P.J., Austin, W.E.N., Bard, E., Bayliss, A., Blackwell, P.G., Ramsey, C.B., Butzin, M., Cheng, H., Edwards, R.L., and Friedrich, M., 2020, The IntCal20 Northern Hemisphere radiocarbon age calibration curve (0–55 cal kBP): Radiocarbon, v. 62, p. 725–757.

Sawai, Y., Horton, B.P., Kemp, A.C., Hawkes, A.D., Nagumo, T., and Nelson, A.R., 2016, Relationships between diatoms and tidal environments in Oregon and Washington, USA: Diatom Research, v. 31, p. 17–38, doi:10.1080/0269249X.2015.1126359.

Shennan, I., Bruhn, R., Barlow, N., Good, K., and Hocking, E., 2014, Late Holocene great earthquakes in the eastern part of the Aleutian megathrust: Quaternary Science Reviews, v. 84, p. 86–97, doi:10.1016/j.quascirev.2013.11.010.

Shennan, I., Garrett, E., and Barlow, N., 2016, Detection limits of tidal-wetland sequences to identify variable rupture modes of megathrust earthquakes: Quaternary Science Reviews, v. 150, p. 1–30, doi:10.1016/j.quascirev.2016.08.003.

Shennan, I., Long, A.J., Rutherford, M.M., Innes, J.B., Green, F.M., and Walker, K.J., 1998, TIDAL MARSH STRATIGRAPHY, SEA-LEVEL CHANGE AND LARGE EARTHQUAKES—II: SUBMERGENCE EVENTS DURING THE LAST 3500 YEARS AT NETARTS BAY, OREGON, USA: Quaternary Science Reviews, v. 17, p. 365–393, doi:10.1016/s0277-3791(97)00055-3.

Spaulding, S.A., Potapova, M.G., Bishop, I.W., Lee, S.S., Gasperak, T.S., Jovanoska, E., Furey, P.C., and Edlund, M.B., 2021, Diatoms. org: supporting taxonomists, connecting communities: Diatom Research, v. 36, p. 291–304.

Suleimani, E., and Freymueller, J.T., 2020, Near-field modeling of the 1964 Alaska tsunami: The role of splay faults and horizontal displacements: Journal of Geophysical Research: Solid Earth, v. 125, p. e2020JB019620.

Troels-Smith, J., 1955, Characterization of unconsolidated sediments:, doi:10.1163/_q3_SIM_00374.

Vancouver, G., 1801, A voyage of discovery to the North Pacific Ocean: And round the world: J. Stockdale, v. 5.

Vos, P.C., and de Wolf, H., 1993, Diatoms as a tool for reconstructing sedimentary environments in coastal wetlands; methodological aspects: Hydrobiologia, v. 269–270, p. 285–296, doi:10.1007/BF00028027.

Wilson, B.W., and Tørum, A., 1972, Runup heights of the major tsunami on North American coasts in The Great Alaska Earthquake of 1964: Oceanography and Coastal Engineering: NAS Pub, v. 1605, p. 158–180.

Witter, R.C., Kelsey, H.M., and Hemphill-Haley, E., 2003, Great Cascadia earthquakes and tsunamis of the past 6700 years, Coquille River estuary, southern coastal Oregon: Bulletin of the Geological Society of America, v. 115, p. 1289–1306, doi:10.1130/B25189.1.

Witter, R. C., LeWinter, A., Filiano, D. L., Haeussler, P. J. and Bender, A. M., 2020, Airborne lidar-based digital elevation models of coastal Montague Island (Alaska) acquired September 2018: U.S. Geological Survey data release, https://doi.org/10.5066/P9FLQROT

Witter, R.C., Bender, A.M., DePaolis, J.M., 2023, Radiocarbon data from coastal environments on Montague Island, Alaska: U.S. Geological Survey data release, https://doi.org/10.5066/P9OSRE0J

Chapter 3: Determining the source of lacustrine turbidites using diatoms (Ozette Lake, Washington, USA)

Jessica M. DePaolis[1], Tina Dura[1], Daniel Brothers[2], Drake Singleton[2], Brian Sherrod[3]

[1]*Department of Geosciences, Virginia Polytechnic Institute and State University, Blacksburg, VA, USA*
[2]*United State Geological Survey, Pacific Coastal and Marine Science Center, Santa Cruz, CA, USA*
[3]*United States Geological Survey, Earthquake Science Center, University of Washington, Seattle, WA, USA*

ABSTRACT

Offshore turbidites and onshore tidal wetland stratigraphy have provided exceptional geologic records of great (M_w >8.5) earthquakes along the Cascadia subduction zone (CSZ). However, a limited onshore tidal wetland record of past earthquakes and tsunamis in the northern CSZ leaves questions about the spatial and temporal variability of past events along the entire megathrust boundary. Coastal lakes located in the northern CSZ may provide a more complete picture of past megathrust earthquakes since earthquake magnitude thresholds for generating depositional signatures in lakes are typically lower (MMI ~5.5) than other environments (e.g., coastal marshes).

Ozette Lake, located on the coastal rim of the Olympic Peninsula in northern Washington state, preserves >30 Holocene subaqueous mass transport deposits (turbidites) inferred to represent seismic-induced deposition over ~14,000 years. However, questions about whether sedimentary and geophysical characteristics alone can distinguish between seismic- and climate-induced deposition remain. Diatoms, a type of siliceous microalgae, preserved within lacustrine sediments may act as bioindicators for turbidite origin (i.e., seismic versus climatic). Here, we explore the grain size and diatom signature across the youngest six turbidites emplaced over a ~3,000-year period to address questions about source mechanism. Results suggest diatoms record distinctly

different signatures during seismic- and climate-induced deposition in Ozette Lake, even in cores where grain size analysis does not clearly show turbidites. We conclude that diatoms are a viable proxy for distinguishing the sediment origin and source mechanism of lacustrine turbidites, adding a valuable tool to onshore paleoseismic studies.

3.1 INTRODUCTION

The Cascadia subduction zone (CSZ), a 1,100 km margin stretching from northern Vancouver Island, British Columbia to northern California, has not generated a great (M_w >8.5) earthquake since the last rupture on January 26, 1700 (estimated M8.5-9.0; Nelson et al., 1995). The lack of modern or historic earthquakes along the CSZ has created interest in using onshore and offshore geologic records to understand the recurrence and spatial correlation of earthquakes along the boundary. Offshore turbidite records document up to 19 great earthquakes at the CSZ over the last 10,000 years (Goldfinger, 2011; Walton, Staisch et al., 2021). Of the 19 inferred great earthquakes along the margin, 12 of them are recorded in onshore tidal marsh stratigraphy. However, most onshore evidence is concentrated in the central and southern CSZ (Oregon) where records extend thousands of years longer than the northern CSZ (Washington state and Canada) making it difficult to corroborate offshore evidence with the onshore record. The challenge of spatially and temporally correlating onshore and offshore records between the southern and northern CSZ leaves questions about the recurrence of great earthquakes along the entire CSZ margin.

An additional onshore sedimentary archive that can be used to expand the spatial and temporal range of northern CSZ earthquake records is coastal lakes. Coastal lakes are sensitive depositional environments that can provide continuous, long-term records of seismically-induced environmental changes that can be preserved as chemical, ecological, and sedimentological

evidence (Sabatier et al., 2022). Lake studies around the world have used primary (e.g., tsunami inundation and deposition or direct fault displacement) and/or secondary (e.g., seismically-induced subaqueous or subaerial slope failure) evidence to reconstruct regional earthquake recurrence history and intensity (Moernaut et al., 2014; Praet et al., 2017; Van Daele et al., 2019; Molenaar et al., 2021; Oswald et al., 2021; Brothers et al., 2022). Secondary evidence of regional seismicity often appears as widespread turbidite layers interrupting the usually fine-grained (silt/clay) deep lake sediments (Strasser et al., 2007; Sabatier et al., 2022). However, climate-induced processes (e.g., hydrologically-induced subaerial landslides, flooding during storms or rapid snowmelt, etc.) may also produce turbidites, emplacing resuspended benthic and/or onshore terrestrial material into deeper lake settings (Osleger et al., 2009; Smith et al., 2019; Praet et al., 2020; Vandekerkhove et al., 2020). Differentiating seismic- and climate-induced lake deposition can be a challenge, especially when relying only on sedimentological and subsurface imaging of lake stratigraphy, leading to potential over- or under-interpretations of prehistoric earthquake recurrence. Therefore, it is crucial to have an additional proxy that will enhance existing criteria to be able to differentiate deposit origins.

Diatoms, a type of siliceous microalgae common in lake environments that are sensitive to specific lake conditions (e.g., lake depth, vegetation, substrate) have been successfully applied in tsunami lake studies (e.g., Kelsey et al., 2005) and to differentiate intra-lake versus extreme event deposits (e.g., Orpin et al., 2010). However, diatoms have not been broadly applied to lacustrine paleoseismology studies, providing an opportunity to develop a new proxy for testing inferences of the sediment origin and source mechanism (i.e., seismic versus climate) of lacustrine turbidites.

Here, we use grain size and diatom analysis to explore the sediment origin and source mechanism of a series of six inferred seismic-induced lacustrine turbidites emplaced over a ~3,000-year history at Ozette Lake, Washington (Brothers at al., in review). We first characterize

the grain size and diatom signature of modern source sediments (e.g., river, delta, shallow lake, and deep lake depositional environments) and develop a conceptual model for the signature of seismic-induced versus climate-induced turbidites in the lake. Then, using this framework, we link turbidites to their likely modern source sediment based on their grain size and diatom composition. Our results suggest that diatoms record a distinct signature during seismic-induced deposition as compared to climate-induced flooding events, even in cores where grain size analysis does not clearly show turbidites. We conclude that diatoms are a viable proxy for distinguishing the sediment origin and source mechanism of lacustrine turbidites, adding a valuable tool to onshore paleoseismic studies.

3.2 BACKGROUND

3.2.1 Lacustrine paleoseismology at subduction zones

Lacustrine paleoseismology has been an effective tool along subduction zones spanning Alaska to Chile to examine and expand subduction and intraslab earthquake chronologies (e.g., Morey et al., 2013; Moernaut et al., 2017; Van Daele et al., 2019; Praet et al., 2020; Vandekerkhove et al., 2020; Singleton et al., 2023). However, the differentiation between seismic- and climate-induced turbidites has been a challenge since both mechanisms may produce thick, coarse, and widespread deposition in the form of turbidites or other mass transport deposition in lake settings (Sabatier et al., 2022). Grain size has been established as being a key proxy for differentiating source mechanism where some variation in the depositional process may be reflected in the sedimentology (Jenny et al., 2014; Sabatier et al., 2022). In Eklutna Lake, a varved, proglacial lake in Alaska, Vandekerkhove et al. (2020) found that historical floods created turbidites with very similar macroscopic appearance to the seismic-induced turbidites, but

discussed that flood-induced deposition displays a more gradual transition from the coarse base towards the top of the turbidites compared to seismic-induced turbidites which display an exponential-type transition from coarser basal sediment to fine cap sediment (Arnaud et al., 2002; Beck, 2009; Boes et al., 2018; Praet et al., 2020; Sabatier et al., 2022). They also found that a coarser grain size and more erosive basal contact may be indicative of a higher peak flow velocity more common in seismic-induced deposition compared to floods (Mulder et al., 2003; Talling, 2014; Vandekerkhove et al., 2020). Additionally, flood deposition was determined to be more evenly spread over the lake compared to the locally thick seismic-induced deposition (Vandekerkhove et al., 2020).

Paleoseismic studies have been implemented on Vancouver Island (Adams, 1996; López, 2012) and in Washington state (Karlin and Abella, 1996; Karlin et al., 2004; Leithold et al., 2018, 2019; Vo, 2018; Brothers et al., in review) along the northern CSZ in an effort to develop longer subduction zone earthquake chronologies to fill spatial and temporal gaps. High-resolution subsurface mapping with seismic profiles, detailed coring, and sedimentary characteristics have been used to recognize seismic- versus climate-induced deposition in a number of these studies (Karlin et al., 2004; Vo, 2018; Slajus, 2020). Studies farther inland (Karlin et al., 2004; Leithold et al., 2018b, 2019; Vo, 2018) record subduction zone earthquakes and intraslab earthquakes, creating records that are necessary for paleoseismology, but that cloud our understanding of subduction zone earthquake recurrence. Ozette Lake, located much closer to the coast and inferred to record only subduction zone earthquakes, may provide a unique opportunity to use diatom-based methods to develop an additional proxy that may enhance our criteria for differentiating seismic- versus climate-induced deposition (Brothers et al., in review).

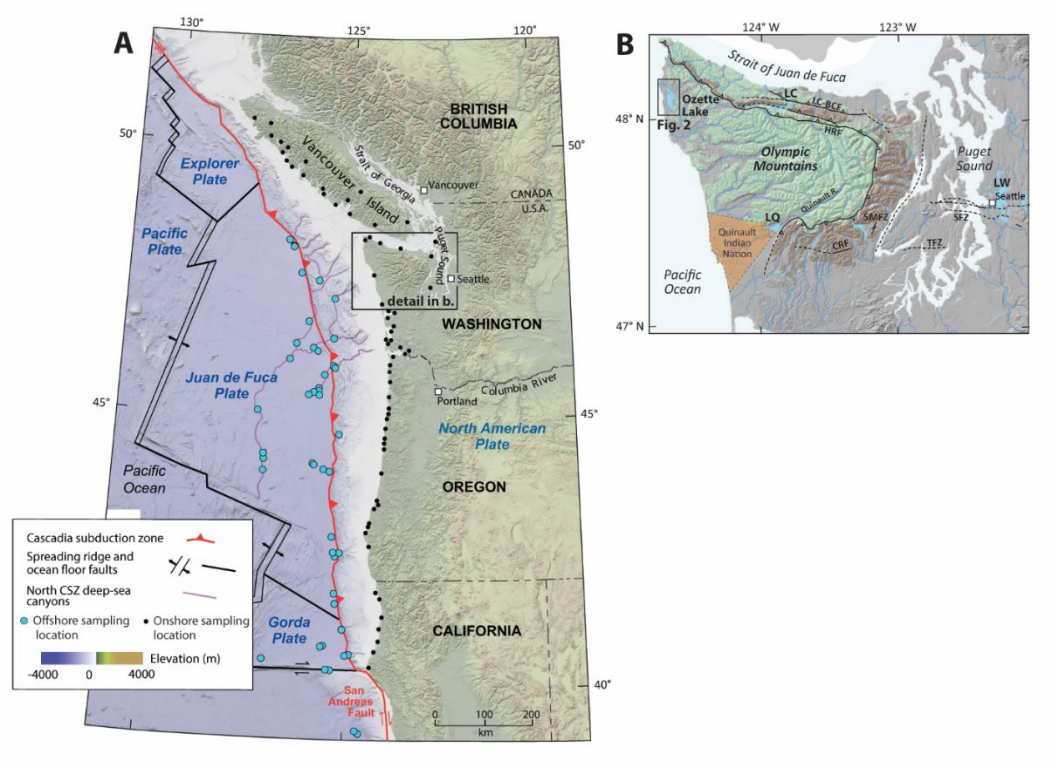

Figure 3.1. a) Regional and tectonic setting above the Cascadia subduction zone from Nelson et al. (2021). b) Olympic Peninsula marked with the Quaternary crustal faults (CRF = Canyon River Fault; SMFZ = Saddle Mountain Fault Zone; TFZ = Tacoma Fault Zone; SFZ = Seattle Fault Zone; HRF = Hurricane Ridge Fault; LC-BCF = Lake Creek-Boundary Creek Fault) and regional lakes with paleoseismic studies (LC = Lake Crescent; LQ = Lake Quinault; LW = Lake Washington). The location of Ozette Lake is marked with a black rectangle (details in Figure 2). Figure from Smith et al. (2019).

3.2.2 Ozette Lake setting and previous work

Ozette Lake is located ~1 km from the Pacific coast of the Olympic Peninsula of Washington state where it is sensitive to shaking caused by great earthquakes on the CSZ, but too far-field for smaller regional and local intraslab and deep crustal earthquakes (Wirth et al., 2021; Fig. 3.1). Brothers et al. (in review) distinguishes three depositional basins (northern, proximal, and distal) within Ozette Lake (Fig. 3.2). The northern basin is a shallow depositional basin towards the far north arm of the lake. The rest of the lake is divided in between the proximal (eastern) and distal (western) depositional basins divided by a subaqueous ridge that runs north to

south through the center of the lake (Fig. 3.2). Maximum depths reach ~100 m in the proximal basin (Ritchie and Bourgeois, 2009). Sediment accumulation rates are ~1 mm/yr between ~2,800 yrs ago and ~1960 CE when rates increased nearly 8-fold due to the increase in logging in the surrounding watersheds (Ritchie and Bourgeois, 2009). Mean water surface elevation is 10.4 m above MSL with a max range of ~3.4 m (Ritchie and Bourgeois 2009). There are four fluvial inflow points with delta formation – Umbrella Creek, Crooked Creek, Big River, and Siwash Creek – which are all feeding in through the north and east coastlines of the lake. Ozette River is the sole outflow located at the northernmost end of the lake and flows northwest to the Pacific Ocean (Ritchie and Bourgeois 2009).

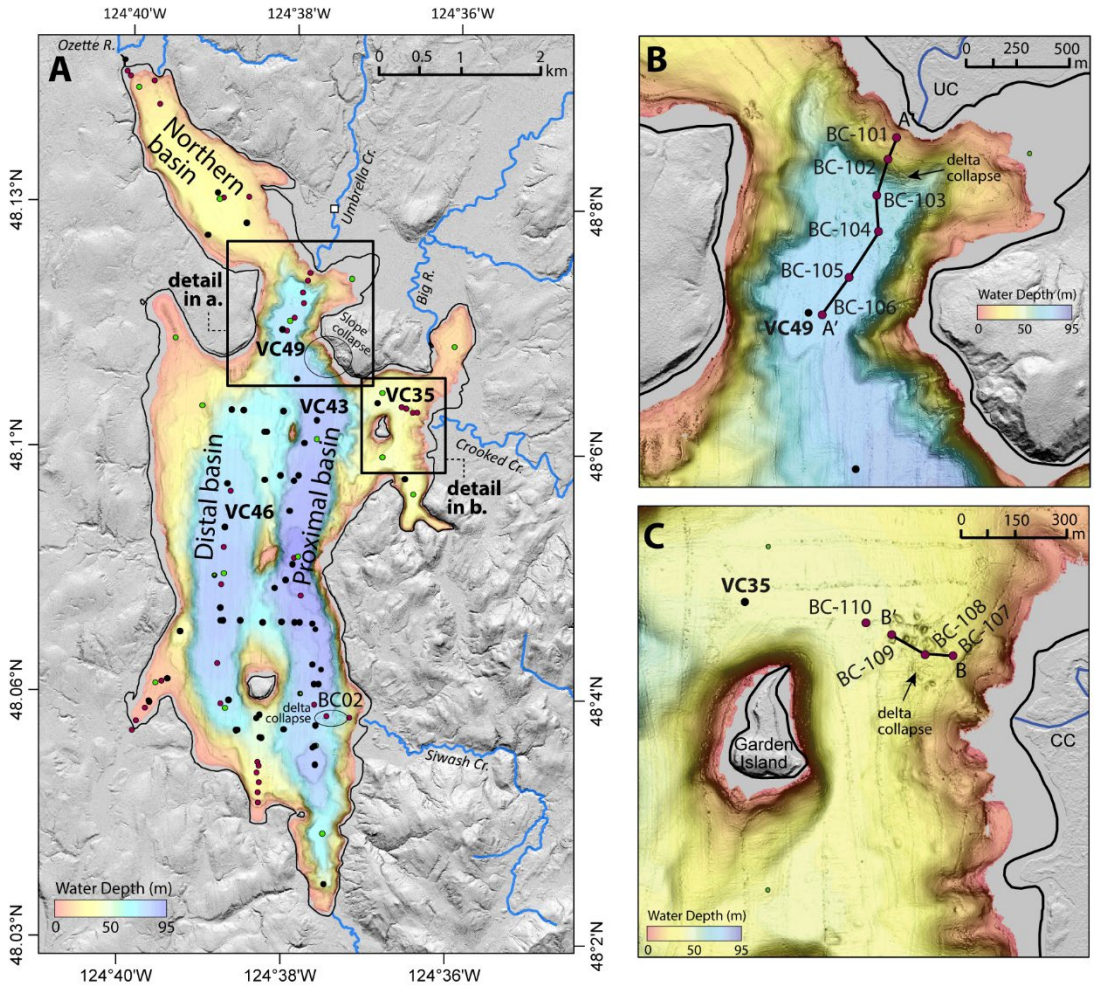

Figure 3.2. a) High-resolution bathymetric map of Ozette Lake with vibracore (black cirlces), short gravity cores (maroon circles), and cores aquired by Ritchie and Bourgeois (2009) (green

circles). White square indicates location of modern creek sample. b, c) Core sampling locations along the Umbrella Creek delta (A-A') and the Crooked Creek delta (B-B').

Geophysical and stratigraphic mapping of Ozette Lake stratigraphy, core sampling, and sedimentologic analysis was completed over two sampling expeditions led by researchers at the United States Geological Survey (USGS) with detailed methods described in Brothers et al. (in review). Dense grids of sub-bottom Chirp (Compressed High-Intensity Radiated Pulse), multibeam bathymetry, and seismic reflection survey profiles were collected to provide wide-spread surface and subsurface characterization. Short (1-2 m) gravity cores, intermediate (2-5 m) vibracores, and deep (10-20 m) vibracores acquired using a Uwitch platform were collected throughout the lake to map the subsurface and sample for grain size, radiocarbon, and fossil diatoms. Brothers et al. (in review) observe a total of 30-34 coarse-grained turbidites in Ozette Lake representing ~14,000 years of depositional history. All turbidites appear in the sub-bottom Chirp profiles as high amplitude reflections across two sub-basins and >5 km. The turbidites are thickest near their inferred sediment source, the Umbrella Creek Delta, and thin and fine away from the delta. Based on sedimentological characteristics and criteria developed by Vanderkerkhove et al. (2020), Brothers et al. (in review) infer the turbidites to be seismic-induced correlating 11 of the 12 turbidites in their study to local and regional onshore earthquake records. However, the interpretation hinges on broader scale turbidite characteristics like thinning and fining from the inferred sediment source, and the increase in basal grain size in turbidites proximal to the inferred sediment source. Because climate-induced turbidites could display similar characteristics that a climate-induced turbidite could display. Could climate-induced events from Umbrella Creek produce sediment deposition in the form of widespread turbidites? Are there multiple sediment sources for the distal basin turbidites?

3.3 APPROACH AND METHODS

Brothers et al. (in review) characterize the main sediment source of the inferred seismic-induced turbidites in Ozette Lake as the Umbrella Creek delta. To test this interpretation, and evaluate possible climate-induced deposition, we conducted high-resolution diatom and grain size analysis on a variety of samples from potential sediment sources within the lake and surrounding environment, and from samples below, within, and above the turbidites. We collected modern sediment samples during a field campaign in summer 2019. Samples from inferred turbidites were collected from archive cores VC49, VC43, VC46 stored at USGS Pacific Coastal and Marine Science Center, and described in Brothers et al. (in review). We analyzed a total of 11 samples from potential modern sediment sources within the lake and surrounding environment and 136 samples from below, within, and above the turbidites.

3.3.1 Diatoms as a proxy for reconstructing turbidite source at Ozette Lake

Diatoms are a photosynthetic, unicellular microalgae that inhabit freshwater, brackish, and marine environments. Diatoms create elaborate siliceous shells (valves) ranging in size from ~5 μm to ~200 μm that are resistant to degradation from dissolution and abrasion from transport (Dura et al., 2016). Diatoms are a valuable tool in reconstructing paleoenvironmental changes in lake environments because of their sensitivity to environmental factors including pH, water depth, substrate (i.e., mud, sand, vegetation, rock, etc.) and nutrient supply (Potapova and Charles, 2007; Pilarczyk et al., 2014). During long-term sediment accumulation within lake basins, diatoms settle in the stratigraphic layers and reflect the changes in environmental conditions through time. During a disturbance that produces rapid sediment accumulation (i.e., earthquake-induced slope failure or climate-induced flooding), diatoms are entrained in the allochthonous sediments that are carried and deposited throughout the deeper lake setting and may provide evidence for sediment origin.

To characterize the diatom signature of the modern environments in Ozette Lake, we collected modern shallow grab samples from the inlet (Umbrella Creek) and the top centimeter of shallow lake cores within the Umbrella Creek (A-A') and Crooked Creek (B-B') deltas (Fig. 3.2, Fig. S1). Detailed grain size and diatom analyses were conducted to capture the signature (i.e., diatom species abundances, sediment size, etc.) of potential source sediment to compare to downcore turbidites.

We explored the grain size and diatom signature of inferred seismic-induced turbidites in three lake basin cores (VC49, VC43, VC46) that are in proximal, intermediate, and distal locations, respectively, relative to the inferred Umbrella Creek Delta sediment source (Fig. 3.3). Core VC49 contains two inferred turbidites, core VC43 contains five inferred turbidites, and core VC46 contains five inferred turbidites. We sampled below, within, and above the turbidites in cores VC49, VC43, VC46 at 1- to 2-cm resolution to document changes in grain size and fossil diatoms. We also analyzed turbidites documented in core VC35 which represents potential seismic-induced deposition at shallower depths (Fig. S2). We followed the methods of Dura and Hemphill-Haley (2020) and pretreated sediment samples with hydrogen peroxide (30% concentration) to remove organic material. Diatoms were identified to the species level with a minimum of 300 valves counted in 147 samples. We used global diatom ecological classifications (Krammer and Lange-Bertalot, 1988; Vos and de Wolf, 1993; Spaulding et al., 2021) to group species that exceeded 1% of the total diatoms counted into two main ecological groups (planktonic and benthic). **Planktonic** diatom species float within the water column and are common in deeper water where they can maintain depths in the photic zone (Fig. S3). **Benthic** diatom species live within or just above the water-sediment interface and are therefore constrained to shallower water depths where light can penetrate to the lake floor. Within the benthic category, we further defined three ecological subgroups (shallow lake benthic, delta, and terrestrial). The **shallow lake benthic subgroup**

diatom species are found in high abundance in both shallow and deep lake settings, as well as within background lake sediments (Fig. S4). The **delta subgroup** is associated with higher grain size and intermediate water depths on creek deltas but is absent or found in very low abundance in the creeks (Fig. S5). This includes epipsammic (live attached to sand grains) and specific epipelic (live attached to or within finer sediments) species that favor the delta conditions. The **terrestrial subgroup** contains diatoms commonly found in onshore and creek settings (Fig. S6). This includes a higher abundance of aerophilic (resistant to drier environments) and epiphytic (live attached to vegetation) species.

To establish the diatom assemblage present in background lake conditions (i.e., between turbidite disturbances), we average the percent abundance of the diatoms present in each ecological group in samples below turbidites in each core. The average background diatom abundances are calculated for each individual core because the background lake diatom assemblages vary slightly due to their location within the lake. We avoid incorporating samples above turbidites in the average due to the potential lasting environmental change in the lake following a widespread disturbance.

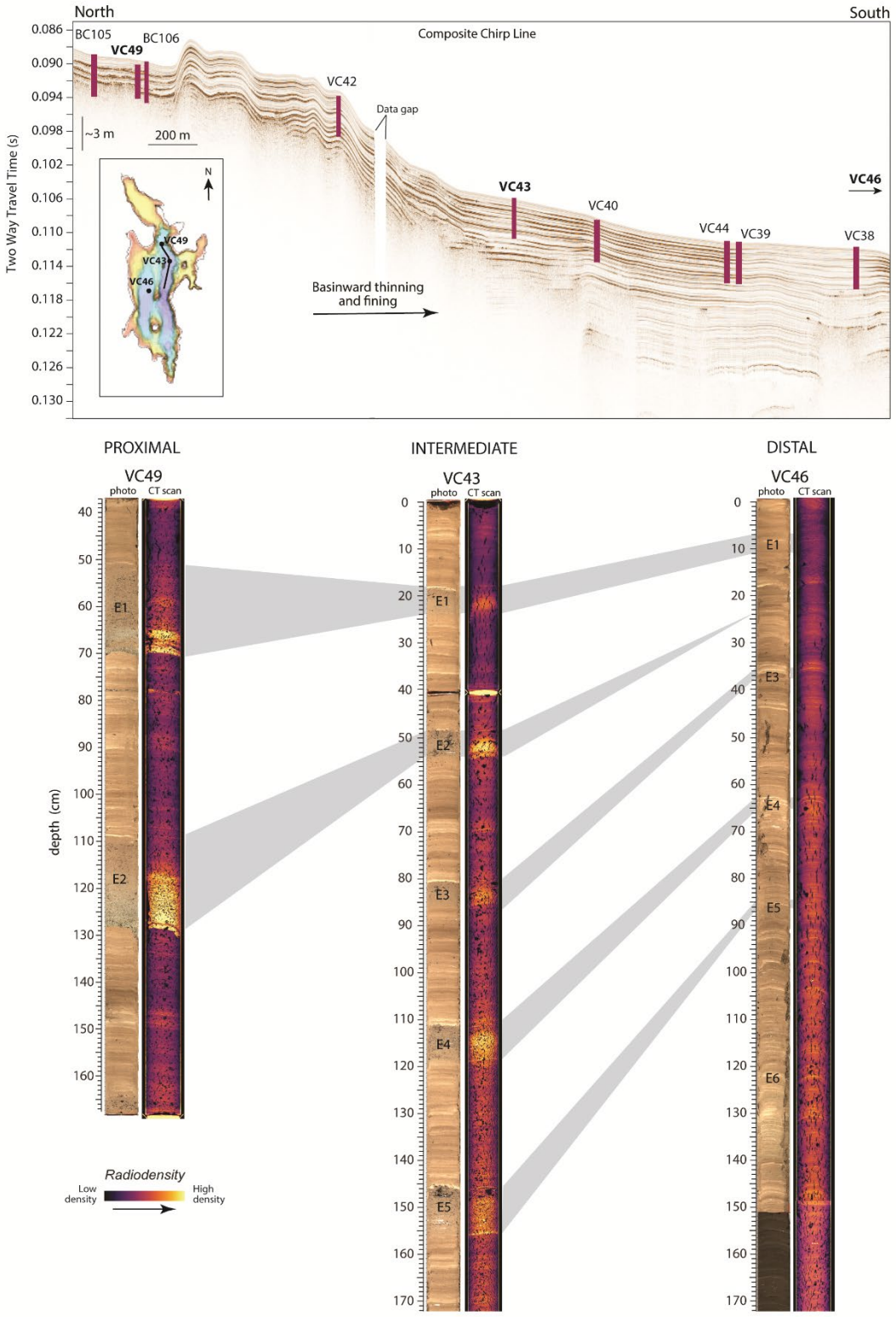

Figure 3.3. Composite Chirp transect through the northern Ozette Lake proximal basin. Cores VC49, VC43, and VC46 represent proximal, intermediate, and distal locations, respectfully, from the Umbrella Creek delta. Turbidite layers sampled for this study are labeled E1-E6.

3.3.2 Grain size analysis

We pretreated sediment samples with hydrogen peroxide (30% concentration) to remove organic material prior to conducting grain size analysis. We characterized the grain size of each modern sample, turbidite, and background sediment with high-resolution (i.e., 1-cm) grain size analysis using a Malvern Mastersizer 3000 laser-particle size analyzer equipped with a Hydro LV (large volume) module for wet sample dispersion and analysis. Each sample was analyzed three consecutive times and averaged to provide one representative grain size result per sample. We calculated sample statistics using the GRADISTAT statistical software package (Blott and Pye, 2001) and used Wentworth classification mean and median (D50) results (in phi) to characterize the background and turbidite sediment (Table 1).

We plot grain size as a function of depth to study the evolution of grain size through the depositional process as standard for sedimentological analysis (Vandekerkhove et al., 2020; Sabatier et al., 2022). Brothers et al. (in review) provide detailed, high-resolution grain size statistics for E1 and E2 in VC49 and examine the grain size transition with depth. We build on this data and provide similar high-resolution grain size for the intermediate and distal turbidites for comparison.

3.4 RESULTS

3.4.1 Potential Turbidite Source Sediment

3.4.1.1 Umbrella Creek modern samples

A grab sample (1-2-cm of surface sediment) was collected from a shallow point bar of Umbrella Creek about 1 km up-creek of the inlet (Fig 3.2, Fig. S7). The modern creek sediment is composed of medium to coarse sand (estimated mean = ~1 φ; D50 = ~1 φ) with a diatom

assemblage that has a high abundance (91%) and high diversity (16 species) of benthic species and a low abundance (2%) and low diversity (2 species) of planktonic species. The terrestrial subgroup species are the most abundant in this sample comprising ~52% of the benthic species followed by the shallow lake benthic subgroup comprising ~37%, and <3% categorized as delta subgroup species (Fig. 4; Table 1).

We establish a set of diatom species that represent the terrestrial subgroup ecology based on their presence and abundance within the creek, but absence or low abundance in lake samples. The species include *Achnanthidium spp*., *Cocconeis placentula, Gomphonema spp., Encyonema silesiacum,* and *Fragilaria vaucheriae* (Table 3.2). These species are used to calculate the terrestrial subgroup abundance in all study samples.

3.4.1.2 Umbrella Creek and Crooked Creek delta transects

The Umbrella Creek delta transect (A-A') runs from the inlet mouth of Umbrella Creek at BC101 south to BC106 (Fig. 3.2b). Umbrella Creek is a major inlet into Ozette Lake with sub-bottom Chirp profiles showing evidence of continual accumulation and progradation of a prominent subaqueous delta south into the basin (Fig. 3.2a). The length of the cores along the transect range between ~85-130 cm. The top centimeter of each core was used to represent modern sediment and diatom assemblage distribution from shallow to deeper lake. The sediment at BC101 is composed of fine sand (mean = 3.32 φ; D50 = 3.02 φ) which transitions to coarse silt (mean = 5.22 φ; D50 = 4.91 φ) at BC102 and to medium silt (mean = 6.36 φ; D50 = 6.43 φ) at BC106, consistent with a creek distributing coarser sediment closest to the inlet and finer sediment further into the lake during floods (Fig. 3.4; Table 1).

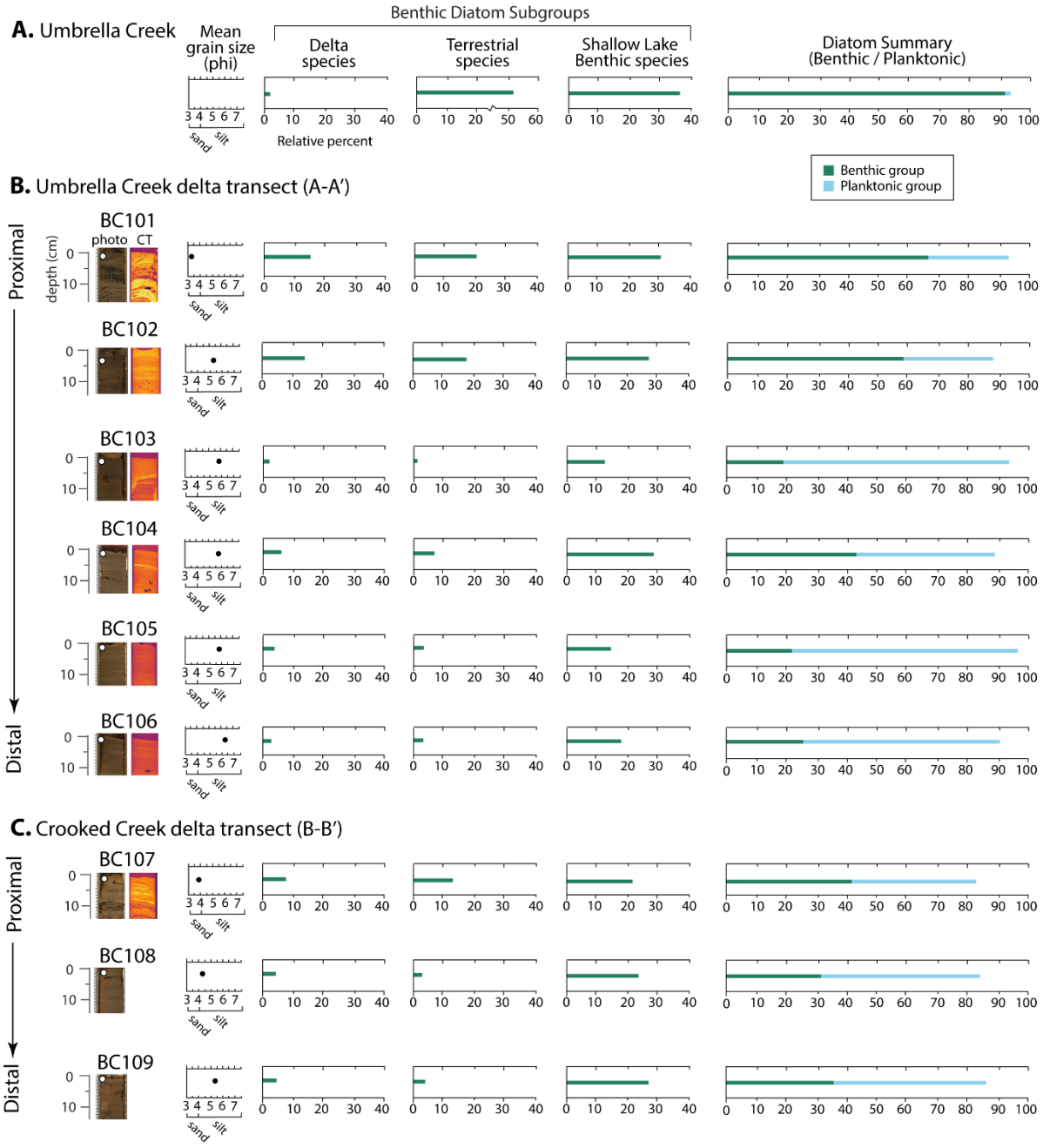

Figure 3.4. Photograph and CT scans for a) the Umbrella Creek grab sample, b) Umbrella Creek delta transect (A-A'), and c) Crooked Creek delta transect (B-B'). Grain size/diatom sample locations are shown by white circles. Mean grain size results (in phi) are shown with black circles. Relative abundances of diatom analysis are organized by three ecologic subgroups (delta, terrestrial, and shallow lake benthic) followed by a summary plot showing the total benthic (green bar) to total planktonic (blue bar) species in each sample.

At BC101, the modern diatom flora is abundant (62%) in benthic species with a lower abundance (24%) of planktonic species. Because this core is located at the shallowest depths with the closest proximity to Umbrella Creek delta, it contains the coarsest sediment and the greatest diatom diversity. Of the benthic species, 15.5% are delta subgroup species, ~20% are considered terrestrial subgroup species, and ~32% are categorized as shallow lake benthic subgroup species, consistent with being at a location with direct deposition from the creek and terrestrial runoff. At BC102, the modern diatom flora remains abundant (56%) in benthic species and much lower abundance (28%) of planktonic species. Of the benthic species, 14% are categorized as part of the delta subgroup and 17% are terrestrial subgroup species, and ~28% are shallow lake benthic subgroup species. BC103 drops by 40% in benthic species and increases by >45% in abundance of planktonic species. Of the benthic species, ~3% are delta subgroup species, ~2% are categorized as terrestrial species, and ~14% are shallow lake benthic subgroup species, possibly representing the unstable slope of the delta. At the bottom of the slope, BC104 contains a nearly equal ratio (41% to 44%) of benthic species to planktonic species, respectively. Of the benthic species, ~6% are delta subgroup species, 8% are terrestrial subgroup species, and ~30% are shallow lake benthic subgroup species. At the deepest parts of the transect, BC105 is less abundant (21%) in benthic species and significantly more abundant (74%) in planktonic species. Similarly, BC106 contains 22% benthic species and 65% planktonic species. Of the benthic species at BC105 and BC106, ~3% are delta subgroup species, ~4% are terrestrial subgroup species, and 15-18% are shallow lake benthic subgroup species.

The Crooked Creek delta transect (B-B') runs from the inlet mouth of Crooked Creek at BC107 northwest to BC110 (Fig. 3.2c). The inlet enters Ozette Lake from the east and produces a small, shallow delta that extends west onto the shelf (Fig. 3.2b). The top centimeter of each core was sampled to represent modern sediment and diatom assemblage distribution from shallow lake

to lake shelf zones. The grain size across this transect is characterized by a transition from coarse silt to very fine sand (average top 2 cm: mean = 4.5 φ; D50 = 4.12 φ) at BC107 to very coarse silt (mean = 4.28 φ; D50 = 3.76 φ) at BC108 and coarse silt (mean = 5.22 φ; D50 = 4.87 φ) at BC109, consistent with expected sediment distribution during floods (Fig. 3.4; Table 1). We did not collect a modern sediment sample from BC110.

Similar to the Umbrella Creek delta transect, modern diatom samples along the Crooked Creek delta transect reflect a transition from shallow lake to deep lake environments. BC107 contains 41% benthic and 42% planktonic species consistent with the proximity of BC107 to the river inlet. Of the benthic species, ~7% are delta subgroup species, ~13% are considered terrestrial subgroup species, and ~21% are categorized as shallow lake benthic subgroup species. BC108 contains a lower abundance (31%) of benthic species and higher abundance (55%) of planktonic species. Of the benthic species, ~4.5% are delta subgroup species, 5.7% are considered terrestrial subgroup species, and ~24% are categorized as shallow lake benthic subgroup species. BC109 is consistent with BC108, with less (36%) benthic species and a higher abundance (50%) of planktonic species. Both BC108 and BC109 represent modern locations farther from the creek inlet and farther from settings where terrestrial and delta species would likely thrive. Of the benthic species, ~4.5% are delta subgroup species, ~4% are terrestrial subgroup species, and ~27% are categorized as shallow lake benthic subgroup species.

We establish a set of diatom species that represent the ecology of the delta surfaces based on their presence and abundance on the deltas, but absence or low abundance in cores in the deeper lake or creek. The species include *Planothidium spp*., *Brachysira spp*., *Ulnaria delicatissima, Odontidium mesodon*, *Encyonema pergracile* and *E. procerum*, and *Stauroforma exiguiformis* (Table 2). These species are used to calculate the delta subgroup abundance in all lake samples.

3.4.2 Climate-induced deposition (Floods)

Following Slajus (2020), Brothers et al. (in review) recognize fine-grained (silt/clay), thin, denser deposits from BC02 (northeast proximal basin) as possible flood deposits in Ozette Lake. Slajus (2020) proposes that a broader pattern of light and dark banding within the background sediment indicates hydroclimate responses of the watershed to the Pacific Decadal Oscillation represented by dominant periodicities in the sediments of roughly 15 to 75 years. The lighter, thinner deposits were sampled from BC02 at 24 cm and 44.5 cm (Fig. 3.5; Table 1). The two samples are composed of medium silt (mean = 6.86 φ; D50 = 7.11 φ) and between 15-20% benthic diatom species and 65-75% planktonic species. Of the benthic species, the most abundant subgroup was the shallow lake benthic species ranging between 11-17%, with <2% categorized as delta subgroup species, and <1.5% categorized as terrestrial subgroup species.

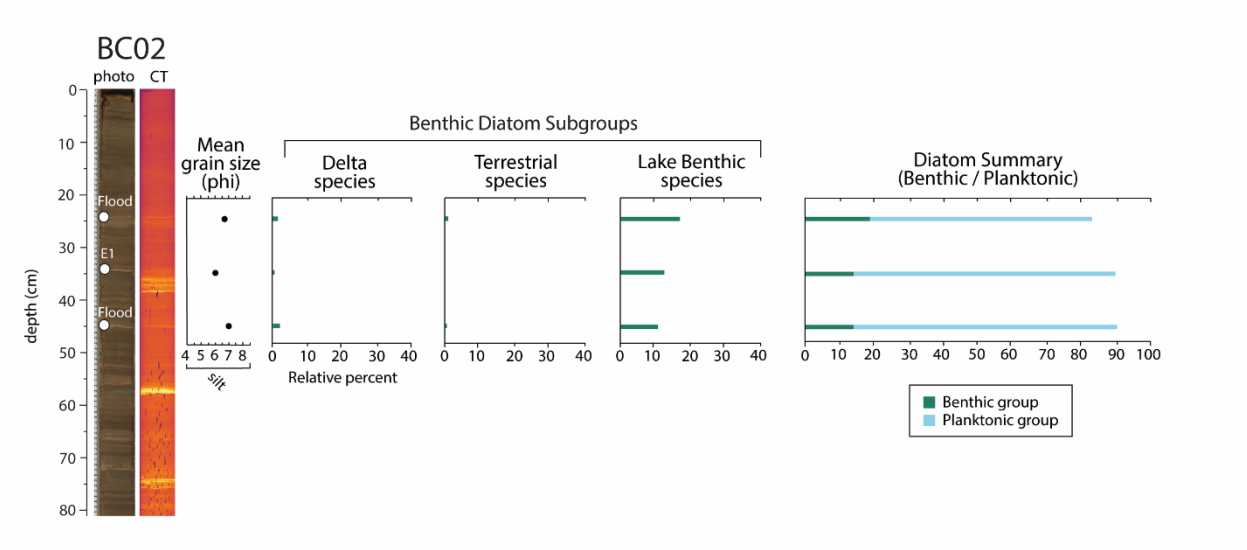

Figure 3.5. Photograph and CT scan for BC02, encompassing two flood deposits (24 cm and 44 cm depth) and one turbidite (E1). Grain size/diatom sample locations are shown by white circles. Mean grain size results (in phi) are shown in black circles. Relative abundances of diatom analysis are organized by three ecologic subgroups (delta, terrestrial, and shallow lake benthic) followed by a summary plot showing the total benthic (green bar) to total planktonic (blue bar) species in each sample.

3.4.3 Turbidites (Event layers)

3.4.3.1 Core VC49 (Proximal)

A 149-cm-long core (VC49) was taken ~70 m to the southwest of BC106 at the end of the Umbrella Creek transect located in the proximal basin (Fig. 3.6). There are two turbidites in core VC49: E1 (18 cm thick) and E2 (20 cm thick). The background lake sediment below both turbidites is composed of gray fine to medium silt (mean = 6.91 φ D50 = 6.98 φ), which is then sharply overlain by the coarser turbidite. The turbidites are normally graded with of 2-3 cm of fine sand (mean = 3.67 φ; D50 = 2.25 φ) at their base, which then rapidly transitions to a medium to fine silt (mean = 6.95 φ; D50 = 6.86 φ) towards the top of the turbidites. Both turbidites are capped with thin silt/clay layers. There is visible detrital organic matter within the turbidites that is not present in background lake sediments.

Diatom assemblages within the background lake sediments below the turbidites are dominated by planktonic species (64-87%; Average = 78.5%) compared to the low abundance of benthic species (7-24%; Average = 15%). Of the benthic diatom species in the background lake sediments, the shallow lake benthic subgroup is the most abundant (~7-20%; Average = 12%), while the delta and terrestrial subgroups make up less than 5% of the benthic species. The diatom flora in the background lake sediment is consistent with deep lake ecology that is high in planktonic species with very low sedimentological and ecological influence from shallow lake inputs.

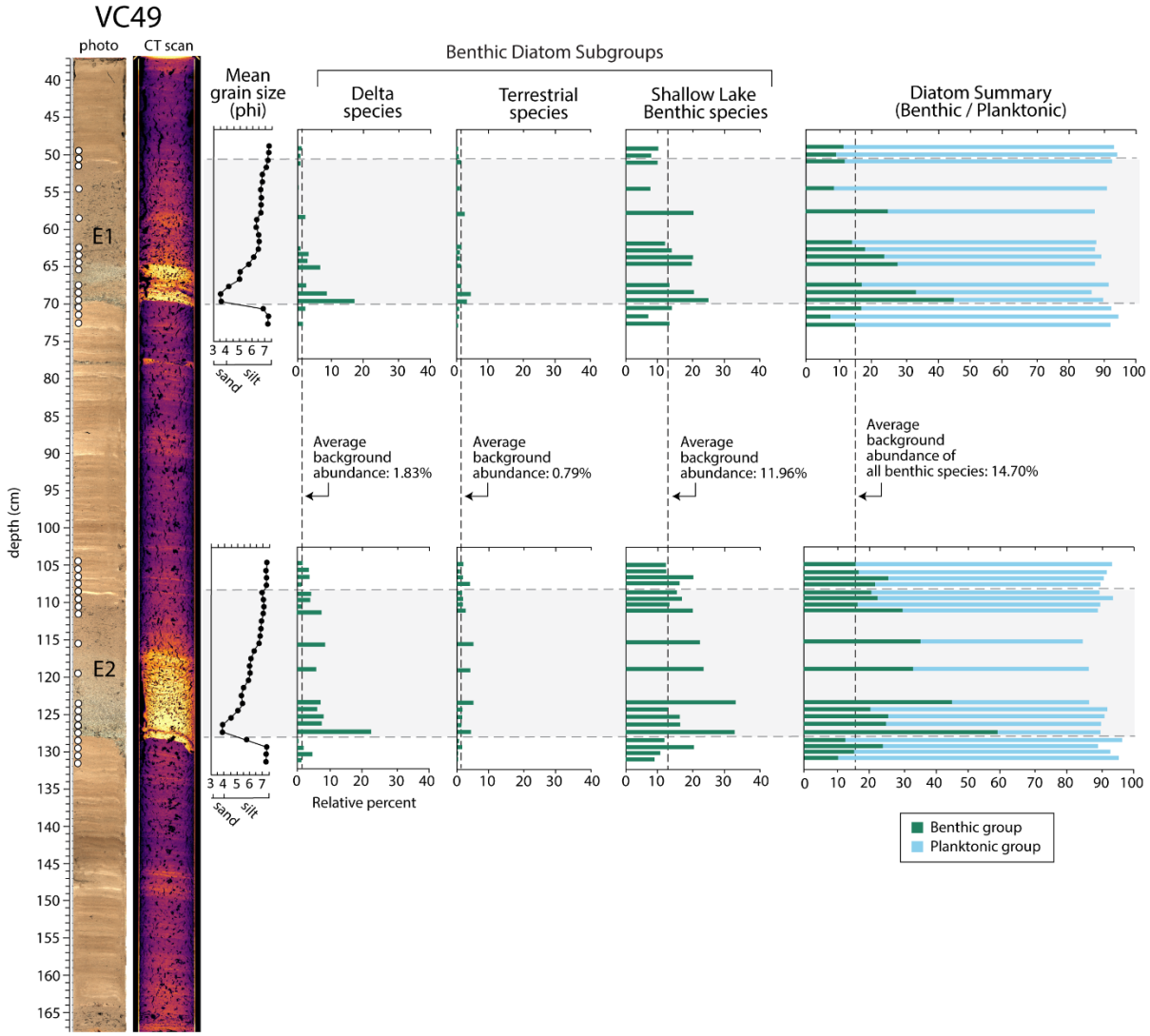

Figure 3.6. Photograph and CT scan for the proximal core VC49, encompassing two turbidites (E1 and E2). Diatom sample depths are shown by white circles. Mean grain size results (in phi) are shown in black circles and correlate to proper sample depths. Relative abundances of diatom analysis are organized by three ecologic subgroups (delta, terrestrial, and shallow lake benthic) followed by a summary plot showing the total benthic (green bar) to total planktonic (blue bar) species in each sample.

The diatom assemblage at the base of both turbidites is characterized by a sudden increase in benthic species (45-60%; Average = 52%) from the background lake average (15%). The delta subgroup, common in sandy sediment, increases significantly (17-22%; Average = 20%) from the background lake averages (2%) at the base of the turbidites and gradually decreases in abundance

towards the top of the turbidites. The shallow lake benthic subgroup also increases in abundance (25-32%; Average = 29%) from average (12%) at the base of the turbidites and fluctuates between 8-32% abundance throughout the turbidites. The terrestrial subgroup shows a slight increase but remains below 5%.

3.4.3.2 Core VC43 (Intermediate)

A ~190-cm-long core (VC43) was taken <1 km southeast of VC49 located in the proximal depositional basin (Fig. 3.7). There are five turbidites in core VC43: E1 (6 cm thick), E2 (7 cm thick), E3 (5 cm thick), E4 (9 cm thick), E5 (10 cm thick). The background lake sediment below the turbidites is composed of gray fine to medium silt (mean = 5.50 φ; D50 = 5.55 φ), which is then sharply overlain by the coarser turbidite layers. The base of turbidites E1 and E3 is composed of very coarse silt (mean = 4.92 φ; D50 = 4.67 φ) that fines upward gradually into fine silt (mean = 6.10 φ; D50 = 6.08 φ). The base of turbidites E2, E4, and E5 is composed of very fine sand (mean = 4.50 φ; D50 = 3.94 φ) that also fines upwards into fine to medium silt (mean = 5.97 φ; D50 = 6.24 φ). All turbidites are capped with dense, thin silt/clay layers.

Diatom assemblages within the background lake sediments below the turbidites are dominated by planktonic species (74.5-88%; Average = ~81%) compared to the low abundance of benthic species (5-14%; Average = ~12%). Of the benthic diatom species in the background lake sediments, the shallow lake benthic subgroup is the most abundant (4-17.5%; Average = 11%), while the delta and terrestrial subgroup species make up <1% of the benthic species.

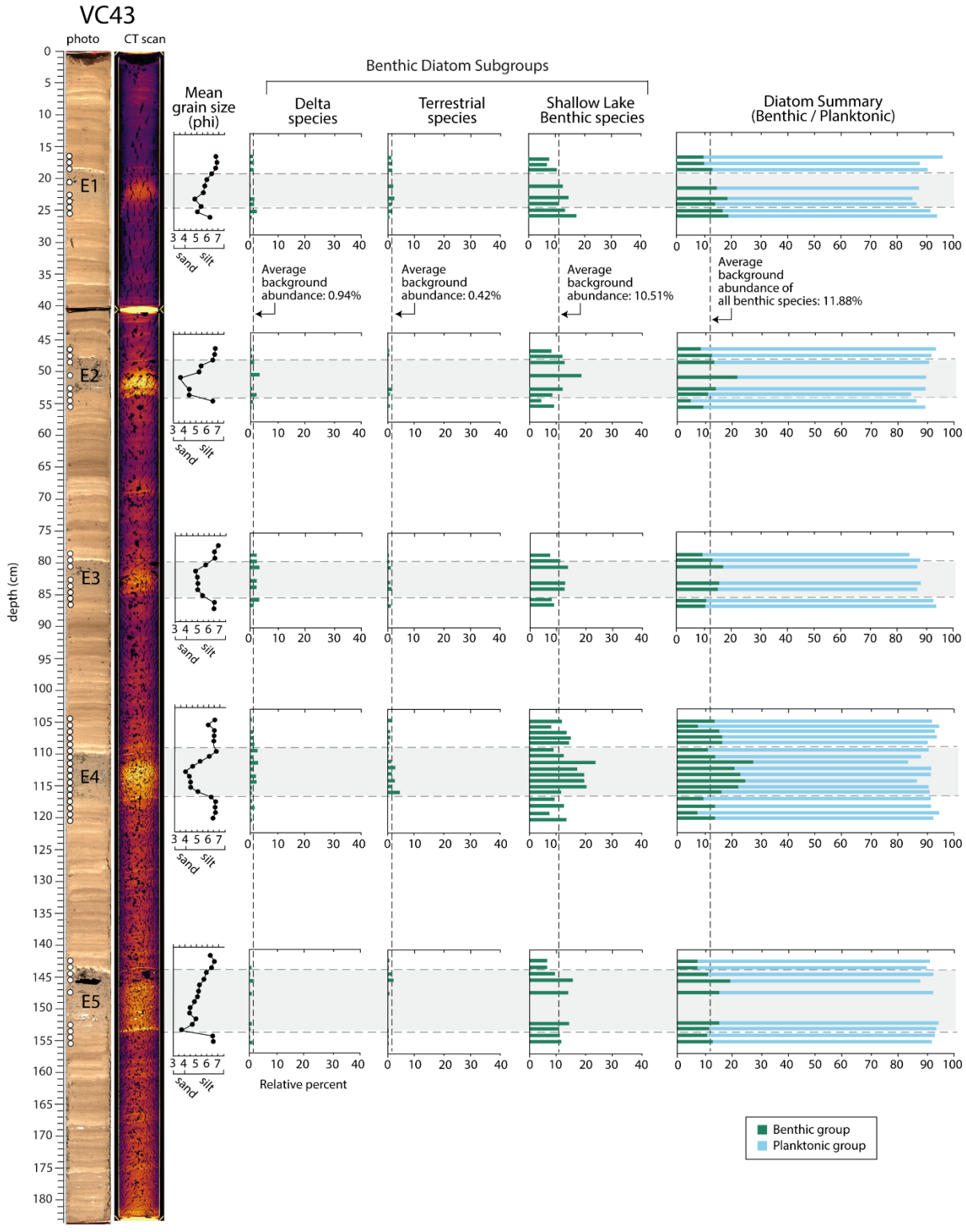

Figure 3.7. Photograph and CT scan for the intermediate core VC43, encompassing two turbidites (E1, E2, E3, E4, E5). Diatom sample depths are shown by white circles. Mean grain size results (in phi) are shown in black circles and correlate to proper sample depths. Relative

abundances of diatom analysis are organized by three ecologic subgroups (delta, terrestrial, and shallow lake benthic) followed by a summary plot showing the total benthic (green bar) to total planktonic (blue bar) species in each sample.

The diatom assemblage at the base of each deposit is characterized by a sudden increase in benthic diatom species (11-27%; Average = 15.8) from background (~12%). The delta subgroup species increase slightly above background average (0.94%) within turbidites E2, E3, and E4, but remain below 5%. The shallow lake benthic subgroup also exhibits an increase (7-24%; Average = 15%) compared to the background (12%), which is consistent for all turbidites in this core.

3.4.3.3 Core VC46 (Distal)

A 305-cm-long core (VC46) was taken ~2 km southwest of VC43 located in the distal depositional basin (Fig. 3.8). There are five turbidites in core VC46: E1 (4 cm thick), E3 (6 cm thick), E4 (4 cm thick), E5 (3 cm thick), E6 (2 cm thick). The turbidites are relatively thin and fine-grained compared to the turbidites in VC49 and VC43. The background lake sediment below the turbidites is composed of gray fine to medium silt (mean = 6.60 φ; D50 = 6.81 φ). Each turbidite contains coarse to very coarse silt (mean = 7.03 φ; D50 = 6.98 φ) with no discernable sedimentary characteristics to distinguish from background sediments.

Diatom assemblages within the background lake sediments below the turbidites are dominated by planktonic species (78-88%; Average = ~83%) compared to the low abundance of benthic species (5-15%; Average = ~10%). Of the benthic species, the shallow lake benthic subgroup is the most dominant (~4.5-14%; Average = ~9%), while the delta and terrestrial species are absent or at very low abundances at this location, making up <0.5% average abundance in background sediments.

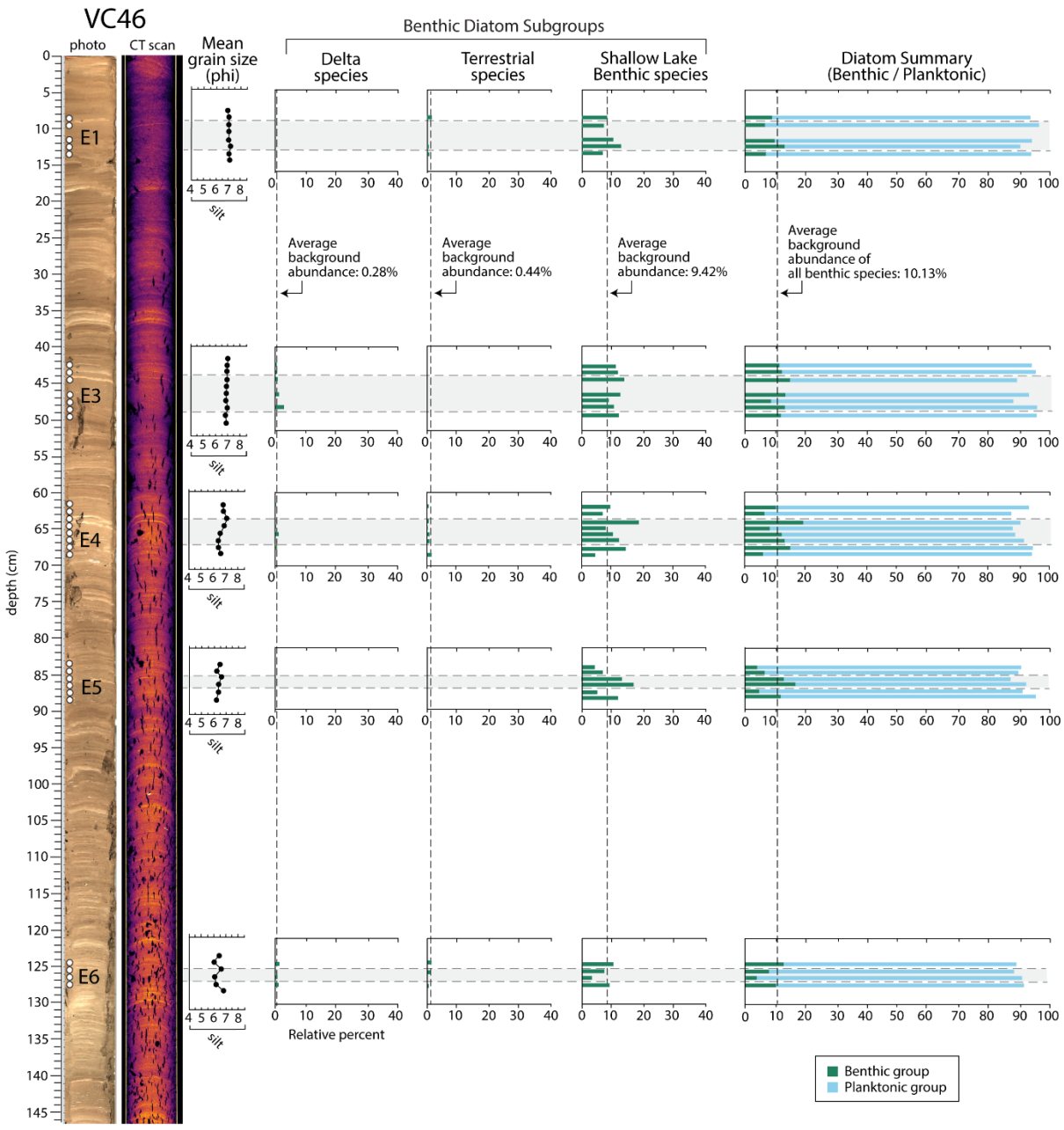

Figure 3.8. Photograph and CT scan for the distal core VC46, encompassing two turbidites (E1, E3, E4, E5, E6). Diatom sample depths are shown by white circles. Mean grain size results (in phi) are shown in black circles and correlate to proper sample depths. Relative abundances of diatom analysis are organized by three ecologic subgroups (delta, terrestrial, and shallow lake benthic) followed by a summary plot showing the total benthic (green bar) to total planktonic (blue bar) species in each sample.

The diatom assemblage at the base of the turbidites are characterized by a muted signal compared to the signatures in the proximal and intermediate cores. The shallow lake benthic subgroup, which significantly increases above background average in the proximal and intermediate turbidites, exhibits a variable trend in turbidites in VC46. The shallow lake benthic subgroup species increases (7-18%; Average = ~12%) from the background average (9.42%) in E1, E2, E3, and E4, but exhibits a ~5% decrease from average in E6. Delta and terrestrial subgroup species are absent or at low abundances (each under 3%) in all turbidites at this location.

We note that this core is missing a turbidite that correlates with E2. Brothers et al. (in review) found that E2 is much thinner than other turbidites basin-ward from the VC49 and most cores in the distal depositional basin do not observe this turbidite.

3.5 DISCUSSION

3.5.1 Framework for seismic- vs. climate-induced deposition

Brothers et al. (in review) infer a seismogenic source for the top 12 turbidites recorded in Ozette Lake based on a set of criteria developed by Vandekerkhove et al. (2020). The Vandekerkhove et al. (2020) criteria uses sedimentological characteristics to differentiate seismic versus climate triggers using a dataset from Eklutna Lake, Alaska. Sedimentary indicators of seismic-induced deposition include: (1) increase in deposit thickness towards main inferred sediment sources, (2) increase in basal grain size, (3) change in deposit color contrasting the background sedimentation, and (4) time synchronicity with local or regional earthquake history. Turbidites in Ozette Lake exhibit these characteristics leading to the interpretation by Brothers et al (in review) that the turbidites are consistent with a short-lived, energetic flow distinctive of

seismic-induced slope failures. However, these criteria do not interrogate the sediment sources of the turbidites and cannot rule out the possibility of climate-induced sediment deposition into Ozette Lake, especially for turbidites observed in distal locations from the inferred sediment source that have a lower concentration of coarse sediment. Do large precipitation events transport enough sediment into the lake from terrestrial environments to produce turbidity currents that mimic seismic-induced turbidites?

Below, we establish a framework to differentiate the source mechanism of the youngest six turbidites preserved at Ozette Lake using grain size and diatom analysis. By characterizing the grain size and diatom signature of potential turbidite source sediments and of the turbidites themselves, we can link turbidites to their likely modern source sediment. We demonstrate that seismic- and climate-induced depositional mechanisms create distinctly different grain size and diatom signatures in Ozette Lake and establish diatoms as a valuable tool in differentiating sediment origin in lacustrine paleoseismology studies.

3.5.2 Grain size and diatom signature of seismic-induced vs. climate-induced deposition in Ozette Lake

In order to understand how seismic- and climate-induced deposition is expressed in Ozette Lake, we must first establish the expected background lake grain size and diatom signature that is interrupted by turbidites. Our analysis shows that background lake diatom assemblages in our proximal, intermediate, and distal cores are composed of fine to medium silt sediment dominated by planktonic species that float within the water column in the photic zone, and over time, die and settle into the bottom lake sediments. Background lake sediments also include lesser amounts (<12%) of shallow lake benthic species that are common in shallower parts of the lake and can be transported basin-ward through lake currents, wind, and/or bioturbation.

In the context of the observed background lake diatom assemblages, we build two conceptual models of the expected diatom signature for seismic- and climate-induced deposition in Ozette Lake (Fig. 3.9). Seismic-induced deposition is triggered by extreme shaking due to subduction zone earthquakes that destabilize subaqueous deltas and shallow shelves, generating mass flows that transport and deposit anomalous in-situ delta and shallow lake sediment throughout the lake basins (Beck, 2009; Vandekerkhove et al., 2020). Based on our grain size and diatom analyses of source sediments, we expect a seismic-induced turbidite that is proximal to the main delta sediment source to contain a pulse of fine sand from the delta and an increase in delta and shallow lake benthic species reflective of a short-lived, energetic event. We expect turbidites in cores collected in intermediate and distal locations relative to the main delta sediment source to contain a similar, but muted, grain size and diatom signature as the turbidite thins and becomes finer with increasing distance from the delta. Shallow lake benthic species, common to shallow lake environments, may increase in intermediate and distal turbidites without a strong signature of delta diatom species as a sign of widespread subaqueous slope failures and resuspension of shallower sediments. We do not expect a significant increase in terrestrial diatom species coming from outside of the lake in seismic-induced turbidites, although these species are likely part of the assemblage present in delta sediments since precipitation events transport terrestrial species onto the delta through regular creek discharge and floods.

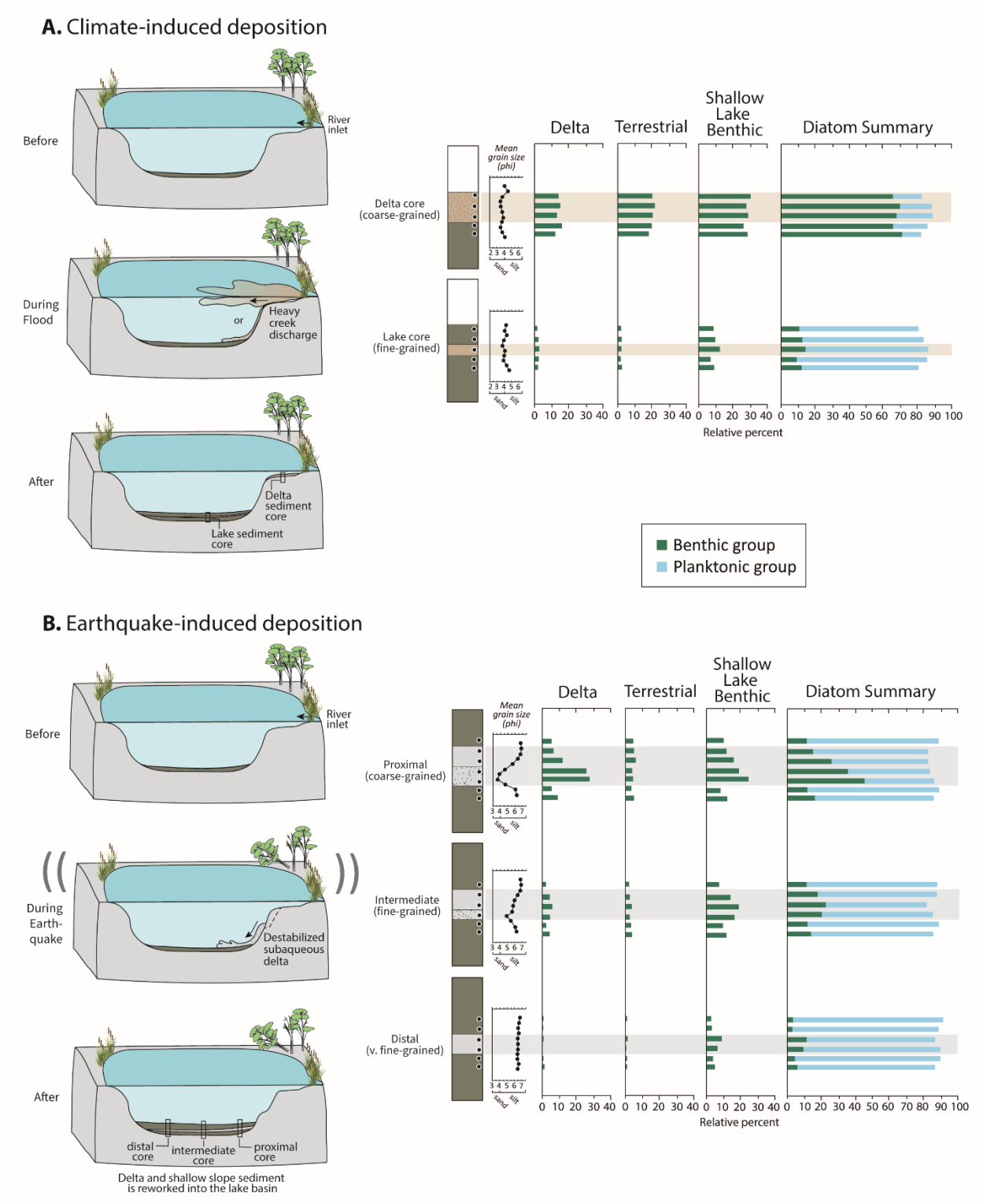

Figure 3.9. Schematics showing the inferred mechanism and sedimentary response for before, during, and after a) climate-induced (flood) and b) earthquake-induced deposition at Ozette Lake. Core summaries display observed grain size and diatom results for inferred flood and turbidite deposition.

Climate-induced deposition in Ozette Lake is triggered by large precipitation events or snowmelt that transport terrestrial sediment from the creeks to deeper lake settings through hypopycnal (low-density surficial distribution) or, more commonly, hyperpycnal (high-density lake-bottom turbidite) flows (Beck, 2009; Jenny et al., 2014; Vandekerkhove et al., 2020; Fig. 3.9). Hypopycnal flows are likely to create widespread deposition of fine-grained sediment, but deposits are less distinguishable within the lake stratigraphy (Sabatier et al., 2022). Hyperpycnal flows can create widespread distribution of anomalous coarse sediment (as turbidites or other mass transport deposition) during floods, distributing sediment evenly over many days (Jenny et al., 2014; Wilhelm et al., 2015; Vandekerkhove et al., 2020). Based on our grain size and diatom analyses of source sediments, we expect a climate-induced turbidite emplaced through hyperpycnal flow to transport coarser sediments from the delta and creek, but contain a significant increase in benthic terrestrial diatoms, common in creeks and runoff sediment, and otherwise absent from background lake sediments. It is possible that deposition could include some resuspended benthic delta and shallow lake benthic species, but we expect a persistent signature from terrestrial diatoms that would reflect distribution of sediment from creeks over an extended period of time (i.e., duration of the climatic-induced event).

3.5.3 Reconstructing turbidite source mechanism based on grain size and diatom analysis

Based on our diatom and grain size analysis, we support a seismic origin for the youngest six turbidites in Ozette Lake, consistent with seismic-induced failure of the Umbrella Creek delta. Our high-resolution grain size results for the proximal core (VC49) build on data collected by Brothers et al. (in review) and show a close match between the fine sand observed on the Umbrella Creek delta and the fine sand observed at the base of turbidites E1 and E2 (Fig. 3.6). The grain

size rapidly fines above the coarse base, consistent with a grain size distribution observed in other seismic-induced turbidites in lakes around the world signaling short but energetic flow (Beck, 2009; Vandekerkhove et al., 2020). Our diatom data support a significant delta sediment source, with a 15-20% increase in delta subgroup species above background averages at the base of the turbidites, indicating a pulse of sediment sourced from the delta slope and/or delta surface. We also observe an increase in shallow lake benthic species above background levels in turbidites E1 and E2, consistent with the destabilization of shallow shelf sediment into the lake basin. We do not observe a significant increase in terrestrial diatoms in the turbidites as we would expect during climate-induced hyperpycnal flows into the lake, supporting a seismic-induced delta slope failure as the source of the proximal core turbidites.

Our high-resolution grain size results for the intermediate core (VC43) show a coarsening at the base of the turbidites from background sediments, with E2, E4, and E5 containing very fine sand matching the fine sand of the Umbrella Creek delta (Fig. 7). The turbidites are thinner than in the proximal core, consistent with the basin-ward thinning expected from a delta slope failure. In contrast to proximal core VC49, delta diatom species increase only slightly over background averages in E2, E3, and E4. However, like VC49, shallow lake benthic species common to shallow lake environments increase above background levels in all turbidites. This suggests that turbidites in the intermediate coring location contain less delta sediment than proximal cores, and are instead mainly sourced from the destabilization or resuspension of shallow shelf sediment into the lake basin during seismic activity. We do not observe a significant increase in terrestrial diatoms in the intermediate turbidites, which we would expect for climate-induced deposition.

The sedimentary signature of distal basin turbidite deposition in core VC46 is nearly undiscernible from the background lake laminations without the help of CT or high-resolution Chirp (Fig. 3.8). Because VC46 is located in the distal depositional basin of Ozette Lake and is

separated from the proximal basin (i.e., location of cores VC49 and VC43) by the subaqueous ridge, it is unlikely that a delta shelf collapse would contribute significant sediment to the turbidites at this location. For this reason, it is an important location to rule out hyperpycnal flows as the turbidite sediment source. Turbidites at VC46 are much thinner and finer than proximal basin turbidites (Fig. 2, 4). High-resolution grain size results show no clear difference between background sediments and turbidites, and delta and terrestrial benthic diatom species are nearly absent from the turbidites. However, shallow lake benthic diatoms increase above background average within most turbidites (i.e., E1, E3, E4, E5). Based on our grain size and diatom results, we infer that the distal core turbidites are composed of mostly localized remobilization of shallow shelf sediments rather than the distal extents of delta destabilization, consistent with the interpretation of Brothers et al. (in review). The lack of influx of terrestrial diatoms in any of the subtle distal turbidite deposits supports that climate-induced hypopycnal and hyperpycnal flows are not the source of the sediment.

3.5.4 Possible additional turbidite sediment sources in and around Ozette Lake

We consider additional or alternative sediment sources, besides the Umbrella Creek delta, that may contribute to the turbidite deposits in the proximal and distal lake basins. In addition to Umbrella Creek, Brothers et al. (in review) point out scarps and debris aprons that are evidence of past slope and delta failures at Siwash Creek and Crooked Creek inlets and slopes around Ozette Lake suggesting potential lake-wide remobilization of sediment (Fig. 2).

It is possible to have earthquake-induced subaerial landslides deposit significant sediment loads into the lake as seen in lidar between the Umbrella Creek and Crooked Creek deltas (Fig. 2). We would expect proximal locations to have much thicker deposition with much coarser grains

than sediments within the lake. Additionally, diatoms may reflect the displacement from non-aquatic environments by showing pulses of sediment absent of diatoms or possibly more abundant in aerophilic (living in drier conditions) diatom species. Because there are no pulses of extremely coarse sediment or terrestrial and aerophilic diatom species in any of the lake turbidites, we infer all sediment input is sourced from inside the lake.

We also note that our sedimentary and diatom analyses cannot account for turbidites derived from spontaneous slope failures (Girardclos et al., 2007; Hilbe and Anselmetti, 2014). Processes such as sediment loading on delta surfaces or oversaturated subaerial slopes may produce turbidites with sedimentary and diatom characteristics that match seismic-induced slope failures. Brothers et al. (in review) use modeled radiocarbon ages for the youngest 12 turbidites to compare the Ozette Lake record with regional northern Cascadia paleoseismic records. Overall, 11 of the 12 Ozette Lake turbidites were estimated to overlap, sometimes weakly, with local and regional onshore chronologies. However, the uncertainties in radiocarbon age estimates for individual turbidites are broad enough that inferred seismic-induced slope failures could correspond with non-seismic spontaneous slope failures occurring within several decades of earthquake ruptures. Therefore, we cannot rule out the possibility that our turbidites (some or all) represent spontaneous slope failures that occur close in time with major earthquakes along the CSZ.

3.5.5 Is there evidence of climate-induced deposition (floods) in Ozette Lake basins?

Based on our grain size and diatom results, we do not observe evidence for climate-induced flood deposits within the basins of Ozette Lake. Our results instead suggest that flood deposits appear as discrete sedimentation in deeper lake settings and/or are contained to the shallow lake

and subaqueous deltas (Chaumillon et al., 2017; Sabatier et al., 2022). Small catchments of Umbrella Creek and Crooked Creek are reflected in the size of the subaqueous deltas and the absence of obvious flood deposits in the deeper basins. Ozette Lake receives a mean rainfall of 266 cm (105 in) annually and accumulations of snowfall do not exceed of 25 cm (10 in) in the winter months. With the lack of high elevations within the relatively small catchments, it is unlikely to have significant snowfall that would be capable of carrying high volumes of sediment downstream to Ozette Lake during snowmelt (Ritchie and Bourgeois, 2009). Additionally, until the onset of logging in the 1960s, the catchments around Ozette Lake remained heavily vegetated with temperate rainforests, suggesting that sediment availability remained low and sediment-rich floods were less likely (Ritchie and Bourgeois, 2009).

Based on our diatom analysis, we estimate that the heavier flow from the inlets into Ozette Lake are unable to reach beyond the extents of the deltas and therefore concentrate most of the coarser sediments and terrestrial diatoms closest to the inlet. We also infer that floods from Umbrella Creek will likely distribute into the lake as a low-density hypopycnal flow due to the lack of sediment to create a higher-density hyperpycnal distribution. We expect hypopycnal flow to distribute coarser sediment and diatoms on top of the subaqueous deltas and gradually distribute suspended finer-grained (silt/clay) sediments and diatoms basin-ward. This is evident in the inferred flood deposits analyzed in core BC02. The flood deposits have a similar lighter color and sedimentary characteristics to the silt/clay cap of most turbidite deposits in Ozette Lake. Comparing the characteristics of the flood deposits to the silt/clay cap of a turbidite in the same core, we observe similarities in diatom diversity, species present, and grain size (Fig. 5; Table 1). The silt/clay caps of the turbidites represent the final stages of turbidite deposition with the settling of suspended fine-grained sediment and diatoms. We infer hypopycnal flow during climate-

induced floods produce a similar sedimentological and ecological signal as the distal, far fringes of flood deposits in core BC02.

3.6 CONCLUSION

We use high-resolution grain size and diatom analysis to demonstrate that the turbidites preserved in the stratigraphy of Ozette Lake likely represent seismic-induced, rather than climate-induced, deposition. The sudden pulse of coarse sediment and delta benthic diatom species found at the base of proximal turbidites is consistent with a seismic-induced failure of the Umbrella Creek delta. The increase in shallow lake benthic diatom species in the proximal turbidites suggests localized failure of shallow lake shelfs also contributes finer sediment to the proximal turbidites. Grain size and diatom results also indicate intermediate core turbidites are sourced from a combination of Umbrella Creek delta sediment and localized failures of shallow shelfs contributing finer sediment, while distal core turbidites are sourced from remobilized shallow lake sediment only. The lack of a distinct terrestrial diatom signature in any background lake sediment or within the turbidites in the proximal or distal lake basins leads us to infer there is not consistent deposition/sedimentary influence from outside of the lake. Our results instead suggest that climate-induced floods deliver coarse sediment and terrestrial species mostly onto the delta surfaces on the fringes of the lake, and only produce discrete deposition within the deeper lake basins. Guided by our framework, we infer seismic-induced deposition of the six youngest turbidites across the ~3,000-year depositional history analyzed in this study, consistent with the findings of Brothers et al. (in review).

Ozette Lake, representing the longest continuous onshore earthquake record along the CSZ, has the potential to bridge offshore (e.g., deep marine) and other onshore (e.g., coastal marsh)

records, expanding the spatio-temporal history of the northern CSZ earthquake record. Our results show that diatoms are a viable proxy for distinguishing the origin of deposits in the sediment record at Ozette Lake and provide a potential tool for future paleoseismic studies. We note, however, that lake settings can be extremely variable (e.g., slope steepness, sediment input, sedimentation rate, climate factors/seasonality changes, number of tributaries, catchment characteristics, etc.) and it is important to characterize the diatom signature of potential source sediments and background lake conditions at every site when conducting diatom-based lacustrine paleoseismology studies.

3.7 ACKNOWLEDGMENTS

Partial field work and summer funding was provided through the Virginia Tech Department of Geosciences.

We would like to thank Andy Ritchie for sharing insights and assisting with sample collection during field work, David Bruce for assisting with field work, and Brian Romans for helpful discussions about lake turbidite behavior.

REFERENCES CITED

Adams, J., 1996, Paleoseismology in Canada: a dozen years of progress: Journal of Geophysical Research: Solid Earth, v. 101, p. 6193–6207.

Arnaud, F., Lignier, V., Revel, M., Desmet, M., Beck, C., Pourchet, M., Charlet, F., Trentesaux, A., and Tribovillard, N., 2002, Flood and earthquake disturbance of 210Pb geochronology (Lake Anterne, NW Alps): Terra Nova, v. 14, p. 225–232.

Beck, C., 2009, Late Quaternary lacustrine paleo-seismic archives in north-western Alps: Examples of earthquake-origin assessment of sedimentary disturbances: Earth-Science Reviews, v. 96, p. 327–344.

Blott, S.J., and Pye, K., 2001, GRADISTAT: A grain size distribution and statistics package for the analysis of unconsolidated sediments: Earth Surface Processes and Landforms, v. 26, p. 1237–1248, doi:10.1016/S0167-5648(08)70015-7.

Boes, E., Van Daele, M., Moernaut, J., Schmidt, S., Jensen, B.J.L., Praet, N., Kaufman, D., Haeussler, P., Loso, M.G., and De Batist, M., 2018, Varve formation during the past three centuries in three large proglacial lakes in south-central Alaska: GSA Bulletin, v. 130, p. 757–774.

Brothers, D.S., Driscoll, N.W., Kent, G.M., Baskin, R.L., Harding, A.J., and Kell, A.M., 2022, Seismostratigraphic analysis of Lake Cahuilla sedimentation cycles and fault displacement history beneath the Salton Sea, California, USA: Geosphere, v. 18, p. 1354–1376.

Chaumillon, E., Bertin, X., Fortunato, A.B., Bajo, M., Schneider, J.-L., Dezileau, L., Walsh, J.P., Michelot, A., Chauveau, E., and Créach, A., 2017, Storm-induced marine flooding: Lessons from a multidisciplinary approach: Earth-Science Reviews, v. 165, p. 151–184.

Dura, T., Engelhart, S.E., Vacchi, M., Horton, B.P., Kopp, R.E., Peltier, W.R., and Bradley, S., 2016, The Role of Holocene Relative Sea-Level Change in Preserving Records of

Subduction Zone Earthquakes: Current Climate Change Reports, v. 2, p. 86–100, doi:10.1007/s40641-016-0041-y.

Dura, T., and Hemphill-Haley, E., 2020, Diatoms in tsunami deposits, *in* Geologic Records of Tsunamis and Other Extreme Waves, p. 291–322.

Girardclos, S., Schmidt, O.T., Sturm, M., Ariztegui, D., Pugin, A., and Anselmetti, F.S., 2007, The 1996 AD delta collapse and large turbidite in Lake Brienz: Marine Geology, v. 241, p. 137–154.

Goldfinger, C., 2011, Submarine Paleoseismology Based on Turbidite Records: Annual Review of Marine Science, v. 3, p. 35–66, doi:10.1146/annurev-marine-120709-142852.

Hilbe, M., and Anselmetti, F.S., 2014, Signatures of slope failures and river-delta collapses in a perialpine lake (Lake Lucerne, Switzerland): Sedimentology, v. 61, p. 1883–1907.

Jenny, J.-P., Wilhelm, B., Arnaud, F., Sabatier, P., Giguet Covex, C., Melo, A., Fanget, B., Malet, E., Ployon, E., and Perga, M.E., 2014, A 4D sedimentological approach to reconstructing the flood frequency and intensity of the Rhône River (Lake Bourget, NW European Alps): Journal of Paleolimnology, v. 51, p. 469–483.

Karlin, R.E., and Abella, S.E.B., 1996, A history of Pacific Northwest earthquakes recorded in Holocene sediments from Lake Washington: Journal of Geophysical Research: Solid Earth, v. 101, p. 6137–6150, doi:10.1029/95jb01626.

Karlin, R.E., Holmes, M., Abella, S.E.B., and Sylwester, R., 2004, Holocene landslides and a 3500-year record of Pacific Northwest earthquakes from sediments in Lake Washington: Bulletin of the Geological Society of America, v. 116, p. 94–108, doi:10.1130/B25158.1.

Krammer, K., and Lange-Bertalot, H., 1988, Süßwasserflora von Mitteleuropa, Bd 2/2. Bacillariophyceae. 2. Teil: Bacillariaceae, Epithemiaceae, Surirellaceae: Gustav Fischer,.

Leithold, E.L., Wegmann, K.W., Bohnenstiehl, D.R., Joyner, C.N., and Pollen, A.F., 2019,

Repeated megaturbidite deposition in Lake Crescent, Washington, USA, triggered by Holocene ruptures of the Lake Creek-Boundary Creek fault system: Bulletin of the Geological Society of America, v. 131, p. 2039–2055, doi:10.1130/B35076.1.

Leithold, E.L., Wegmann, K.W., Bohnenstiehl, D.R., Smith, S.G., Noren, A., and O'Grady, R., 2018a, Slope failures within and upstream of Lake Quinault, Washington, as uneven responses to Holocene earthquakes along the Cascadia subduction zone: Quaternary Research, v. 89, p. 178.

Leithold, E.L., Wegmann, K.W., Bohnenstiehl, D.R., Smith, S.G., Noren, A., and O'Grady, R., 2018b, Slope failures within and upstream of Lake Quinault, Washington, as uneven responses to Holocene earthquakes along the Cascadia subduction zone: Quaternary Research (United States), v. 89, p. 178–200, doi:10.1017/qua.2017.96.

López, G.I., 2012, Evidence for mid-to late-Holocene palaeotsunami deposits, Kakawis Lake, Vancouver Island, British Columbia: Natural hazards, v. 60, p. 43–68.

Moernaut, J. et al., 2017, Lacustrine turbidites produced by surficial slope sediment remobilization: A mechanism for continuous and sensitive turbidite paleoseismic records: Marine Geology, v. 384, p. 159–176, doi:10.1016/j.margeo.2015.10.009.

Moernaut, J., Van Daele, M., Heirman, K., Fontijn, K., Strasser, M., Pino, M., Urrutia, R., and De Batist, M., 2014, Lacustrine turbidites as a tool for quantitative earthquake reconstruction: New evidence for a variable rupture mode in south central Chile: Journal of Geophysical Research: Solid Earth, v. 119, p. 1607–1633.

Molenaar, A., Van Daele, M., Vandorpe, T., Degenhart, G., De Batist, M., Urrutia, R., Pino, M., Strasser, M., and Moernaut, J., 2021, What controls the remobilization and deformation of surficial sediment by seismic shaking? Linking lacustrine slope stratigraphy to great earthquakes in South–Central Chile: Sedimentology, v. 68, p. 2365–2396.

Morey, A.E., Goldfinger, C., Briles, C.E., Gavin, D.G., Colombaroli, D., and Kusler, J.E., 2013, Are great Cascadia earthquakes recorded in the sedimentary records from small forearc lakes? Natural Hazards and Earth System Sciences, v. 13, p. 2441–2463, doi:10.5194/nhess-13-2441-2013.

Mulder, T., Syvitski, J.P.M., Migeon, S., Faugères, J.-C., and Savoye, B., 2003, Marine hyperpycnal flows: initiation, behavior and related deposits. A review: Marine and Petroleum Geology, v. 20, p. 861–882.

Nelson, A.R. et al., 1995, Radiocarbon evidence for extensive plate-boundary rupture about 300 years ago at the Cascadia subduction zone: Nature, v. 378, p. 371–374, doi:10.1038/378371a0.

Osleger, D.A., Heyvaert, A.C., Stoner, J.S., and Verosub, K.L., 2009, Lacustrine turbidites as indicators of Holocene storminess and climate: Lake Tahoe, California and Nevada: Journal of Paleolimnology, v. 42, p. 103–122, doi:10.1007/s10933-008-9265-8.

Oswald, P., Strasser, M., Hammerl, C., and Moernaut, J., 2021, Seismic control of large prehistoric rockslides in the Eastern Alps: Nature Communications, v. 12, p. 1–8, doi:10.1038/s41467-021-21327-9.

Pilarczyk, J.E., Dura, T., Horton, B.P., Engelhart, S.E., Kemp, A.C., and Sawai, Y., 2014, Microfossils from coastal environments as indicators of paleo-earthquakes, tsunamis and storms: Palaeogeography, Palaeoclimatology, Palaeoecology, v. 413, p. 144–157, doi:10.1016/j.palaeo.2014.06.033.

Potapova, M., and Charles, D.F., 2007, Diatom metrics for monitoring eutrophication in rivers of the United States: Ecological indicators, v. 7, p. 48–70.

Praet, N., Van Daele, M., Collart, T., Moernaut, J., Vandekerkhove, E., Kempf, P., Haeussler, P.J., and De Batist, M., 2020, Turbidite stratigraphy in proglacial lakes: Deciphering trigger

mechanisms using a statistical approach: Sedimentology, v. 67, p. 2332–2359.

Praet, N., Moernaut, J., Van Daele, M., Boes, E., Haeussler, P.J., Strupler, M., Schmidt, S., Loso, M.G., and De Batist, M., 2017, Paleoseismic potential of sublacustrine landslide records in a high-seismicity setting (south-central Alaska): Marine Geology, v. 384, p. 103–119, doi:https://doi.org/10.1016/j.margeo.2016.05.004.

Ritchie, A., and Bourgeois, J., 2009, Late Quaternary Sediment Source and Deposition History of Lake Ozette:

Sabatier, P., Moernaut, J., Bertrand, S., Van Daele, M., Kremer, K., Chaumillon, E., and Arnaud, F., 2022, A Review of Event Deposits in Lake Sediments: Quaternary, v. 5, p. 1–49, doi:10.3390/quat5030034.

Singleton, D.M., Brothers, D., Haeussler, P.J., Witter, R.C., and Hill, J.C., 2023, Constraining the earthquake recording threshold of intraslab earthquakes with turbidites in southcentral Alaska's lakes and fjords: ESS Open Archive,.

Slajus, L.A., 2020, A Late Holocene Earthquake and Paleoclimate Record from Ozette Lake, Washington: North Carolina State University, https://www.ptonline.com/articles/how-to-get-better-mfi-results.

Smith, S.G., Wegmann, K.W., Leithold, E.L., and Bohnenstiehl, D.R., 2019, A 4000-year record of hydrologic variability from the Olympic Mountains, Washington, USA: Holocene, v. 29, p. 1273–1291, doi:10.1177/0959683619846975.

Spaulding, S.A., Potapova, M.G., Bishop, I.W., Lee, S.S., Gasperak, T.S., Jovanoska, E., Furey, P.C., and Edlund, M.B., 2021, Diatoms. org: supporting taxonomists, connecting communities: Diatom Research, v. 36, p. 291–304.

Strasser, M., Stegmann, S., Bussmann, F., Anselmetti, F.S., Rick, B., and Kopf, A., 2007, Quantifying subaqueous slope stability during seismic shaking: Lake Lucerne as model for

ocean margins: Marine Geology, v. 240, p. 77–97, doi:10.1016/j.margeo.2007.02.016.

Talling, P.J., 2014, On the triggers, resulting flow types and frequencies of subaqueous sediment density flows in different settings: Marine Geology, v. 352, p. 155–182.

VanDaele, M., Araya-Cornejo, C., Pille, T., Vanneste, K., Moernaut, J., Schmidt, S., Kempf, P., Meyer, I., and Cisternas, M., 2019, istinguishing intraplate from megathrust earthquakes using lacustrine turbidites: Geology, v. 47, p. 127–130.

Vandekerkhove, E., Van Daele, M., Praet, N., Cnudde, V., Haeussler, P.J., and De Batist, M., 2020, Flood-triggered versus earthquake-triggered turbidites: A sedimentological study in clastic lake sediments (Eklutna Lake, Alaska): Sedimentology, v. 67, p. 364–389.

Vo, A., 2018, Multiproxy approach to reconstructing a paleoseismology record for Lake Crescent, Washington, USA.

Vos, P.C., and de Wolf, H., 1993, Diatoms as a tool for reconstructing sedimentary environments in coastal wetlands; methodological aspects: Hydrobiologia, v. 269–270, p. 285–296, doi:10.1007/BF00028027.

Walton, M.A.L., Staisch, L.M., Dura, T., Pearl, J.K., Sherrod, B., Gomberg, J., Engelhart, S., Tréhu, A., Watt, J., and Perkins, J., 2021, Toward an integrative geological and geophysical view of Cascadia subduction zone earthquakes: Annual Review of Earth and Planetary Sciences, v. 49, p. 367–398.

Wilhelm, B., Sabatier, P., and Arnaud, F., 2015, Is a regional flood signal reproducible from lake sediments? Sedimentology, v. 62, p. 1103–1117.

Wirth, E.A., Grant, A., Marafi, N.A., and Frankel, A.D., 2021, Ensemble ShakeMaps for magnitude 9 earthquakes on the Cascadia subduction zone: Seismological Research Letters, v. 92, p. 199–211.

Table 1. Grain size and diatom analysis summary

POSSIBLE SOURCE SEDIMENT								
				Benthic subgroups			Mean grain size (phi)	D50 (phi)
Sample name	Depth (cm)	Benthic (all)	Planktonic	Delta	Terrestrial	Lake Benthic		
Umbrella Creek	0-1	91.53	2.28	2.28	51.79	37.46	--	--
BC101	0-1	67.00	24.92	15.49	19.87	31.65	3.32	3.32
BC102	0-1	59.06	28.52	14.09	17.11	27.85	5.22	5.22
BC103	0-1	18.24	75.90	2.61	1.95	13.68	5.73	5.73
BC104	0-1	43.05	44.37	6.29	7.62	29.14	5.73	5.73
BC105	0-1	22.44	73.93	3.30	3.96	15.18	5.68	5.68
BC106	0-1	24.41	65.89	2.68	3.34	18.39	6.37	6.36
BC107	0-1	41.44	42.04	7.21	13.21	21.02	3.87	4.5
BC108	0-1	31.43	54.92	4.44	3.17	23.81	4.28	4.28
BC109	0-1	35.62	50.33	4.58	4.25	26.80	5.22	5.22

TURBIDITES								
				Benthic subgroups			Mean grain size (phi)	D50 (phi)
VC49 E1	Depth (cm)	Benthic (all)	Planktonic	Delta	Terrestrial	Lake Benthic		
	49-50	11.69	81.49	1.30	0.65	9.74	7.11	6.98
	50-51	9.55	84.71	0.96	0.96	7.64	6.98	6.83
	51-52	12.14	80.51	0.96	1.60	9.58	6.69	6.52
	52-53	--	--	--	--	--	6.59	6.54
	53-54	--	--	--	--	--	--	6.41
	54-55	9.00	81.99	0.32	1.29	7.40	6.67	6.56
	55-56	--	--	--	--	--	6.60	6.50
	56-57	--	--	--	--	--	6.58	6.50
	57-58	--	--	--	--	--	6.29	6.31
	58-59	25.25	62.13	2.33	2.66	20.27	6.24	6.23
	59-60	--	--	--	--	--	6.43	6.41
	60-61	--	--	--	--	--	6.46	6.48
	61-62	--	--	--	--	--	6.43	6.47
	62-63	14.47	73.36	0.99	1.64	11.84	6.07	5.98

63-64	18.36	69.18	3.28	1.31	13.77	5.72	5.64
64-65	24.17	65.23	2.98	1.32	19.87	5.03	4.39
65-66	28.16	59.22	6.80	1.62	19.74	5.02	4.63
67-68	17.32	74.18	2.61	1.63	13.07	4.17	2.88
68-69	33.66	52.75	8.74	4.53	20.39	3.56	2.13
69-70	45.07	44.74	17.11	3.29	24.67	3.62	2.11
70-71	17.16	75.25	2.31	0.99	13.86	6.86	6.90
71-72	7.82	86.64	0.00	0.98	6.84	7.21	7.14
72-73	15.41	76.72	1.64	0.66	13.11	6.96	7.13

				Benthic subgroups			Mean grain size	D50 (phi)
VC49 E2	Depth (cm)	Benthic (all)	Planktonic	Delta	Terrestrial	Lake Benthic	(phi)	
	104-105	15.86	77.35	1.94	1.94	11.97	--	--
	105-106	16.77	74.68	3.80	0.95	12.03	--	--
	106-107	25.74	65.02	3.96	1.65	20.13	7.20	7.20
	107-108.2	21.64	67.87	1.64	3.93	16.07	7.13	7.13
	108.2-108.5	18.09	75.33	2.96	0.33	14.80	7.20	7.20
	108.5-109	20.65	68.71	4.52	0.97	15.16	6.80	6.81
	109-110	22.44	70.83	4.17	1.60	16.67	6.99	6.87
	110-111	16.56	72.93	1.59	1.91	13.06	7.02	6.86
	111-112	30.07	58.82	7.52	2.61	19.93	7.00	6.86
	112-113	--	--	--	--	--	6.86	6.72
	113-114	--	--	--	--	--	6.80	6.71
	114-115	--	--	--	--	--	6.71	6.63
	115-116	35.53	48.68	8.55	4.93	22.04	6.68	6.58
	116-117	--	--	--	--	--	6.23	6.14
	117-118	--	--	--	--	--	6.02	6.06
	118-119	--	--	--	--	--	5.97	5.95
	119-120	33.22	52.82	5.98	3.99	23.26	5.82	5.85
	120-121	--	--	--	--	--	5.43	5.18
	121-122	--	--	--	--	--	--	5.41
	122-123	--	--	--	--	--	5.32	5.03
	123-124	45.03	41.06	7.28	4.97	32.78	5.37	5.18
	124-125	20.33	71.48	6.23	1.64	12.46	5.00	4.38

125-126	25.82	65.03	8.17	1.63	16.01	4.47	3.36
126-127	25.08	64.69	7.59	1.32	16.17	3.81	2.42
127-128	58.86	30.63	22.22	4.20	32.43	3.75	2.35
128-129	12.78	83.39	0.64	0.64	11.50	5.71	6.34
129-130	24.12	64.63	2.25	1.61	20.26	7.21	7.13
130-131	15.43	77.17	4.82	0.32	10.29	7.26	7.24
131-132	10.49	84.59	1.64	0.33	8.52	7.19	7.04

				Benthic subgroups			Mean grain size	D50 (phi)
VC43 E1	Depth (cm)	Benthic (all)	Planktonic	Delta	Terrestrial	Lake Benthic	(phi)	
	16-17	9.94	86.02	1.24	1.24	7.45	6.77	6.81
	17-18	10.10	77.52	1.63	1.30	7.17	6.65	6.68
	18-19	13.27	77.02	1.29	1.62	10.36	6.35	6.48
	19-20	--	--	--	--	--	5.85	5.73
	20-21	14.79	72.67	0.32	1.93	12.54	5.71	5.54
	21-22	--	--	--	--	--	5.57	5.43
	22-23	18.69	66.23	1.64	2.30	14.75	4.82	4.41
	23-24	14.19	72.26	1.61	1.29	11.29	5.38	5.34
	24-25	16.99	74.51	2.61	1.31	13.07	5.08	4.78
	25-26	18.79	75.16	0.64	0.64	17.52	6.16	6.28

				Benthic subgroups			Mean grain size	D50 (phi)
VC43 E2	Depth (cm)	Benthic (all)	Planktonic	Delta	Terrestrial	Lake Benthic	(phi)	
	45-46	--	--	--	--	--	6.72	6.79
	46-47	8.70	84.47	0.31	0.62	7.76	6.65	6.73
	47-48	12.86	81.03	0.64	0.64	11.58	6.46	6.52
	48-49	13.68	78.42	1.22	0.30	12.16	5.44	5.18
	49-50	--	--	--	--	--	5.26	5.00
	50-51	21.90	63.40	3.27	0.33	18.30	3.66	3.42
	51-52	--	--	--	--	--	--	--
	52-53	14.07	73.35	0.60	1.80	11.68	4.38	3.80
	53-54	11.36	75.65	2.27	0.97	8.12	4.37	3.86
	54-55	5.14	88.10	0.96	0.00	4.18	6.53	6.56
	55-56	9.91	80.50	0.31	0.93	8.67	--	

VC43 E3	Depth (cm)	Benthic (all)	Planktonic	Benthic subgroups			Mean grain size (phi)	D50 (phi)
				Delta	Terrestrial	Lake Benthic		
	78-79	9.41	75.00	2.35	0.00	7.06	6.63	6.69
	79-80	13.28	75.00	2.34	0.26	10.68	6.67	6.73
	80-81	17.22	70.00	3.33	0.56	13.33	5.84	5.68
	81-82	--	--	--	--	--	4.86	4.47
	82-83	15.77	72.68	2.25	1.13	12.39	5.03	4.72
	83-84	15.21	71.83	2.25	0.85	12.11	5.11	4.86
	84-85	11.42	82.41	0.93	1.23	9.26	5.09	4.93
	85-86	11.14	82.00	3.14	0.29	7.71	5.54	5.76
	86-87	10.67	83.43	1.12	1.12	8.43	6.62	6.71
	86-88	--	--	--	--	--	6.57	6.65

VC43 E4	Depth (cm)	Benthic (all)	Planktonic	Benthic subgroups			Mean grain size (phi)	D50 (phi)
				Delta	Terrestrial	Lake Benthic		
	104-105	13.76	78.59	0.61	1.53	11.62	6.60	6.65
	105-106	7.85	87.01	0.00	0.00	7.85	6.01	6.12
	106-107	15.45	77.88	1.21	0.91	13.33	6.56	6.61
	107-108	16.67	77.36	0.94	0.94	14.78	6.52	6.57
	108-109	16.50	74.11	1.62	0.65	14.24	6.52	6.57
	109-110	11.59	79.47	2.65	0.33	8.61	6.50	6.66
	110-111	14.01	74.27	1.30	0.33	12.38	6.12	6.10
	111-112	27.92	55.52	2.92	1.30	23.70	5.30	5.08
	112-113	20.85	71.00	0.91	2.72	17.22	4.63	4.33
	113-114	23.08	68.64	2.07	1.48	19.53	4.00	3.60
	114-115	24.76	62.06	2.25	2.57	19.94	4.33	3.86
	115-116	22.40	68.51	0.65	1.30	20.45	4.44	3.95
	116-117	16.41	74.92	0.62	4.33	11.46	4.44	3.83
	117-118	9.66	82.24	0.62	0.00	9.03	5.09	4.99
	118-119	14.05	77.78	1.63	0.00	12.42	6.31	6.43
	119-120	7.43	87.31	0.31	0.00	7.12	6.64	6.67
	120-121	13.92	78.80	0.63	0.00	13.29	6.64	6.71

VC43 E5	Depth (cm)	Benthic (all)	Planktonic	Benthic subgroups			Mean grain size (phi)	D50 (phi)
				Delta	Terrestrial	Lake Benthic		
	142-143	7.42	84.52	0.00	0.97	6.45	6.69	6.78
	143-144	7.40	82.32	0.96	0.32	6.11	6.44	6.59
	144-145	11.11	81.05	0.33	1.63	9.15	5.96	7.03
	145-146	19.28	68.37	1.81	2.11	15.36	--	--
	146-147	--	--	--	--	--	5.78	5.65
	147-148	15.41	76.72	0.98	0.66	13.77	5.36	5.08
	148-149	--	--	--	--	--	5.22	4.94
	149-150	--	--	--	--	--	5.15	4.85
	150-151	--	--	--	--	--	4.89	4.53
	151-152	--	--	--	--	--	4.49	3.77
	152-153	15.11	78.78	0.96	0.00	14.15	4.46	3.71
	153-154	11.53	81.62	0.62	0.31	10.59	4.68	4.13
	154-155	11.21	81.93	0.31	0.31	10.59	3.75	3.11
	155-156	12.89	78.93	1.26	0.31	11.32	6.52	6.65

VC46 E1	Depth (cm)	Benthic (all)	Planktonic	Benthic subgroups			Mean grain size (phi)	D50 (phi)
				Delta	Terrestrial	Lake Benthic		
	7-8	--	--	--	--	--	6.93	7.02
	8-9	9.21	84.44	0.00	1.27	7.94	7.00	7.05
	9-10	6.82	89.61	0.00	0.00	6.82	6.99	7.07
	10-11	--	--	--	--	--	6.95	7.05
	11-12	9.90	84.03	0.00	0.00	9.90	6.98	7.08
	12-13	13.13	77.19	0.00	0.63	12.50	7.13	7.20
	13-14	7.08	86.77	0.00	0.62	6.46	7.02	7.10
	14-15	--	--	--	--	--	7.06	7.14

VC46 E3	Depth (cm)	Benthic (all)	Planktonic	Benthic subgroups			Mean grain size (phi)	D50 (phi)
				Delta	Terrestrial	Lake Benthic		
	41-42	--	--	--	--	--	6.99	7.10
	42-43	11.53	82.24	0.62	0.00	10.90	6.94	7.14
	43-44	12.22	82.64	0.64	0.00	11.58	6.91	7.15
	44-45	14.65	74.20	0.96	0.00	13.69	6.94	7.09
	45-46	--	--	--	--	--	6.90	7.08

46-47	13.36	79.48	0.98	0.00	12.38	6.88	7.03
47-48	8.65	79.17	0.00	0.00	8.65	6.80	7.00
48-49	13.18	82.32	2.89	0.00	10.29	6.95	7.07
49-50	12.15	83.18	0.31	0.00	11.84	6.74	6.86
50-51	--	--	--	--	--	6.86	6.97

				Benthic subgroups			Mean grain size	D50 (phi)
VC46 E4	Depth (cm)	Benthic (all)	Planktonic	Delta	Terrestrial	Lake Benthic	(phi)	
	61-62	10.44	82.91	0.32	0.63	9.49	6.78	6.97
	62-63	6.85	80.69	0.00	0.00	6.85	6.80	7.01
	63-64	19.43	71.02	0.32	0.64	18.47	7.08	7.22
	64-65	8.39	79.50	0.31	0.31	7.76	6.87	7.04
	65-66	12.30	76.34	1.26	0.95	10.09	6.46	6.79
	66-67	13.42	78.27	0.32	0.96	12.14	6.35	6.72
	67-68	15.00	79.41	0.59	0.00	14.41	6.39	6.73
	68-69	6.13	88.06	0.00	1.61	4.52	6.58	6.86

				Benthic subgroups			Mean grain size	D50 (phi)
VC46 E5	Depth (cm)	Benthic (all)	Planktonic	Delta	Terrestrial	Lake Benthic	(phi)	
	83-84	4.13	86.03	0.00	0.00	4.13	6.47	6.79
	84-85	6.65	82.48	0.00	0.00	6.65	6.21	6.55
	85-86	12.89	73.90	0.00	0.00	12.89	6.61	6.89
	86-87	16.67	75.16	0.00	0.00	16.67	6.38	6.67
	87-88	4.78	85.67	0.00	0.00	4.78	6.35	6.57
	88-89	11.75	83.17	0.00	0.00	11.75	6.23	6.56

				Benthic subgroups			Mean grain size	D50 (phi)
VC46 E6	Depth (cm)	Benthic (all)	Planktonic	Delta	Terrestrial	Lake Benthic	(phi)	
	123-124	--	--	--	--	--	6.50	6.68
	124-125	12.75	75.82	1.31	1.31	10.13	6.13	6.45
	125-126	7.77	79.94	0.32	0.32	7.12	6.64	6.75
	126-127	3.58	86.64	0.65	0.00	2.93	6.09	6.45
	127-128	10.42	80.78	0.98	0.33	9.12	6.21	6.51
	128-129	--	--	--	--	--	6.83	6.92

FLOOD DEPOSITS								
				Benthic subgroups			Mean grain size (phi)	D50 (phi)
BC-02	Depth (cm)	Benthic (all)	Planktonic	Delta	Terrestrial	Lake Benthic		
Flood	24	19.58	65.36	1.51	1.20	16.87	6.76	7.00
Turbidite cap	34	13.66	76.71	0.31	0.00	13.35	5.99	6.16
Flood	44.5	13.89	77.16	1.85	0.62	11.42	6.98	7.22

APPENDIX A: Supplemental for Chapter 2

OxCal Code:

```
Plot("Hidden Lagoons Phase model 8")
 {
  //4 outlier ages, sample HL-27 317–318 placed ABOVE contact C
  Sequence("27 radiocarbon dates")
  {
   Boundary("start");
   Phase("BEFORE event D")
   {
    R_Date("19HL-17,395.5",3990,15);
   };
   Date("EVENT D",Event D);
   Phase("AFTER event D")
   {
    R_Date("19HL-27, 368–369",3810,130);
    R_Date("19HL-27, 372-373",3730,20);
    R_Date("19HL-17, 380",3730,20);
    R_Date("19HL-17, 352.5–355",3060,15);
   };
   Phase("BEFORE event C")
   {
    R_Date("19HL-30, 346–347",2550,20);
    R_Date("19HL-22, 352-353",2500,20);
    {
     Outlier();
    };
   };
   Date("EVENT C");
   Phase("AFTER event C")
   {
    R_Date("19HL-22, 351-352",2490,20);
    R_Date("19HL-30, 324–326",2430,20);
    R_Date("19HL-27, 317-318cm",2360,25)
    R_Date("19HL-12, 337–339",2290,20);
    R_Date("19HL-27, 315-316cm",2100,25);
   };
   R_Date("19HL-17, 302",2270,15)
   {
    Outlier();
   };
   R_Date("19HL-22, 309",1740,20);
   Phase("BEFORE event B")
   {
    R_Date("19HL-31, 56–58",1000,60);
```

```
 R_Date("19Hl-27, 125-126",1000,20);
 R_Date("19HL-10, 127",920,20);
 R_Date("19HL-32, 110–111",915,15);
 R_Date("19HL-29, 100-102",905,20);
 R_Date("19HL-22, 131-132",880,20)
 {
  Outlier();
 };
};
Date("EVENT B");
Phase("AFTER event B")
{
 R_Date("19Hl-27, 123.5-124.5",1040,20)
 {
  Outlier();
 };
 R_Date("19HL-32, 109–110",1030,20)
 {
  Outlier();
 };
 R_Date("19HL-29, 95-98",915,20);
 R_Date("19HL-17, 143–147",880,15);
 R_Date("19HL-22, 130-131",840,20);
 R_Date("19HL-12, 144–147",825,20);
 R_Date("19HL-19, 78-84",410,20);
};
Boundary("end");
};
};
```

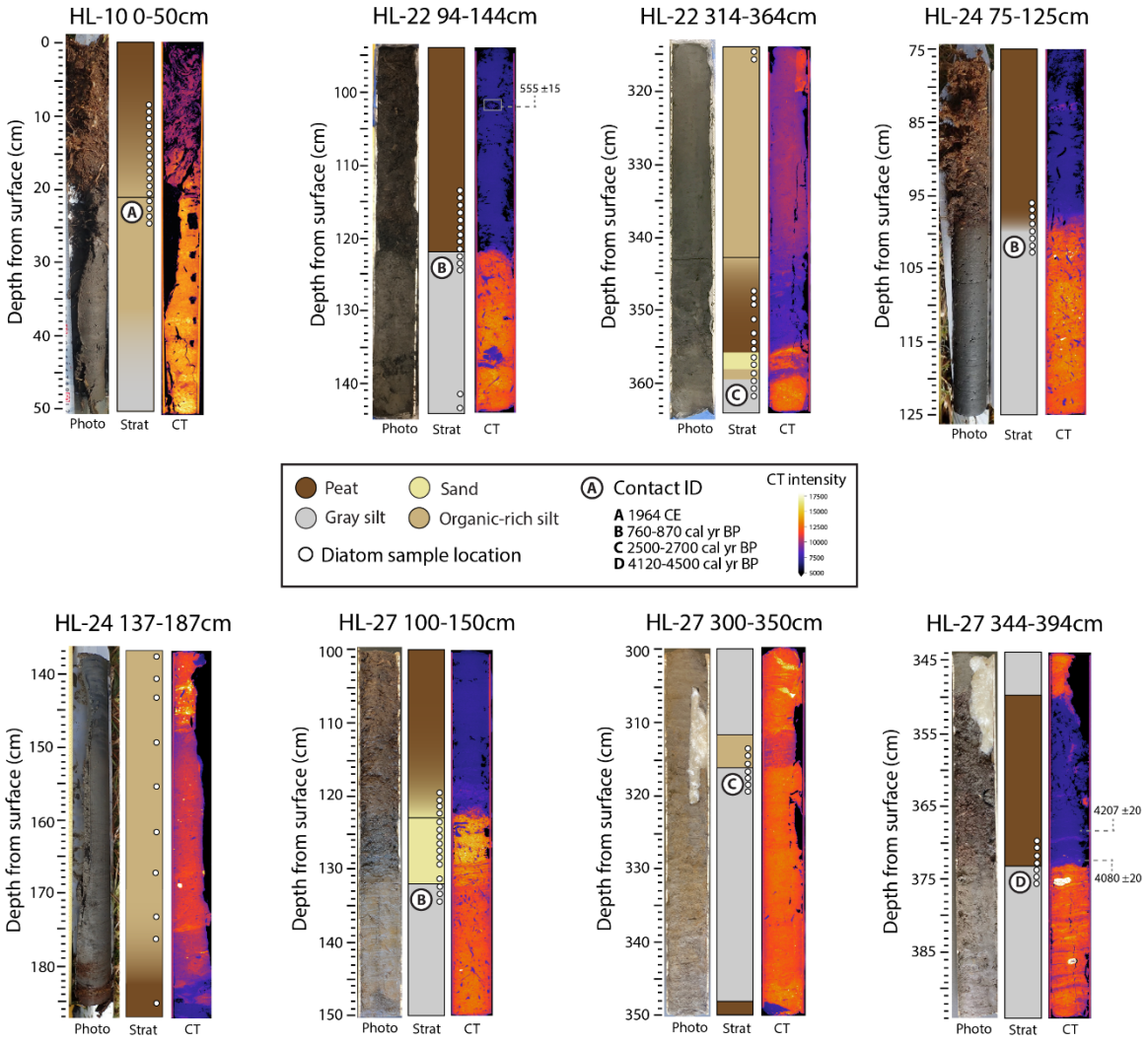

Figure S1. Photograph, cartoon stratigraphy, and CT scans for each 50-cm core sampled at Hidden Lagoons. White circles represent diatom sampling locations.

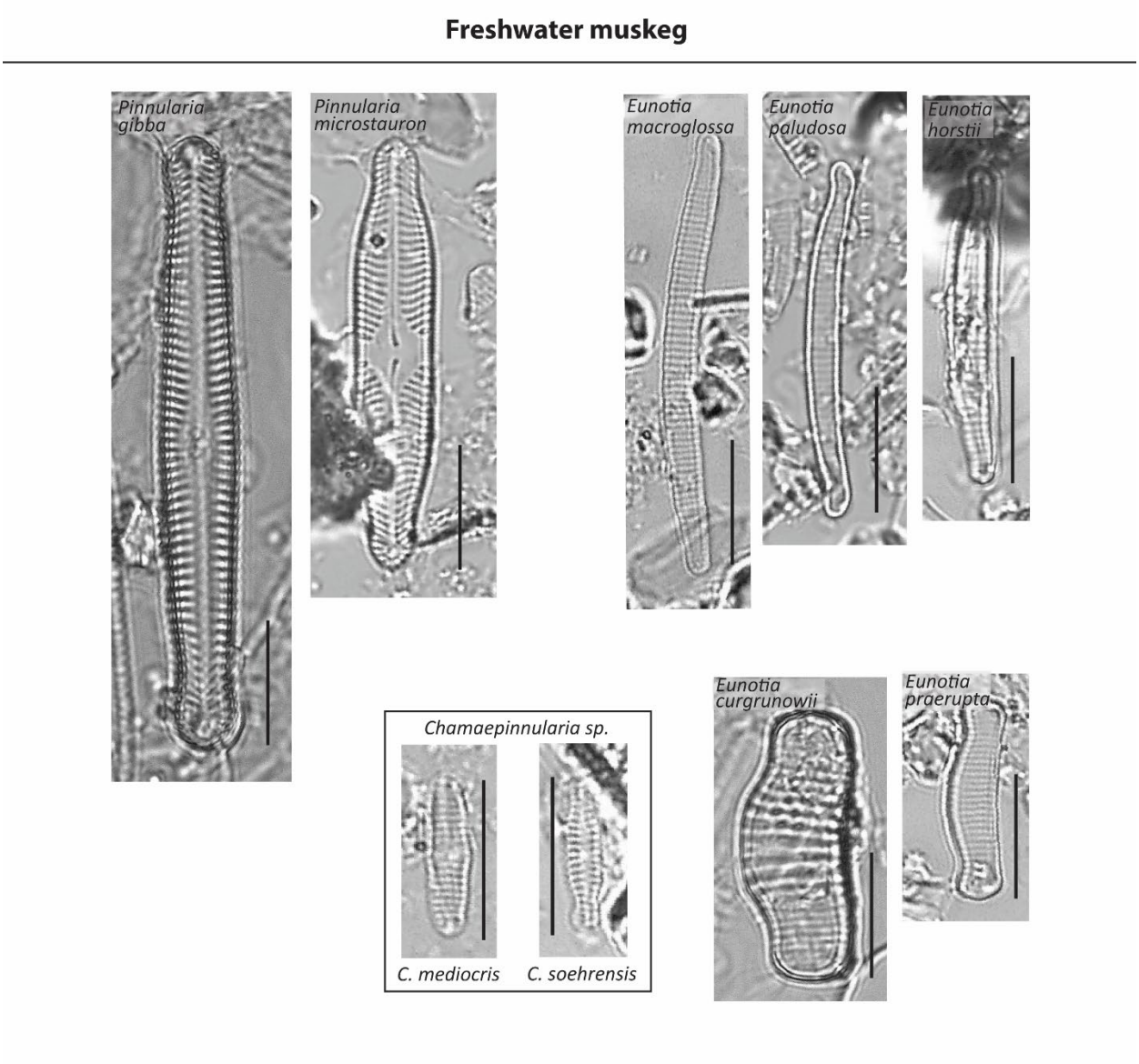

Figure S2. Diatom plate for prominent species within the freshwater muskeg ecological group.

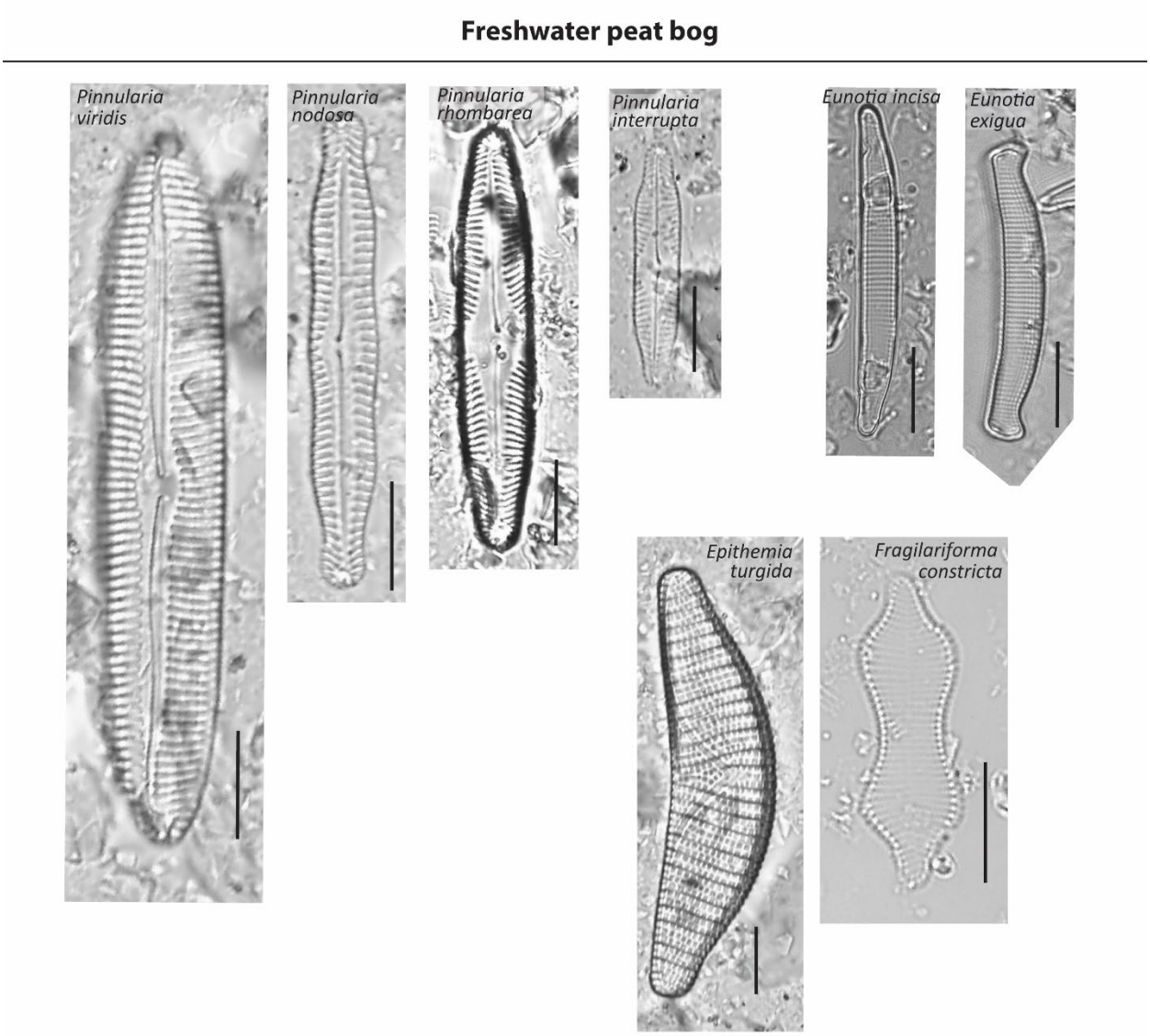

Figure S3. Diatom plate for prominent species within the freshwater peat bog ecological group.

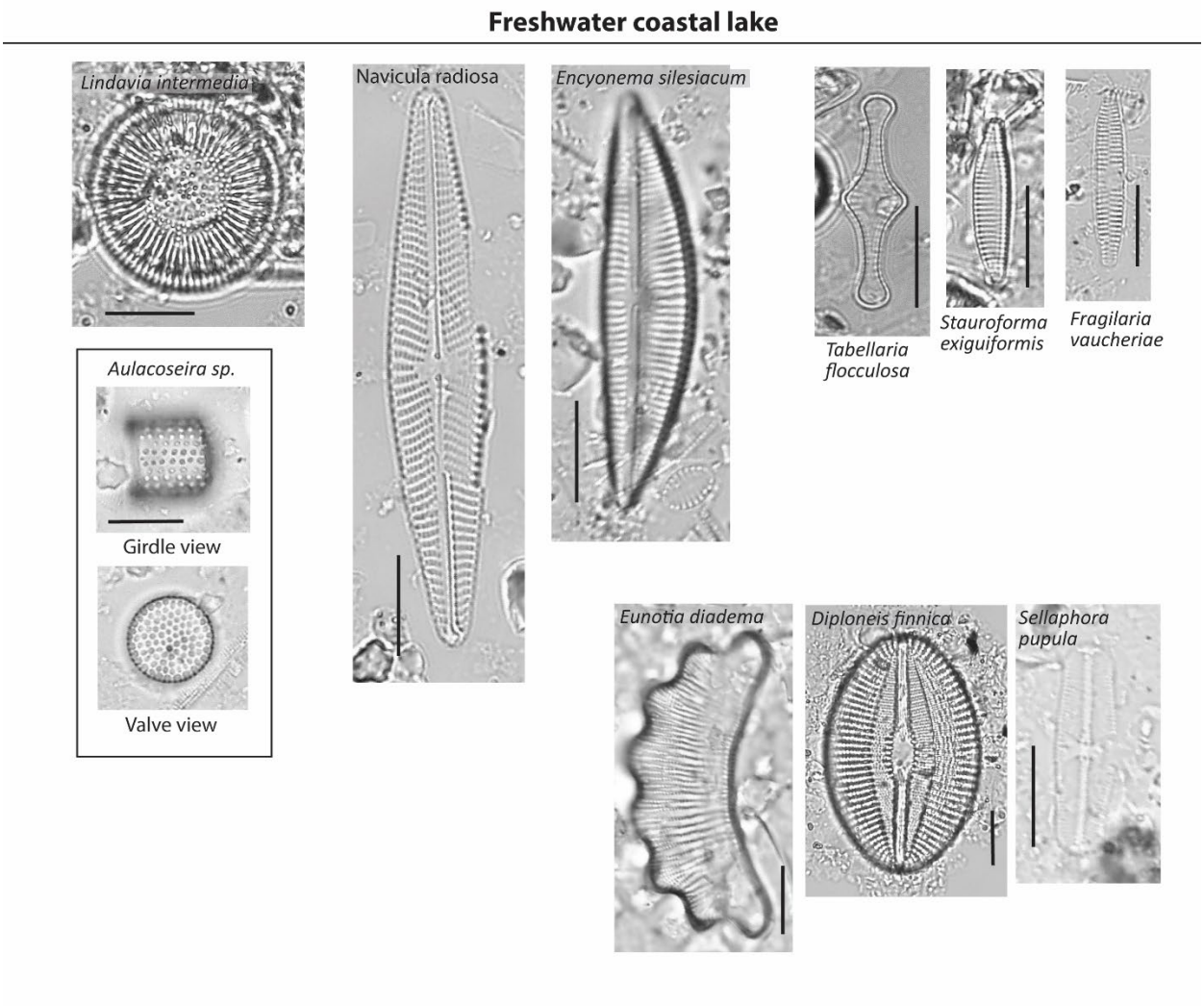

Figure S4. Diatom plate for prominent species within the freshwater coastal lake ecological group.

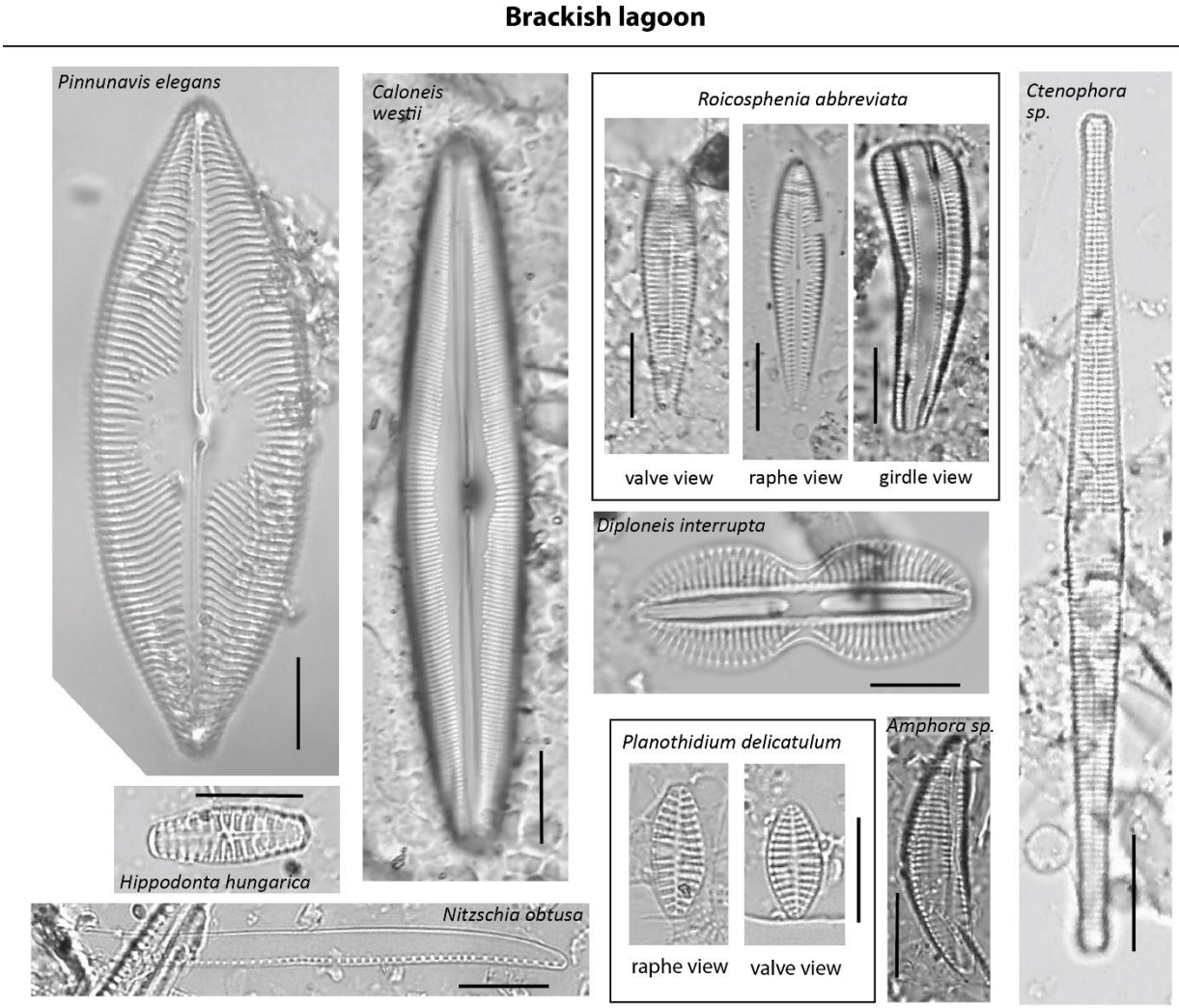

Figure S5. Diatom plate for prominent species within the brackish lagoon ecological group.

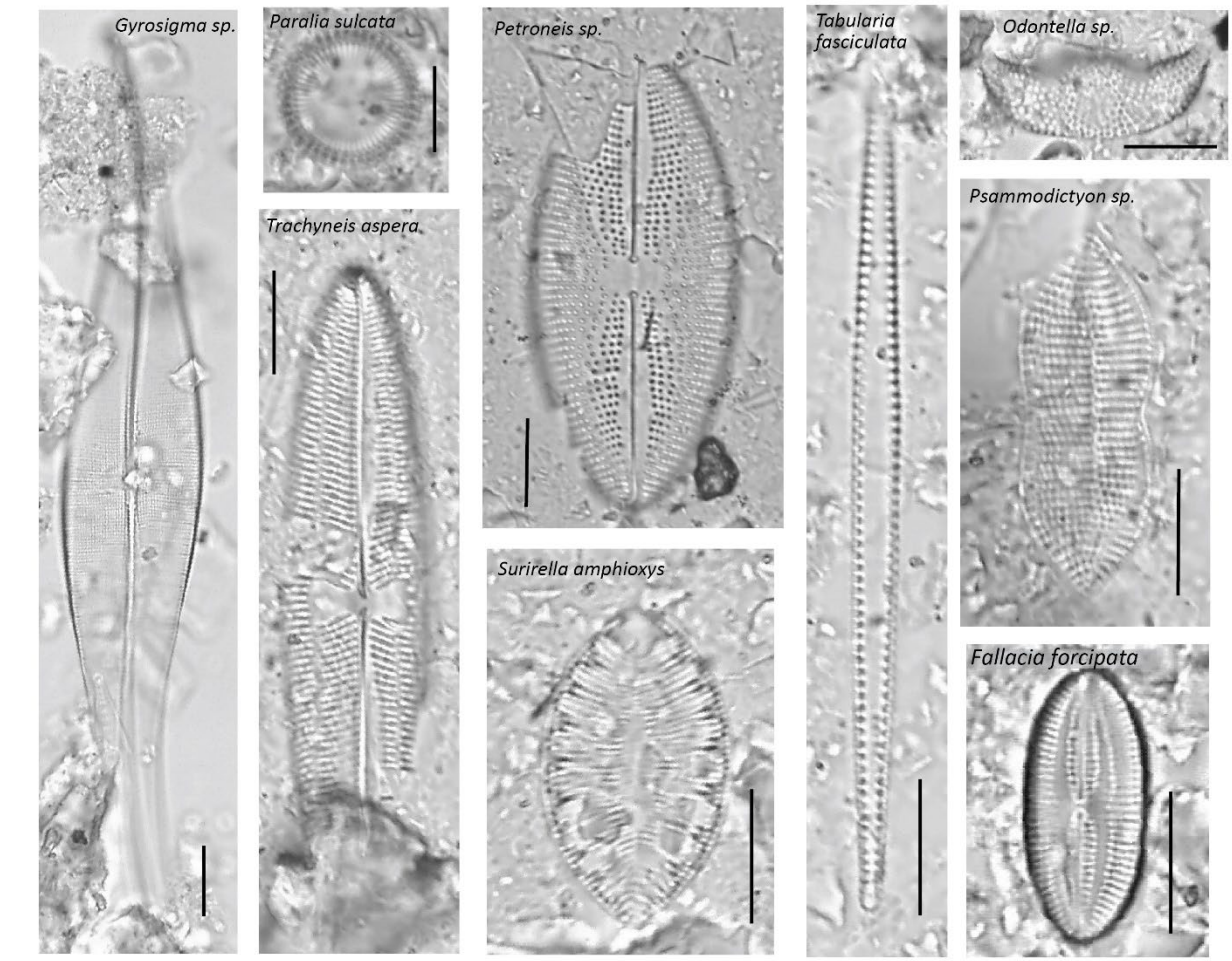

Figure S6. Photograph, cartoon stratigraphy, and CT scans for a) HL-22 Contact B, b) HL-24 Contact B, c) HL-27 Contact C, and d) HL-24 Between contacts B and C. The results of the unweighted pair-group average (UPGMA) cluster analysis are shown to the right of the stratigraphy. The red dotted lines indicate the location of inferred diatom species shift. Results of detrended correspondence analysis (DCA) are shown on the far right. Samples that contain similar diatom assemblages and abundances are grouped together. Trend direction is indicated with dashed black arrows.

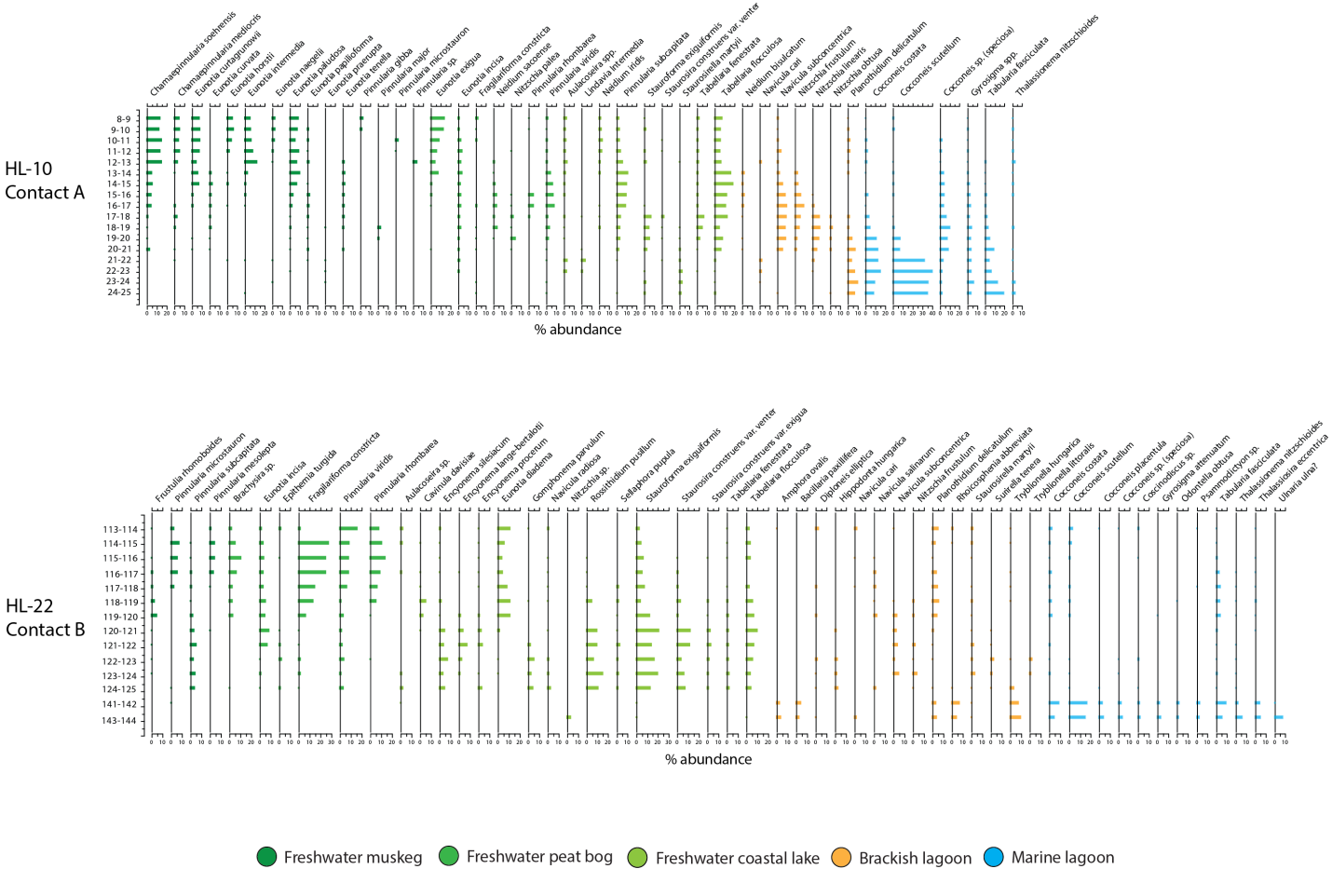
HL-10
Contact A
HL-22
Contact B
% abundance
% abundance
Freshwater muskeg
Freshwater peat bog
Freshwater coastal lake
Brackish lagoon
Marine lagoon

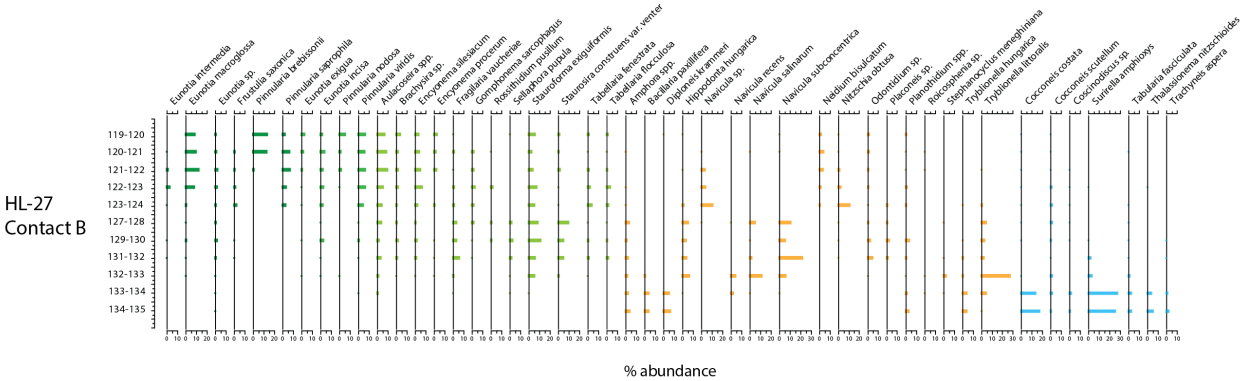
HL-27
Contact B
Eunotia intermedia
Eunotia macroglossa
Eunotia sp.
Frustulia saxonica
Pinnularia bredaisonii
Pinnularia saprophila
Eunotia exigua
Eunotia incisa
Pinnularia nodosa
Pinnularia viridis
Aulacoseira spp.
Brachysira sp.
Encyonema dilesiacum
Encyonema prcerum
Fragilaria vaucheriae
Gomphonema sarcophagus
Rossithidium pusillum
Sellaphora pupula
Staurosira construens var.venter
Staurosirella exiguiformis
Tabellaria fenestrata
Tabellaria flocculosa
Amphora spp.
Bacillaria paxillifera
Diploneis krammeri
Hippodonta hungarica
Mastogloia sp.
Navicula spp.
Navicula recens
Navicula salinarum
Navicula subconcentrica
Nedium bisulcatum
Nitzschia obtusa
Odontidium sp.
Placoneis sp.
Planothidium spp.
Rhoicosphenia sp.
Stephanocyclus meneghiniana
Tryblionella hungarica
Tryblionella litoralis
Cocconeis costata
Cocconeis scutellum
Cosmioneis sp.
Surirella amphioxys
Tabularia fasciculata
Thalassionema nitzschioides
Trachyneis aspera
119-120
120-121
121-122
122-123
123-124
127-128
129-130
131-132
132-133
133-134
134-135
% abundance
HL-27
Contact C
Prestauroneis sp.
Stauroforma exiguiformis
Staurosira construens var exigua
Tabellaria flocculosa
Cocconeis placentula sensu lato
Hippodonta hungarica
Navicula lanceolata
Navicula subconcentrica
Planothidium delicatulum
Puncticostata sp.
Rhoicosphenia sp.
Tryblionella hungarica
Cocconeis costata
Cocconeis scutellum
Gyrosigma spp.
Parlia sulcata
Seminavis sp.
Tabularia fasciculata
313-314
314-315
315-316
316-317
317-318
318-319
319-320
% abundance
Freshwater muskeg
Freshwater peat bog
Freshwater coastal lake
Brackish lagoon
Marine lagoon

HL-22
Contact C

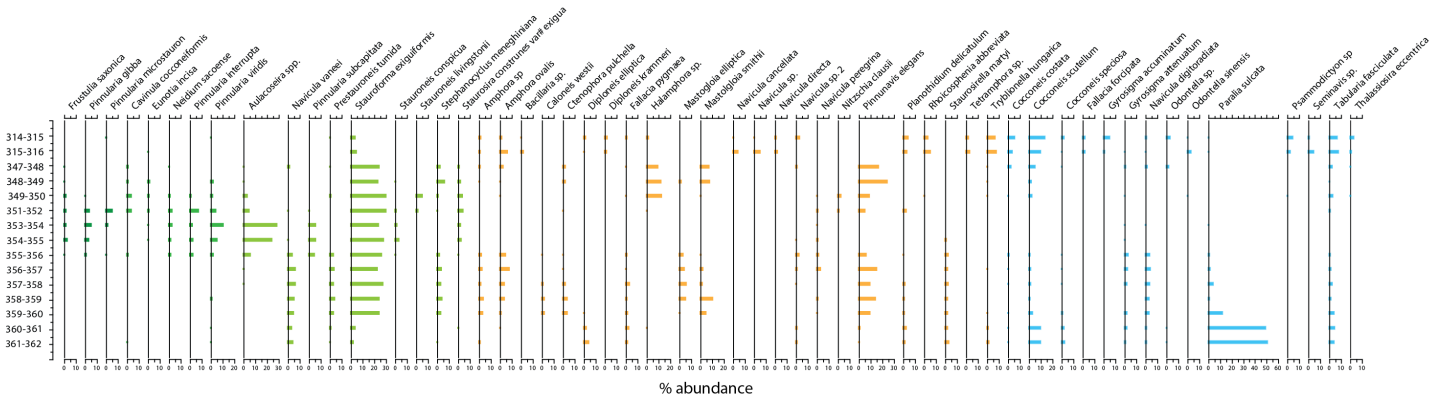

HL-24
Contact B

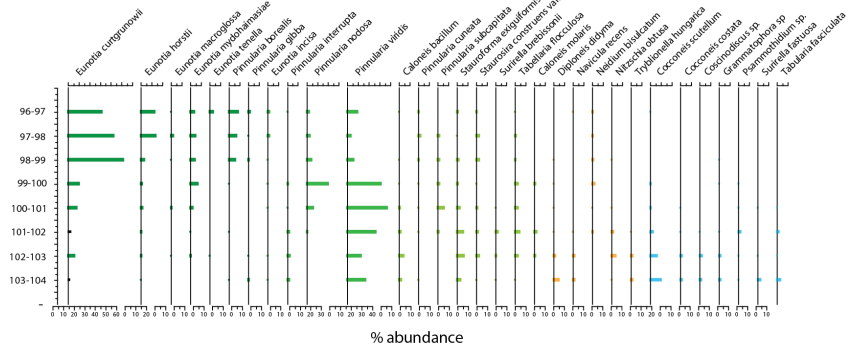

Freshwater muskeg
Freshwater peat bog
Freshwater coastal lake
Brackish lagoon
Marine lagoon

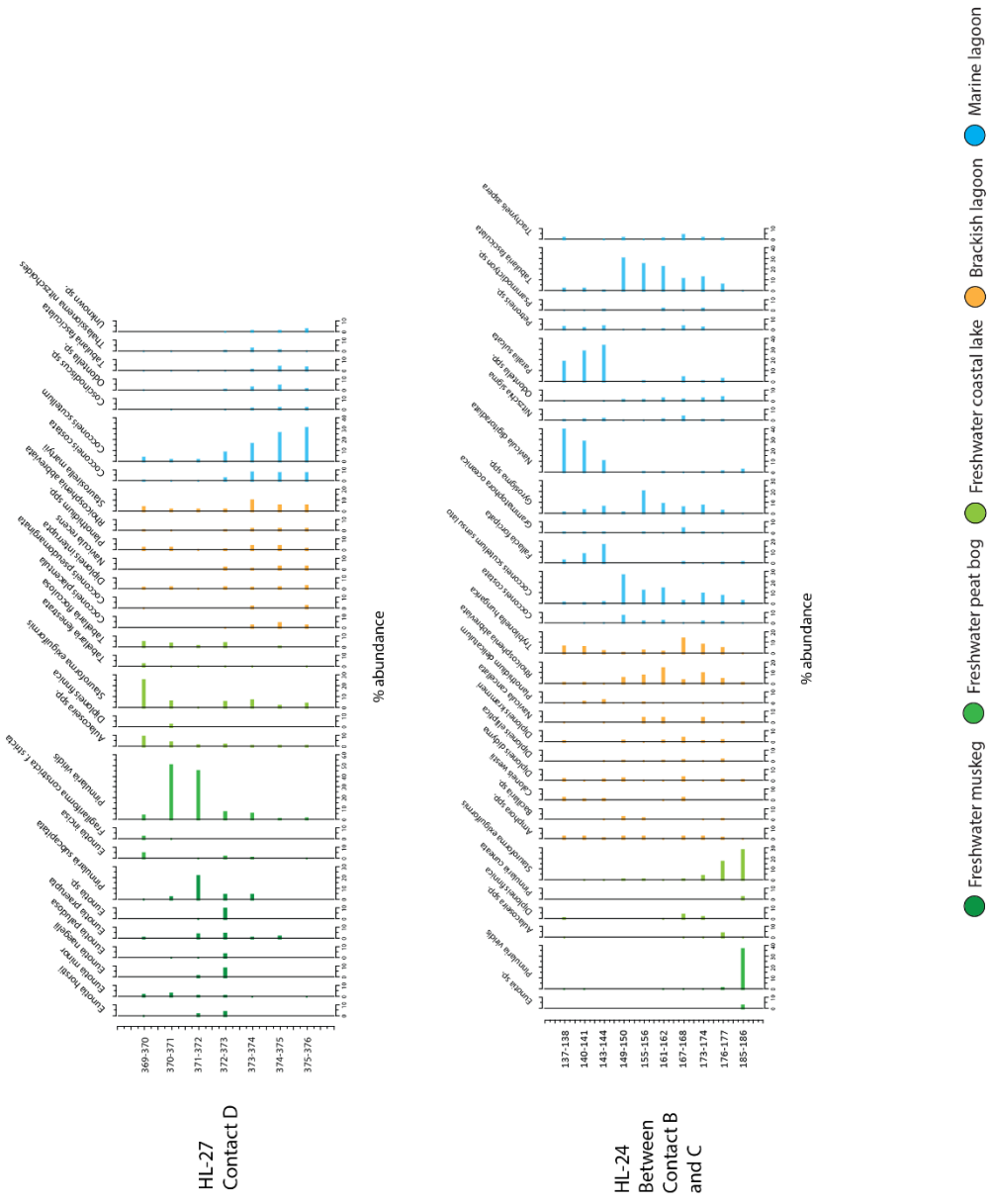

Figure S8. Full diatom ecology counts colored by ecological group for all sampled cores from Hidden Lagoons.

Table 1. Comprehensive list of the most abundant (>2%) species in each salinity group from all contacts.

Group 1: Freshwater muskeg
Chamaepinnularia mediocris
Chamaepinnularia soehrensis
Eunotia curtgrunowii
Eunotia curvata
Eunotia diadema
Eunotia horstii
Eunotia intermedia
Eunotia macroglossa
Eunotia mydohaimasiae
Eunotia minor
Eunotia naeglii
Eunotia paludosa
Eunotia papilioforma
Eunotia praerupta
Eunotia tenella
Frustulia saxonica
Frustulia rhomboides
Pinnularia borealis
Pinnularia brebissonii
Pinnularia gibba
Pinnularia major
Pinnularia mesolepta
Pinnularia microstauron
Pinnularia saprophila
Pinnularia subcapitata

Group 2: Freshwater peat bog
Brachysira sp.
Cavinula cocconeiformis
Epithemia turgida
Eunotia exigua
Eunotia incisa
Fragilariaforma constricta
Neidium sacoense
Nitzschia palea
Pinnularia interrupta
Pinnularia nodosa
Pinnularia rhombarea
Pinnularia viridis

Group 3: Freshwater coastal lake
Aulacoseira spp. (planktonic)
Caloneis bacillum
Cavinula davisiae
Diploneis finnica
Encyonema procerum
Encyonema lange-bertalotii
Encyonema silesiacum
Eunotia diadema
Fragilaria vaucheriae
Gomphonema parvulum/sarcophagus
Lindavia intermedia (planktonic)
Navicula radiosa
Navicula vaneei
Neidium iridis
Pinnularia cuneata
Prestauroneis tumida
Rossithidium pusillum
Sellaphora pupula
Stauroforma exiguiformis
Stauroneis livingstonii
Staurosira construens var. exigua
Staurosira construens var. venter
Surirella brebissonii
Tabellaria fenestrata
Tabellaria flocculosa

Group 4: Brackish lagoon
Amphora sp.
Amphora ovalis
Bacillaria sp.
Caloneis molaris
Caloneis westii
Cocconeis placentula
Cocconeis pseudomarginata
Ctenophora pulchella
Diploneis didyma
Diploneis elliptica
Diploneis interrupta
Diploneis krammeri
Fallacia pygmaea
Halamphora sp.
Hippodonta hungarica
Mastogloia elliptica
Mastogloia pumila
Mastogloia smithii
Navicula cari
Navicula cancellata
Navicula directa
Navicula peregrina
Navicula recens
Navicula salinarum
Navicula subconcentrica
Neidium bisulcatum
Nitzschia frustulum
Nitzschia linearis
Nitzschia obtusa
Odontidium sp.
Pinnunavis elegans

Placoneis sp.
Planothidium delicatulum
Punctastriata sp.
Rhoicosphenia abbreviata
Staurosirella martyii
Stephanocyclus meneghiniana (planktonic)
Surirella tenera
Tetramphora sp.
Tryblionella hungarica
Tryblionella littoralis

Group 5: Marine lagoon
Cocconeis costata
Cocconeis scutellum
Cocconeis sp. (speciosa?)
Coscinodiscus sp. (planktonic)
Fallacia forcipata
Grammatophora sp.
Gyrosigma attenuatum
Gyrosigma acuminatum
Navicula digitoradiata
Nitzschia sigma
Odontella sp. (planktonic)
Odontella sinensis
Paralia sulcata (planktonic)
Petroneis sp.
Psammodictyon sp.
Seminavis sp.
Surirella amphioxys
Surirella fastuosa
Tabularia fasciculata
Thalassionema nitzschioides (planktonic)
Thalassiosira sp.
Trachyneis aspera
Ulnaria sp.

Table 2. Diatom database reference list for all Hidden Lagoons diatoms above 2% abundance

Species	Substrate	Benthic/Planktonic	Salinity	References
Amphora ovalis	Epi	B	F	12
Amphora sp.	Epi	B	B	12
Aulacoseira sp.		P	F	11,12
Bacillaria sp.	Epi	B	E	5,10
Brachysira sp.		B	F	11
Caloneis bacillum	Epi	B	BF	3,12
Caloneis molaris	Epi	B	B	
Caloneis westii	Epi	B	BM	13
Cavinula cocconeiformis		B	F	11
Cavinula davisiae	Epi	B	F	
Chamaepinnularia mediocris	Aer	B	F	11
Chamaepinnularia soehrensis	Aer	B	F	6
Cocconeis costata	Ept	B	BM	14
Cocconeis placentula	Ept	B	BF	3,12
Cocconeis pseudomarginata	Ept	B	BF	14
Cocconeis scutellum	Ept	B	BM	3,12
Cocconeis sp. (speciosa?)	Ept	B	BM	14
Coscinodiscus sp.	Tyc	P	M	13
Ctenophora pulchella	Ept	B	BM	12
Diploneis didyma	Epi	B	B	12
Diploneis elliptica	Epi	B	B/BM	11
Diploneis finnica	Epi	B	BF	7
Diploneis interrupta	Epi	B	E	12
Diploneis krammeri/smithii	Epi	B	BM	12
Encyonema lange-bertalotii	Epi	B	F	11
Encyonema procerum	Epi	B	F	6,11
Encyonema silesiacum	Epi	B	F	11
Epithemia turgida	Ept	B	F	6,12
Eunotia curtagrunowii	Epi	B	F	14
Eunotia diadema	Epi	B	F	11
Eunotia exigua	Ept, Aer	B	F	1,2,8,12
Eunotia horstii	Epi	B	F	14
Eunotia incisa	Aer	B	F	4,9
Eunotia macroglossa	Epi	B	F	
Eunotia mydohaimasiae	Epi	B	F	
Eunotia naeglii	Epi	B	F	14
Eunotia paludosa	Aer	B	F	2,4,12
Eunotia papilioforma	Epi	B	F	14
Eunotia praerupta	Ept, Aer	B	F	2,8
Eunotia tenella	Aer	B	F	1,4
Fallacia forcipata	Epi	B	BM	13
Fallacia pygmaea	Epi	B	B	12
Fragilaria vaucheriae	Epi	B	F	9
Fragilariforma constricta	Epi	B	F	11

Frustulia saxonica	Aer	B	F	6
Gomphonema parvulum/sarcophagus	Ept	B	BF	5,12,14
Grammatophora sp.	Ept	B	M	12
Gyrosigma attenuatum	Epi	B	M/B	12
Gyrosigma gibbyae	Epi	B	B/BM	12
Halamphora sp.	Epi	B	B	10
Hippodonta hungarica	Epi	B	B	7,11
Lindavia intermedia	Epi	P	F	11
Mastogloia pumila	Epi	B	B	11
Mastogloia elliptica	Epi	B	BM	11
Mastogloia smithii	Epi	B	BM	11
Navicula cancellata	Epi	B	M	12
Navicula cari	Epi	B	B	7
Navicula digitoradiata	Epi	B	B/M	12
Navicula directa	Epi	B	M	14
Navicula peregrina	Epi	B	BM	12
Navicula radiosa	Epi	B	F	12
Navicula recens	Epi	B	B	11
Navicula salinarum	Epi	B	B	11,14
Navicula subconcentrica	Epi	B	B	14
Navicula vaneei	Epi	B	F	6
Neidium bisulcatum	Epi	B	B	14
Neidium iridis	Epi	B	F	6
Neidium sacoense		B	F	11
Nitzschia frustulum	Epi	B	E	14
Nitzschia linearis		B	FB	7
Nitzschia obtusa		B	B/BM	7
Nitzschia palea	Ept	B	F	12,13
Nitzschia sigma	Epi	B	BM	12,13
Odontella sp.	Tyc	P	M	12
Odontidium sp.		B	B	14
Paralia sulcata	Tyc	P	BM	12
Petroneis sp.	Eps	B	BM	14
Pinnularia borealis	Aer	B	F	12
Pinnularia brebessonii	Epi	B	F	14
Pinnularia cuneata	Epi	B	BF	14
Pinnularia gibba	Aer	B	F	1,7
Pinnularia interrupta	Epi	B	F	7
Pinnularia major	Epi	B	F	13,14
Pinnularia mesolepta	Epi	B	F	12
Pinnularia microstauron	Aer	B	F	1,8
Pinnularia nodosa	Epi	B	F	9
Pinnularia rhombarea	Epi	B	F	11
Pinnularia subcapitata	Aer	B	F	2,8
Pinnularia viridis	Epi	B	F	9
Pinnunavis elegans	Epi	B	B	12

Placoneis sp.	Epi	B	BF	11
Planothidium delicatulum	Eps	B	BM	6
Prestauroneis tumida		B	F	6
Psammodictyon sp.	Eps	B	M	11
Punctastriata sp.	Epi	B	B	11
Rhoicosphenia abbreviata	Ept	B	BF	12,13
Rossithidium pusillum		B	F	11
Sellaphora pupula	Epi	B	F	12
Seminavis sp.		B	M	11,14
Stauroforma exiguiformis	Epi	B	F	9
Stauroneis acidoclinata		B	F	14
Stauroneis livingstonii		B	F	11
Staurosira construens var. exigua		B	F	14
Staurosira construens var. venter		B	BF	11,12
Staurosirella martyii	Eps	B	BF	14
Stephanocyclus meneghiniana	Tyc	P	B	3,12
Surirella amphioxys	Epi	B	M	14
Surirella brebissonii	Epi	B	BF	9
Surirella fastuosa	Epi	B	BM	14
Surirella tenera	Epi	B	B	11
Tabellaria fenestrata	Ept	B/P	F	3
Tabellaria flocculosa	Ept	P	F	6
Tabularia fasciculata	Ept	B	B/BM	3
Tetramphora sp./Plagiotropis sp.	Epi	B	B	11
Thalassionema nitzschioides	Tyc	P	M	3
Trachyneis aspera	Epi	B	M	12
Tryblionella hungarica	Epi	B	B/BM	6,12
Tryblionella littoralis	Epi	B	B/BM	13
Ulnaria sp.	Epi, Tyc	B	BM	11

Key for Substrate: (Aer, aerophilous; Tyc, Tychoplanktonic; Ept, epiphytic, Epi, epipelic; Eps, epipsammic

Key for Salinity Classification: (F, freshwater; BF = oligohalobous indifferent; E = euryhaline; B = brackish; M/BM = marine or brackish-marine)

Reference Key:

(1) Beyens (1989)
(2) Carballeira et al. (2020)
(3) Dura and Hemphill-Haley (2020)
(4) Frankova et al. (2009)
(5) Foged (1981)
(6) Guiry et al. (2014)
(7) Hamilton and Shennan (2005)
(8) Lund (1946)
(9) Nelson et al. (2015)
(10) Sherrod (1999)
(11) Spaulding et al. (2021)
(12) Vos and De Wolf (1993)
(13) Witter et al. (2009)
(14) CSZ/Oregon modern associations

Ecology Key:

Freshwater muskeg
Freshwater peat bog
Freshwater coastal lake
Brackish lagoon
Marine lagoon

REFENCES CITED

Beyens, Louis. "Moss dwelling diatom assemblages from Edgeøya (Svalbard)." *Polar Biology* 9, no. 7 (1989): 423-430.

Carballeira, R., & Pontevedra-Pombal, X. (2020). Diatoms in paleoenvironmental studies of peatlands. *Quaternary*, *3*(2), 10.

Dura, T., & Hemphill-Haley, E. (2020). Diatoms in tsunami deposits. In *Geological Records of Tsunamis and Other Extreme Waves* (pp. 291-322). Elsevier.

Fránková, M. (2009). *Ecology and taxonomy of diatoms of Western Carpathian spring fens* (Doctoral dissertation, PhD Thesis, Faculty of Science Masaryk University, Brno).

Foged, N. (1981). Diatoms in Alaska. *Bibliotheca phycologica*, *53*, 1-318.

Guiry, M. D., Guiry, G. M., Morrison, L., Rindi, F., Miranda, S. V., Mathieson, A. C., ... & Garbary, D. J. (2014). AlgaeBase: an on-line resource for algae. *Cryptogamie, Algologie*, *35*(2), 105-115.

Hamilton, S., & Shennan, I. (2005). Late Holocene great earthquakes and relative sea-level change at Kenai, southern Alaska. *Journal of Quaternary Science: Published for the Quaternary Research Association*, *20*(2), 95-111.

Lund, J. W. G. (1946). Observations on soil algae. I. The ecology, size and taxonomy of British soil diatoms. *The New Phytologist*, *45*(1), 56-110.

Nelson, A. R., Briggs, R. W., Dura, T., Engelhart, S. E., Gelfenbaum, G., Bradley, L. A., ... & Kelley, K. A. (2015). Tsunami recurrence in the eastern Alaska-Aleutian arc: A Holocene stratigraphic record from Chirikof Island, Alaska. *Geosphere*, *11*(4), 1172-1203.

Nittrouer, C. A., Sternberg, R. W., Carpenter, R., & Bennett, J. T. (1979). The use of Pb-210 geochronology as a sedimentological tool: Application to the Washington continental shelf. *Marine Geology*, *31*(3–4), 297–316. https://doi.org/10.1016/0025-3227(79)90039-2

Sherrod, B. L. (1999). Gradient analysis of diatom assemblages in a Puget Sound salt marsh: can such assemblages be used for quantitative paleoecological reconstructions?. *Palaeogeography, Palaeoclimatology, Palaeoecology*, *149*(1-4), 213-226.

Spaulding, S. A., Potapova, M. G., Bishop, I. W., Lee, S. S., Gasperak, T. S., Jovanoska, E., ... & Edlund, M. B. (2021). Diatoms. org: supporting taxonomists, connecting communities. *Diatom Research*, *36*(4), 291-304.

Vos, P. C., & De Wolf, H. (1993). Diatoms as a tool for reconstructing sedimentary environments in coastal wetlands; methodological aspects. *Hydrobiologia*, *269*, 285-296.

Witter, R. C., Hemphill-Haley, E., Hart, R., & Gay, L. (2009). Tracking Prehistoric Cascadia Tsunami Deposits at Nestucca Bay, Oregon. *US Geological Survey, National Earthquake Hazards Reduction Program Final Technical Report 08HQGR0076*, *92*.

APPENDIX B: Supplemental for Chapter 3

Grain size and diatom analysis of turbidites in core VC35 (Shallow shelf)

Results

A ~73-cm-long core (VC35) was taken ~300 m from BC110 at the end of the Crooked Creek transect (Fig. S2). There are two deposits in core VC35: E1 (6 cm thick) and E2 (8 cm thick). The background lake sediment below the turbidites is composed of medium to coarse silt (mean = 5.86 φ; D50 = 5.77 φ), which is then overlain by the turbidites. The base of turbidite E1 is composed of medium silt (mean = 5.87 φ; D50 = 5.77 φ) with no considerable grain size changes from background sediments, while the base of E2 is composed of very coarse silt (mean = 4.79 φ; D50 = 4.39 φ) that fines upwards to medium silt (mean = 5.88 φ; D50 = 5.78 φ) towards the top.

The diatom assemblage of the background lake sediments below the turbidites are (~72-76%; Average = ~75%) planktonic and (15-18%; Average = ~17%) benthic species. The lake benthic subgroup is the most abundant (10-12%; Average = ~11%), while the delta and terrestrial subgroup species are much less abundant, each making up <3% in background sediments at this location.

The diatom assemblages at the base of turbidites E1 and E2 are characterized by a muted signal. The lake benthic subgroup, which significantly increases above background average in the proximal and distal basin core turbidites, exhibits a variable trend in the turbidites in VC35. The lake benthic subgroup species slightly increases (11-13%; Average = ~12%) from the background average (~11%) in E2, but exhibits a ~6% decrease from average in E1. Delta and terrestrial subgroup species increase slightly (1-3%) in E2, but remain consistent with background averages (~2-3%) in E1.

Interpretation

Core VC35 was taken as a proximal core location to the Crooked Creek transect to act as a representative of potential delta collapse/failure on the subaqueous shallow shelf similar to the motivation to collect core VC49. Our high-resolution grain size and diatom results for core VC35 show variable signatures between turbidites E1 and E2 (Fig. S2, Table S1). At E1, there is no clear difference between background sediments and the turbidite, and all benthic subgroup species remain similar to background abundances. However, grain size results at E2 show coarsening towards the base of turbidite E2 from background sediments and rapid fining upwards to medium silt. Turbidite E1 does not show any increase in grain size from the background sediments. In comparison, E1 and E2 at VC35 are much thinner and finer-grained than turbidites E1 and E2 at VC49. The sedimentary characteristics and lack of strong diatom signature might suggest a shallower and gentler delta slope overall that does not create delta destabilization with the same mechanism of the Umbrella Creek delta.

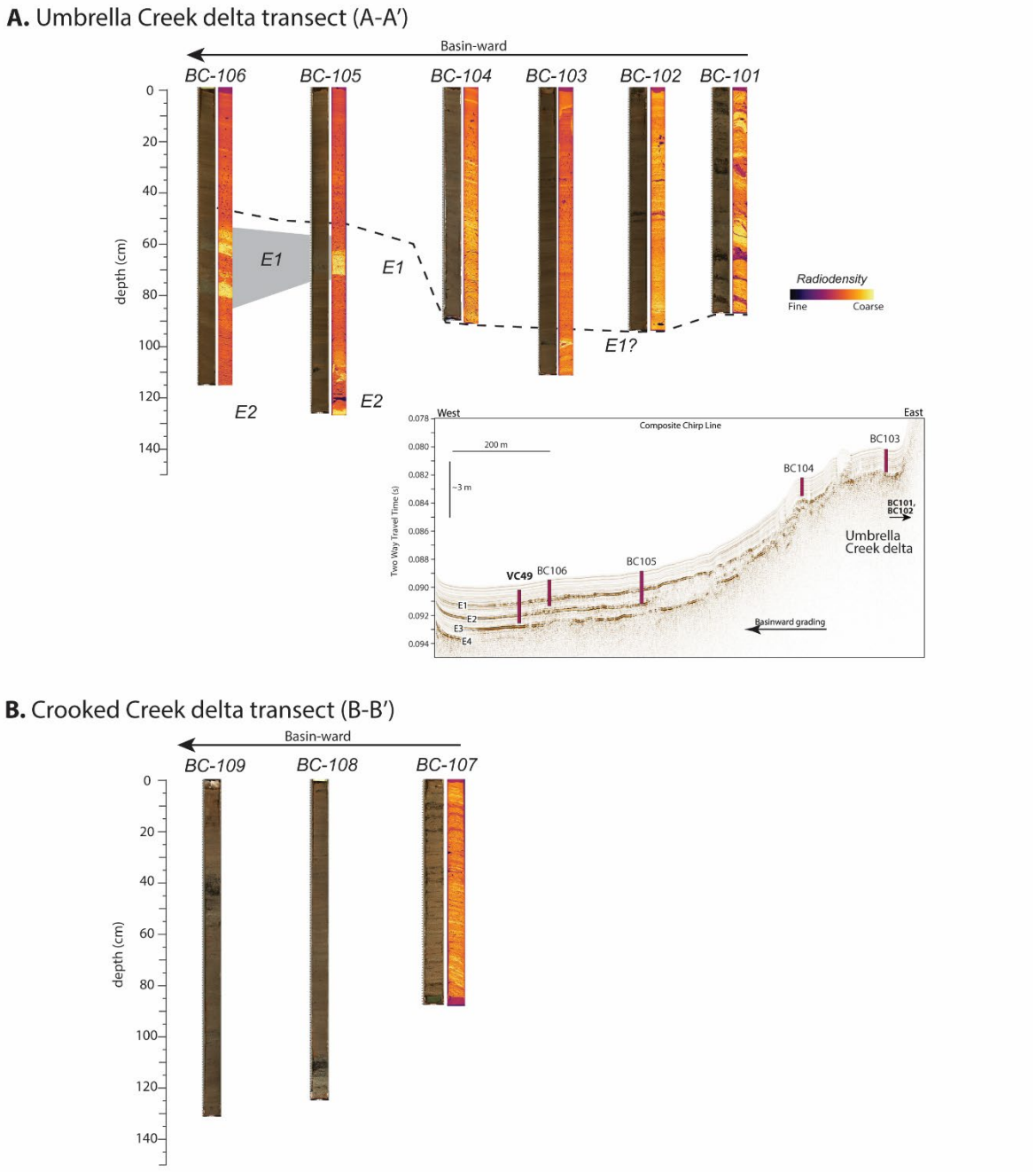

Figure S1. Full length core photograph and CT scans for the cores sampled along the a) Umbrella Creek delta transect (A-A') and b) the Crooked Creek delta transect (B-B').

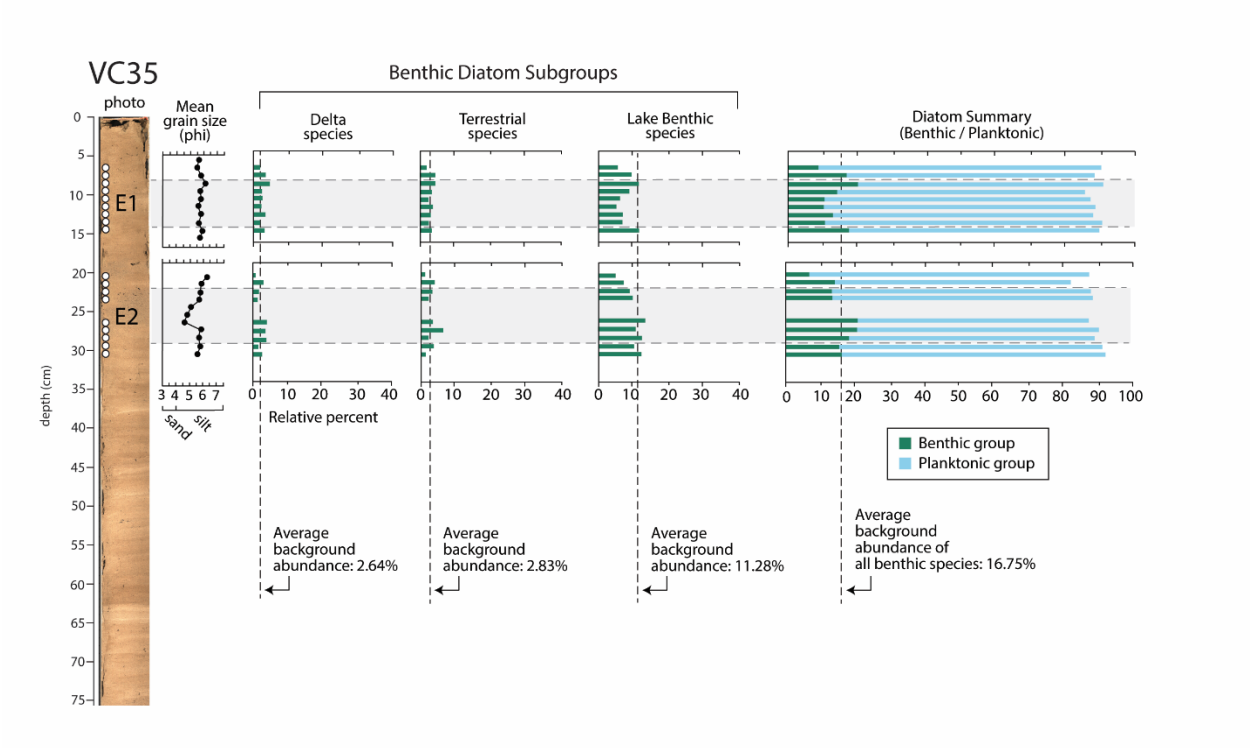

Figure S2. Photograph and CT scans for core VC35, encompassing two turbidites (E1 and E2). Diatom sample depths are shown by white circles. Mean grain size results (in phi) are shown in black circles and correlate to proper sample depths. Relative abundances of diatom analysis are organized by three ecologic subgroups (delta, terrestrial, and lake benthic) followed by a summary plot showing the total benthic (green bar) to total planktonic (blue bar) species in each sample.

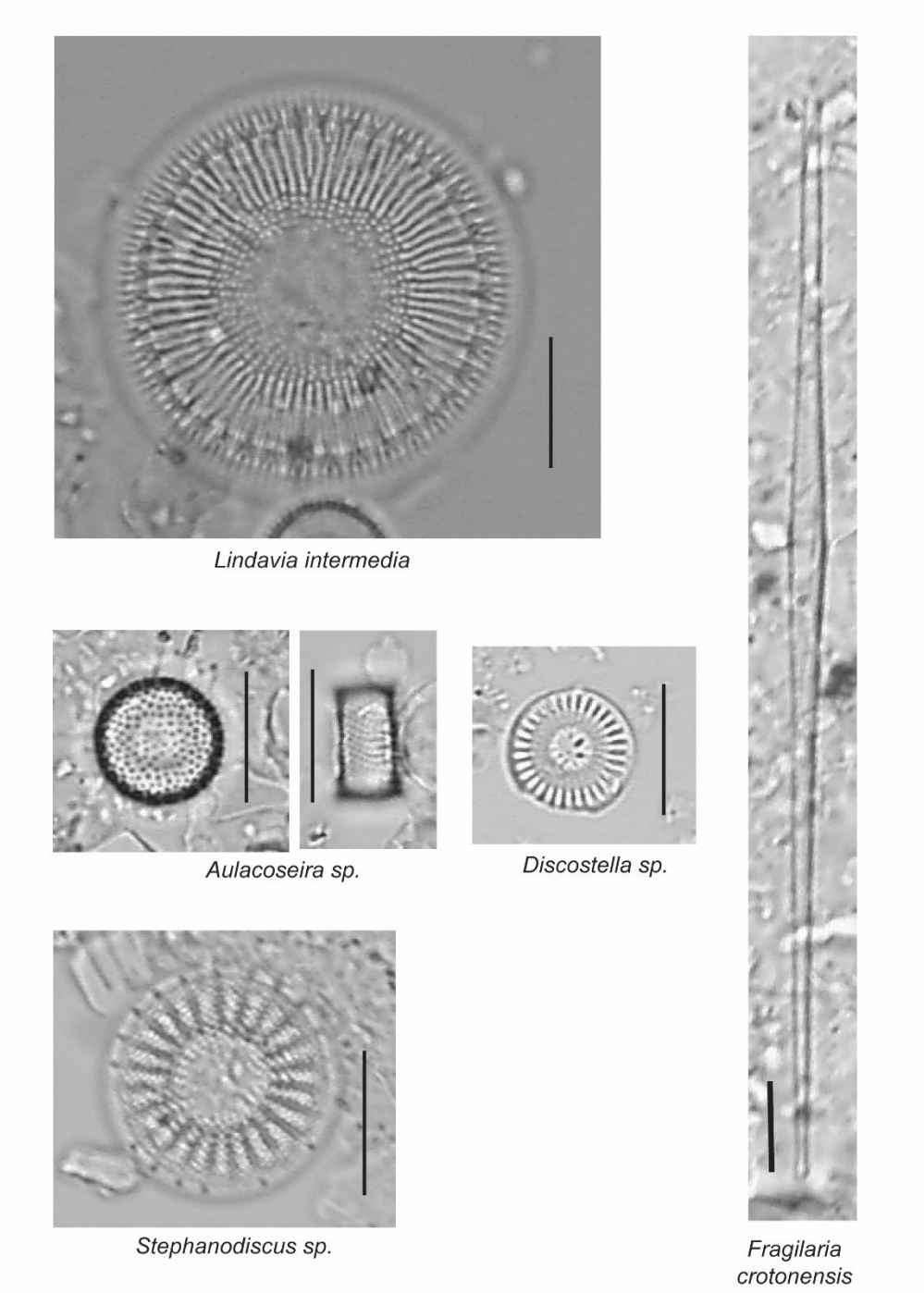

Figure S3. Photomicrographs of the planktonic species from Ozette Lake. (Scale bar = 10 μm).

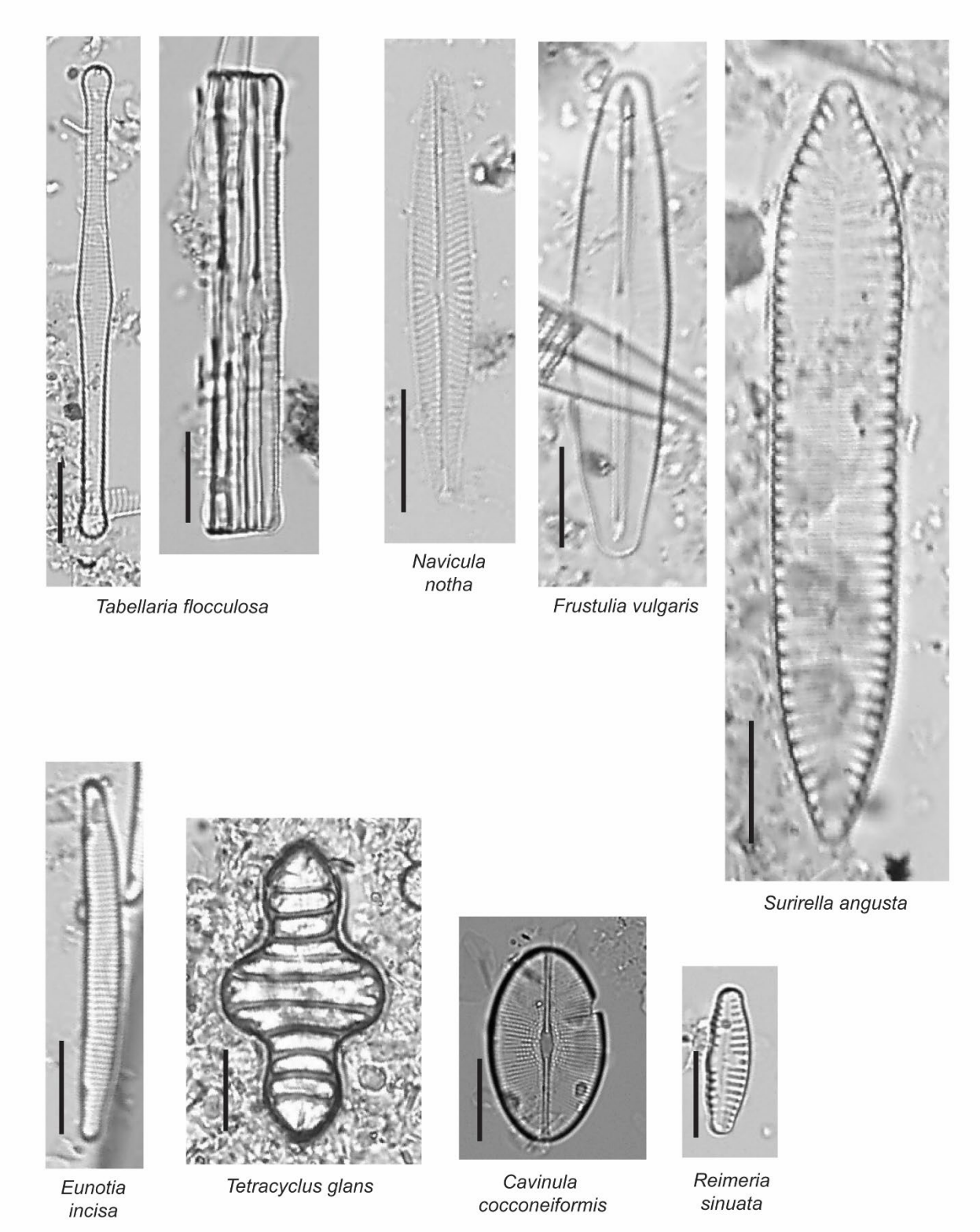

Figure S4. Photomicrographs showing a small sample of the lake benthic subgroup species from Ozette Lake. (Scale bar = 10 µm).

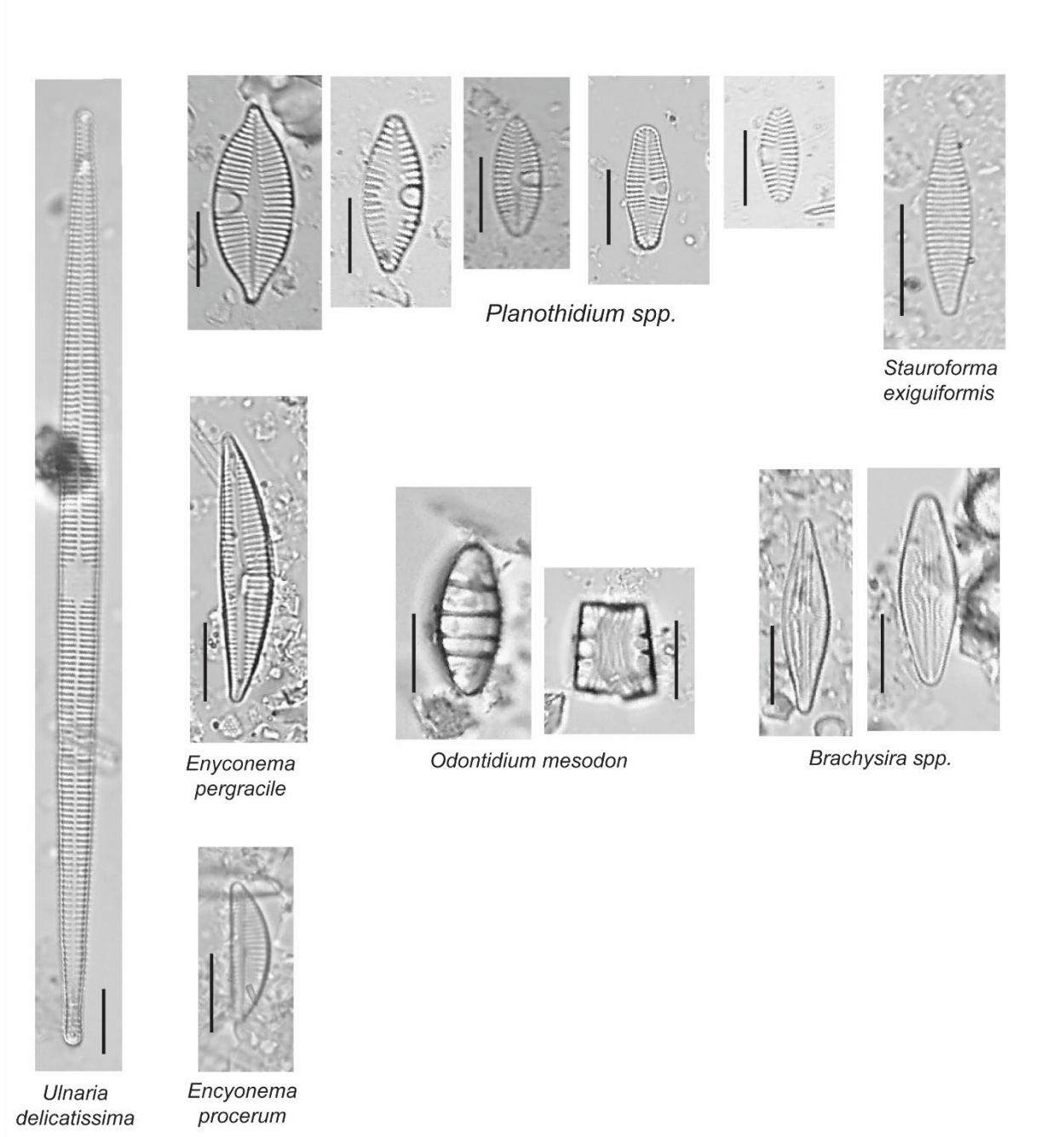

Figure S5. Photomicrographs of the delta subgroup species from Ozette Lake. (Scale bar = 10 μm).

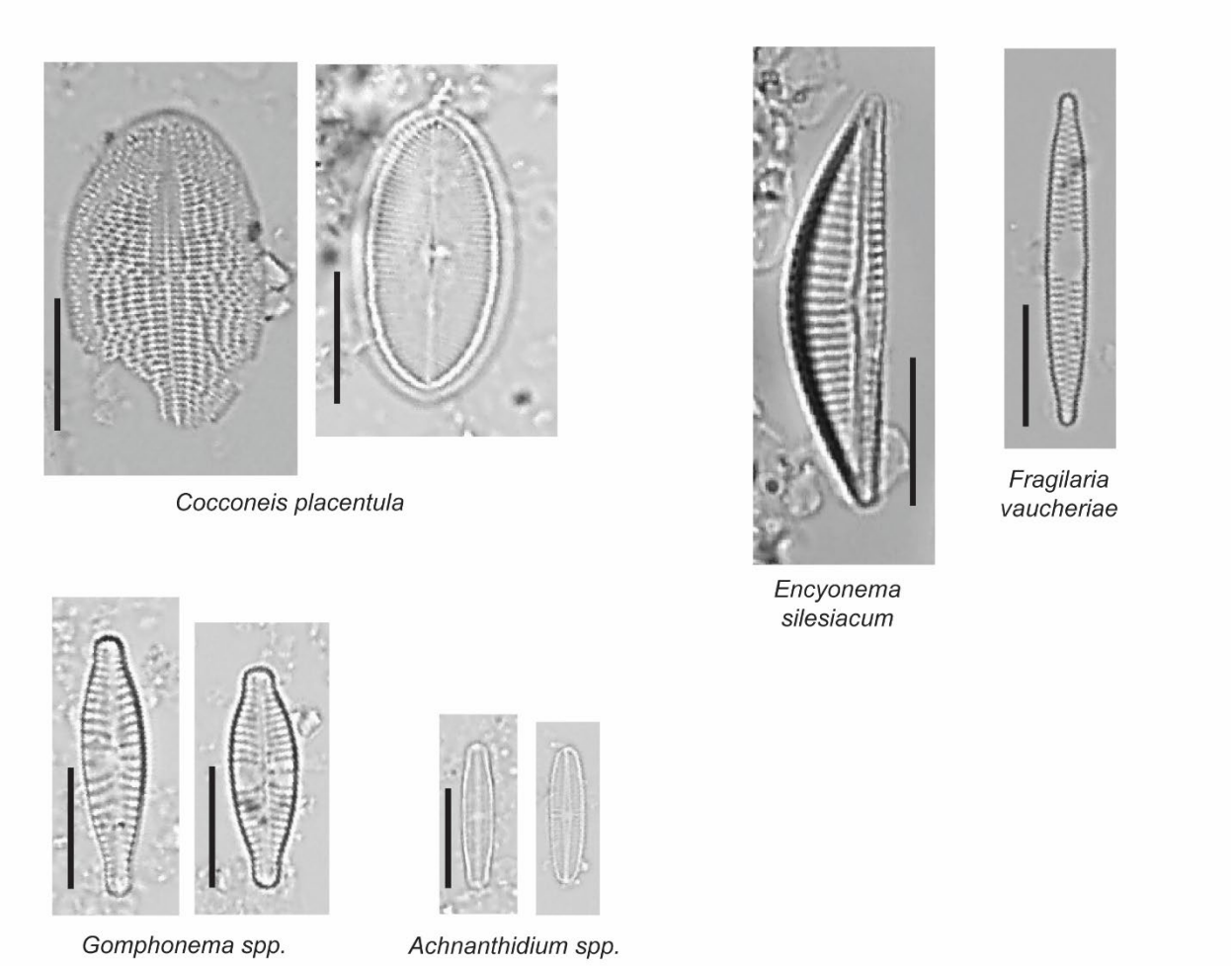

Figure S6. Photomicrographs of the terrestrial subgroup species from Ozette Lake. (Scale bar = 10 µm).

Figure S7. Collecting a modern sample from Umbrella Creek.

Table S1. Grain size and diatom results for samples collected from core VC35.

VC35 E1	Depth (cm)	Benthic (all)	Planktonic	Benthic subgroups			Mean grain size (phi)	D50 (phi)
				Delta	Terrestrial	Lake Benthic		
	6-7	9.09	81.49	1.95	1.62	5.52	5.70	5.581
	7-8	17.15	71.52	3.56	4.21	9.39	5.99	5.988
	8-9	20.52	70.68	4.89	4.23	11.40	6.29	6.314
	9-10	14.55	71.52	2.48	3.10	8.98	5.86	5.788
	10-11	10.82	76.61	2.63	2.05	6.14	5.95	5.912
	11-12	10.65	78.39	2.26	3.23	5.16	5.75	5.598
	12-13	13.25	75.08	3.47	2.84	6.94	5.97	5.911
	13-14	11.11	79.74	1.96	2.29	6.86	5.77	5.624
	14-15	17.89	72.20	3.19	3.19	11.50	5.93	5.889
	16-17	--	--	--	--	--	6.07	6.063

VC35 E2	Depth (cm)	Benthic (all)	Planktonic	Benthic subgroups			Mean grain size (phi)	D50 (phi)
				Delta	Terrestrial	Lake Benthic		
	20-21	7.17	80.46	0.98	1.30	4.89	6.22	6.231
	21-22	14.42	67.79	3.37	3.99	7.06	5.88	5.785
	22-23	13.92	74.43	1.94	3.24	8.74	5.80	5.733
	23-24	13.43	74.86	1.43	2.29	9.71	5.73	5.607
	24-25	--	--	--	--	--	5.10	4.780
	25-26	--	--	--	--	--	4.85	4.477
	26-27	20.90	66.56	4.18	3.54	13.18	4.73	4.289
	27-28	21.04	69.26	3.88	6.47	10.68	6.02	6.042
	28-29	18.83	70.45	4.22	2.27	12.34	5.76	5.698
	29-30	15.69	75.69	1.85	3.69	10.15	5.85	5.785
	30-31	16.67	75.64	2.88	1.60	12.18	5.57	5.360

Table S2. Diatom database for all species observed over 1% abundance in Ozette Lake

	Diatom species	Substrate	Umbrella Creek	Source (UC delta)	VC49 (Proximal)	VC43 (Inter.)	VC46 (Distal)	VC35 (Shelf)	BC02 (Floods)
Delta subgroup	Brachysira spp.	Epi		x	x	x	x	x	
	Encyonema procerum	Ept		x (BC101 + 102)	x	x			
	Encyonema pergracile	Epi		x	x	x			x
	Odontidium mesodon	Tyc?	x	x (BC101+102)			x	x	
	Planothidium spp.	Eps	x	x	x	x	x	x	x
	Stauroforma exiguiformis	Epi		x (BC101)	x				
	Ulnaria delicatissima	Tyc		x (BC101+102)	x	x			
Terrestrial subgroup	Achnanthidium spp.	Aer	x					x	
	Cocconeis placentula	Ept	x	x	x	x			
	Encyonema sileciacum	Epi	x	x	x	x	x	x	
	Fragilaria vaucheriae	Tyc	x	x	x	x	x	x	x
	Gomphonema spp.	Ept	x	x	x	x	x	x	
Lake Benthic subgroup	Amphora spp.	Epi	x	x					
	Cavinula cocconeiformis	Epi			x	x			
	Cavinula vincentii	Epi			x				
	Cocconeis neodiminuta	Epi			x				
	Diploneis spp.	Epi		x	x	x			
	Eunotia incisa	Aer		x	x	x	x	x	x
	Eunotia paludosa	Aer		x	x				
	Fragilaria tenera	Tyc		x				x	
	Frustulia quadrisinuata	Epi		x	x				
	Frustulia vulgaris	Epi, Aer		x (BC101 only)					
	Navicula lanceolata	Epi		x					
	Navicula radiosa	Epi		x	x				
	NAV01		x	x					
	Navicula gregaria		x						
	Navicula notha				x				
	Nitzschia palea	Epi	x						

	Diatom species	Substrate	Umbrella Creek	Source (UC delta)	VC49 (Proximal)	VC43 (Inter.)	VC46 (Distal)	VC35 (Shelf)	BC02 (Floods)
Lake Benthic subgroup	Reimeria sinuata	Epi			x				
	Sellaphora sp.	Epi	x						
	Surirella angusta			x					
	Surirella tenera				x				
	Tabellaria fenestrata	Ept, Tyc		x	x				
	Tabellaria flocculosa	Ept, Tyc		x	x	x	x	x	x
	Tetracyclus glans	Epi			x				
	Ulnaria contracta	Epi	x	x (BC101)					
Planktonic	Aulacoseira sp.		x	x	x	x	x	x	x
	Discostella sp.		x	x	x	x	x	x	x
	Fragilaria crotonensis			x			x	x	x
	Lindavia intermedia			x	x	x	x	x	x
	Stephanodiscus sp.			x	x	x	x	x	x

Substrate: (Aer, aerophilous; Tyc, tychoplanktonic; Ept, epiphytic, Epi, epipelic; Eps, epipsammic